NUREG/CR-1184
SAND79-1787
RV

EVALUATION OF SIMULATOR ADEQUACY FOR THE RADIATION QUALIFICATION OF SAFETY-RELATED EQUIPMENT

Lloyd L. Bonzon
William H. Buckalew

Manuscript Submitted: August 1979
Date Published: May 1980

Sandia National Laboratories
Albuquerque, NM 87185
operated by
Sandia Corporation
for the
US Department of Energy

Prepared for
Research Support Branch
Office of Water Reactor Safety Research
US Nuclear Regulatory Commission
Washington, DC 20555
Under Interagency Agreement DOE 40-550-75
NRC FIN No. A-1051-0

EXECUTIVE SUMMARY

The qualification of Class 1, safety-related, equipment is of continuing concern to the nuclear power industry. Equipment qualification is encompassing in scope and concept; that is, any qualification program must consider the specific functional signature of the equipment under the combined environments of its aging history, followed by the combined environments of its particular design basis accident. The radiation environment is just one of several; if strong interactions occur between radiation and other environments (e.g., temperature), the radiation effects are not clearly separable. It is not precisely correct, therefore, to speak of "radiation qualification." Nonetheless, radiation qualification is addressed in this report to evaluate the adequacy of radiation simulators typically used in qualification testing. Where possible, discussion of combined environment effects is made. "Adequacy" need not be based on one-to-one correspondence of the actual radiation signature with a simulator signature, although that would be sufficient to assure adequacy. Instead, adequacy is judged on the basis of equivalence of equipment "damage" as a result of the exposure; under that definition of adequacy, the radiation signatures may not be identical but the damage (and damage mechanisms) must be quite similar.

Before simulator adequacy could be evaluated, it was necessary to provide background information and calculations in three areas. These are summarized in the report and are detailed in numerous companion topical reports.

First, it was necessary to accurately define the actual loss-of-coolant accident (LOCA) radiation signatures. In fact, it is more nearly correct to describe these LOCA-radiation signatures as "hypothesized". While they are intended to be conservative estimates of releases during the LOCA, they more nearly represent unterminated LOCA conditions. The bases for these reported hypothesized radiation signatures are Regulatory Guide 1.89 and a newer draft of 1.89. It is also recognized that new data

base and new initiatives to describe "best-estimate" LOCA radiation signatures (based on best-estimates of accident time-sequencing, progression, and fission-product release fractions) are currently underway. However, it is generally recognized that these continuing studies will not substantially affect the evaluation of simulator adequacy, because any signature will have (1) gamma and beta radiations, (2) nearly invariant spectral-time shape, and (3) time varying, but shape consistent, magnitudes. The differences will then be primarily manifested in magnitude and in assumptions of "instantaneous" release of the fission products.

Second, from the earliest calculations of accident source signature, it was recognized that the principal concerns in simulator adequacy would be associated with the (1) beta component, (2) time-varying gamma and beta spectra, and (3) time-varying gamma and beta magnitude. Similarly, it was apparent that exposed organic materials would be most (relatively) sensitive to the differences between simulators' and actual signatures. Therefore, it was first necessary to make comparative calculations of exposed organics' response to the various radiation signatures. In the report, a modeled electrical cable is used as an example of a typical Class 1, safety-related, equipment item with significant exposed organic materials. Its significance is as an exposed organic material, not just as an electrical cable. Cobalt and cesium are examined as typical examples of simulators; other gamma sources (e.g., spent-fuel elements) are not expected to strongly influence any judgment of simulator adequacy. Clearly the closer the spectrum (and particle-type) and magnitude match, the more "adequate" is the simulator.

The third area to be addressed, preliminary to the evaluation of simulator adequacy, was the identification of radiation damage mechanisms. For this evaluation, two separate investigations were conducted: the first by IRT Corporation staff and the second by Sandia staff. The major damage mechanisms postulated were

- Electrical changes, charge buildup, electrical noise spikes
- Temperature changes

- Chemical and mechanical changes
- Differential mechanical stress

Each of these is specifically addressed in the report with judgment of its importance to simulator adequacy concerns made.

The trapped charge in the insulator is largely a consequence of the nonuniform dose deposited in the cable. The mechanism that applies here is that the secondary emission leaving a volume element is not balanced by secondary emission from adjacent points because the adjacent points are not receiving the same primary radiation. The gamma source simulators do not show such a strong attenuation as does the true LOCA (particularly, beta) source so they will not precisely simulate the trapped charge and any resultant noise spikes. The amplitude of resultant noise pulses, caused by breakdown in the cable, depends almost completely on the exact details of the cable termination. If the termination is either a small resistive load or a large capacitive load, then the noise spikes will not be large. Because leakage currents are calculated to be small, the noise spikes are small and the choice of simulator is relatively unimportant; the LOCA environment is adequately simulated as long as average doses are "maintained".

Temperature changes in materials may be sufficient to be of concern. Here the beta radiation can be viewed as a total heat source, since the depth-dose features are relatively unimportant. In the same regard, the simulator may be relatively unimportant as long as the heat source is duplicated (where important). Thus, while the simulator is not a factor, the simulation of the heat load is a consideration.

Total chemical and mechanical changes in materials are not a strong function of the radiation source, if the total damage is duplicated as appropriate. That is because the LOCA and simulator energy losses in materials are via the same mechanisms. Further, the available data indicate only minor dose-rate effects in elastomeric materials.

One feature of radiation damage not generally duplicable by the common simulators is the differential stress, due to strong depth-dose profile dependence, from the LOCA beta source. The mechanism involves the shrinkage of a material relative to its remaining elongation; if the surface of an elastomer suffers shrinkage on the order of the remaining elongation, it is plausible that surface crazing or cracking could occur. However, available data show only minimal shrinkage (a few percent), even when the total elongation is reduced to near zero (either thermally or by radiation). Hence, differential stress is not a practical concern.

It is concluded that the standard gamma-radiation simulators can adequately duplicate the damage mechanism and damage in safety-related equipment that result from postulated nuclear plant ambient- and accident-radiation environments. The conclusion can be no stronger than that because the simulators must be intelligently used in an overall qualification program that implies combinations of environments, magnitudes, secondary radiations, and other considerations. Other specialized simulators, which more closely achieve the LOCA-radiation signature, are equally adequate, with similar provisos. However, there seems to be no reason to select one simulator over another. One recommendation is to overstress the equipment/material everywhere to a greater total dose than expected from the combined LOCA-radiation signature; dose rates should also approximate the expected (combined) rates. However, other logical data-based techniques (e.g., averaged dose and rates) may also be acceptable.

In summary, we have seen no evidence of unique damage mechanisms in exposed organic materials that demand unique radiation-simulation techniques. But neither can radiation be arbitrarily applied to the test item without consideration of the complete qualification program. Future work should consider the equivalences of beta/gamma and neutron/gamma ratios in bulk degradation, charge breakdown transient and permanent effects, secondary emissions, and more complex equipment.

CONTENTS

CONTENTS (cont)

CONTENTS (cont)

ILLUSTRATIONS

ILLUSTRATIONS (cont)

ILLUSTRATIONS (cont)

TABLES

EVALUATION OF SIMULATOR ADEQUACY FOR THE RADIATION QUALIFICATION OF SAFETY-RELATED EQUIPMENT

1. Introduction

The qualification of Class 1, safety-related, equipment[1] is a continuing concern to the nuclear power industry. Equipment qualification is encompassing in scope and concept; that is, any qualification program must consider the specific equipment functional signature under the combined environments of its aging history, followed by the combined environments of its particular design basis accident. The radiation environment is just one of the several environments. Thus, radiation is not clearly or cleanly separable; to speak of "radiation qualification" is not precisely correct.

Nonetheless (as a first approximation), radiation qualification will be addressed in this report in order to evaluate the adequacy of radiation simulators typically used in qualification test simulations. Where possible, discussion of combined environment effects will be made. "Adequacy" need not be based on one-to-one correspondence of the actual radiation signature with a simulator signature, although that would be sufficient to assure adequacy. Instead, adequacy is to be judged on the basis of equivalence of equipment "damage" as a result of the exposure; under that definition of adequacy, the radiation signatures may not be identical but the damage (and damage mechanisms) must be quite similar.

1.1 Background, Accident-Radiation Signatures

1.1.1 General

Preliminary to the evaluation of simulator adequacy, it is necessary to accurately define the actual radiation signatures. That has been previously done and reported[2-6] under the Task 2 effort associated with the overall Qualification Testing Evaluation (QTE) program.[7]

In fact, it is more nearly correct to describe these loss-of-coolant accident (LOCA) radiation signatures as "hypothesized". While they are intended to be conservative estimates of releases during the LOCA, they more nearly represent unterminated LOCA conditions. The bases for these reported hypothesized radiation signatures are Regulatory Guide 1.89[8] and a newer draft of 1.89.[9]

Since simulator adequacy is dependent upon the actual radiation signature, a review of this effort is included as Chapter 2 in this report.

1.1.2 New Initiatives in Radiation-Signature Definition

It may be appropriate to note that the LOCA radiation signature has not been finally established. Originally, Regulatory Guide 1.89[8] recognized only one source term for radiation qualification. More recently a draft Guide[9] discusses a two-level source term. The larger term, as originally specified, is to be applied to containment heat-removal and isolation systems, postaccident monitoring (PAM) equipment, and the like. The smaller is to be applied to the majority of the safety-related systems. These two sources are logically based in that the larger is nearly an unterminated LOCA condition, the smaller represents a degraded (not totally dysfunctional) safety-systems response to a LOCA-initiating event; thus the two-tiered source recognizes the circular logic and that it is inappropriate to demand qualification of equipment to environments that can only occur if that same equipment has already been assumed to have failed so as to produce the environments.

Much more recently, under the QTE program,[7] effort has been directed toward a so-called "best-estimate" LOCA-radiation signature incorporating best-estimates of accident time-sequencing, progression, and fission-product release fractions. Full disclosure and distribution of this work by IRT Corporation[10,11] has been made in a Sandia report released as Reference 12. Figures 1.1-1.3 visually summarize some of the key features of the "best-estimate" signature.

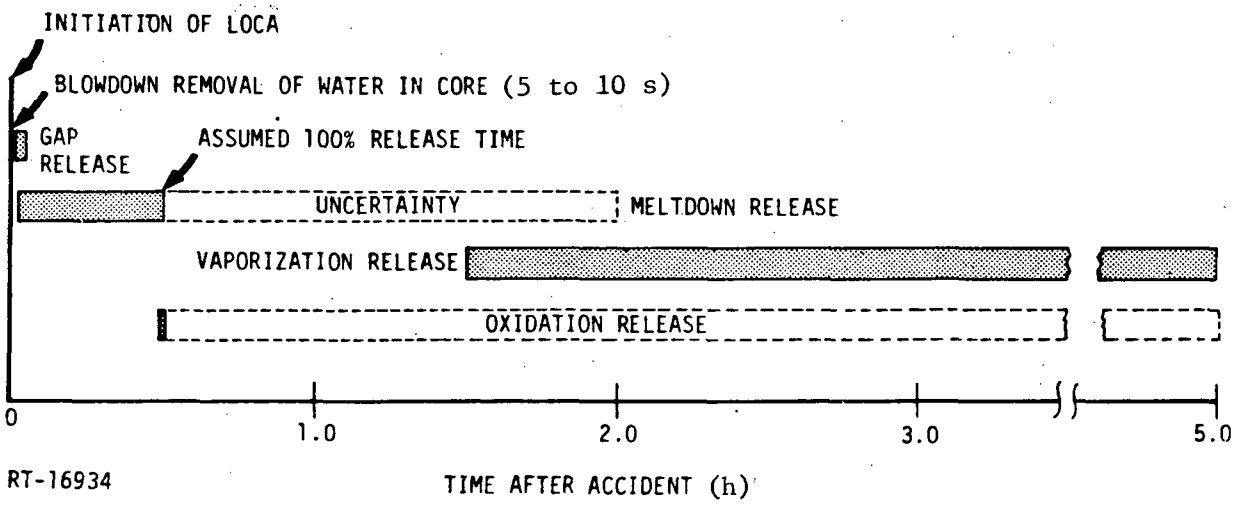

Figure 1.1 Temporal Fission Product Release Sequence - Unterminated LOCA Without Cooling (from Reference 12)

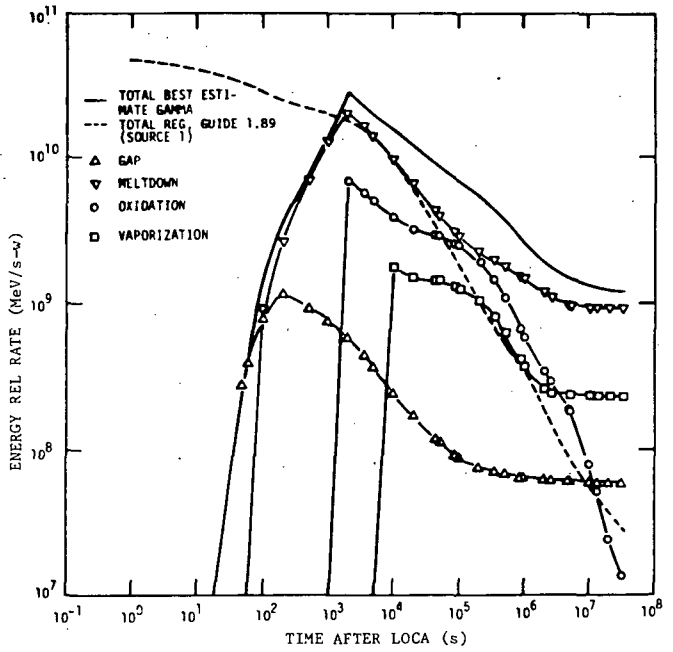

Figure 1.2 Gamma-Ray Energy Release Rate vs Elapsed Time From LOCA - "Best-Estimate" Source (from Reference 12)

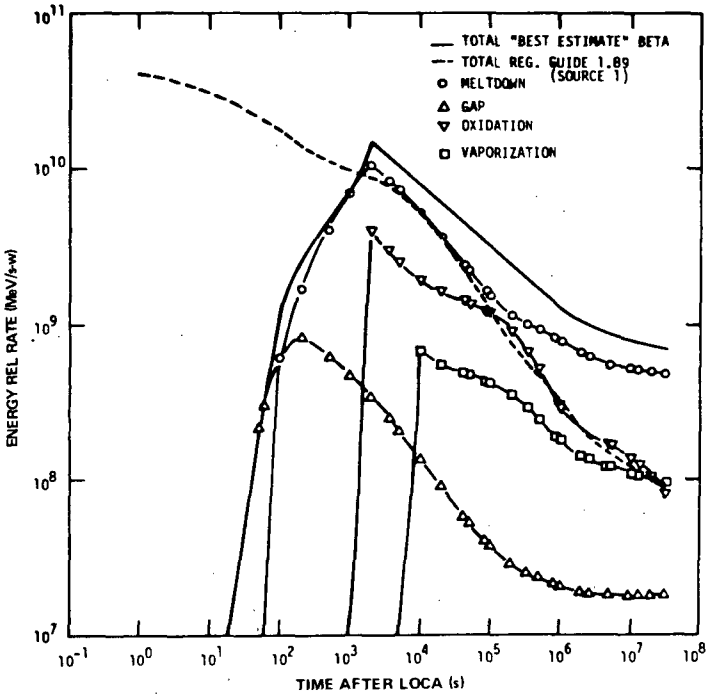

Figure 1.3 Beta Energy Release Rate vs Elapsed Time From LOCA - "Best-Estimate" Source (from Reference 12)

While it is important to understand that the ultimate radiation qualification signature(s) may be modified by these studies and by data-base programs,[13] it should also be realized that they can not substantially affect the evaluation of simulator adequacy. That is, any signature will have (1) gamma and beta radiations; (2) nearly invariant spectral-time shape; and (3) time varying, but shape consistent, magnitudes. The differences will then be primarily manifested in magnitude and "instantaneousness". The evaluation of simulator adequacy in this report will be discussed relative to the larger Regulatory Guide 1.89 source term, also known as Source 1.

1.2 Background, Comparative Calculations

From the earliest calculations (in this series) of accident source signature,[2] it was recognized that the principal concerns in simulator

adequacy would be associated with the (1) beta component, (2) time-varying gamma and beta spectra, and (3) time-varying gamma and beta magnitude. Similarly, it was apparent that exposed organic materials would be particularly susceptible to the differences between simulators' and actual signatures. It was imperative, and preliminarily necessary, to make comparative calculations of exposed organics' response to the various extremes of radiation signatures. Some of this effort has been previously reported in the literature,[6,14] but the full and final report[15] prepared by IRT Corporation is included as Appendix A of this report.

In that report, a modeled electrical cable is used as an example of a typical Class 1, safety-related, equipment item with significant exposed organic materials. Its significance is as an exposed organic material, not just as an electrical cable. Cobalt and cesium are examined as typical examples of simulators; other gamma sources (e.g., spent-fuel elements) are not expected to strongly influence any judgment of simulator adequacy. Specialized sources (e.g., bremsstrahlung, linacs, and the like) were not examined for two major reasons. First, these are generally small-volume sources not amenable to long-term, large-volume irradiations. Second, gamma simulators represent an extreme for the simulator adequacy concerns, specifically the (actual) beta signature; if adequacy can be shown for gamma simulators, the specialized sources may then also be adequate. Besides the simulators examined, the report[15] also addresses unique test conditions (e.g., intervening steel test chambers) and certain test/actual conditions (e.g., 70-psig steam surrounding the test specimens).

Since the comparative calculations influence and are bases for the evaluation of simulator adequacy, a review of this effort is included as Chapter 3 in this report.

1.3 Background, Potential Damage Mechanisms

The third area to be addressed, preliminary to the evaluation of simulator adequacy, is the identification of radiation damage mechanisms, particularly those most influenced by a priori known differences in

simulator and actual signatures. For this evaluation, two separate investigations were conducted: the first by IRT Corporation staff[16] and the second by Sandia staff.[17] The former is included as Appendix B of this report. The major damage mechanisms postulated were

- Electrical changes, charge buildup, electrical noise spikes
- Temperature changes
- Chemical and mechanical changes
- Differential mechanical stress

Since these damage mechanisms are the true bases for simulator adequacy evaluation, they will be discussed and prioritized in Chapter 4 and individually addressed in succedent chapters.

2. LOCA Radiation Signatures

2.1 Origin of Signature Bases

The hypothesized LOCA radiation source for a light-water reactor has been specified by the US Nuclear Regulatory Commission in its Regulatory Guide 1.89[8] for purposes of qualification testing of Class 1, safety-related, equipment in commercial power reactors. The approach taken in the Guide is to specify certain fractions of fission products by categories that are assumed to be released from the reactor core and distributed within the containment structure. More recently a new draft of the Guide[9] suggested a separation of the qualification source into a two-tiered system to be chosen as appropriate to the equipment being qualified (Table 2.1). That draft Guide then calls for two radiation source terms (for containment heat-removal systems and similar equipment, and for other safety-related electrical systems) and three distribution categories for each source (airborne, waterborne, and plateout).

TABLE 2.1

Source Types and Distribution Categories
(From Reference 9)

Source 1 (Containment heat removal systems, etc)	Airborne	100% noble gases, 25% iodines
	Plateout	25% iodines, 1% solids
	Waterborne	50% halogens, 1% solids
Source 2 (Other safety-related electrical systems)	Airborne	10% noble gases (except ^{85}Kr), 30% ^{85}Kr, 5% iodines
	Plateout	5% iodines
	Waterborne	10% halogens

From this specification it remains for the user to translate these source bases into energy release rates and energy spectra for gamma rays and beta particles as a function of time after the accident. Such calculations involve following the buildup and decay of the fission products in the core for some prescribed operating conditions of the reactor. It is useful to examine the variation in energy release rates and spectra that result from different operating conditions or other choices of parameters not specific in the Guide. These parametric calculations have been completed and reported.[4,5,6] The work is summarized in Sections 2.2 and 2.3. In that summary, the emphasis is towards Source 1, the currently required radiation qualification source.[8] In almost every instance, the conclusions reached about Source 1 pertain equally to Source 2; the principal difference is in magnitude.

2.2 Energy-Release Rates -- Source 1

Energy-release rates have been calculated for a wide variety of reactor-operating parameters including fuel composition, power level, duration of operation, and treatment of progeny; the results of these extensive energy-release rate calculations are presented in References 4 and 5. An example of the results is shown in Figure 2.1 where the normalized beta and gamma-ray energy-release rates are plotted as a function of time after LOCA for the case of 200-d continuous operation at 4000 MW(t). Figures 2.2 and 2.3 and Table 2.2 illustrate various parametric calculations and their effect on energy-release rates.

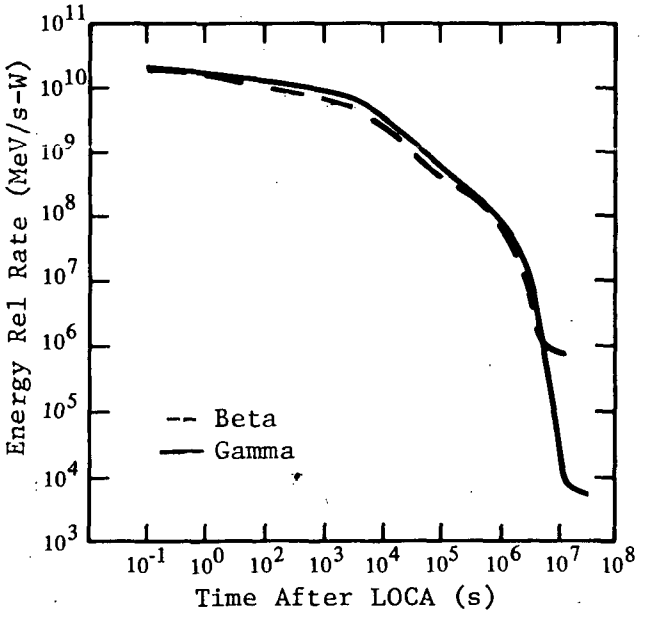

Figure 2.1

Gamma-Ray and Beta Energy Release Rate vs Elapsed Time From LOCA — Source 1 (Airborne), 4000 MW

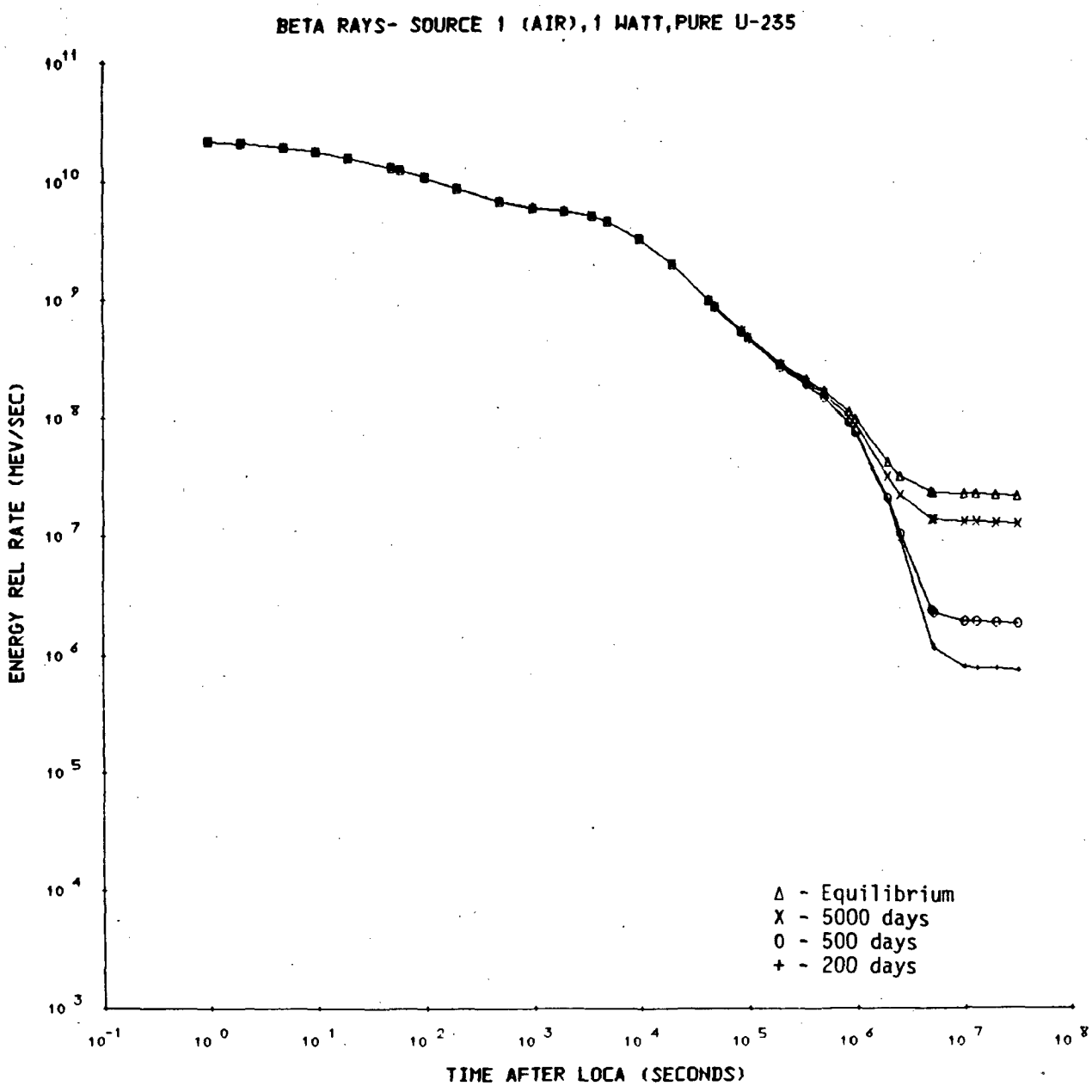

Figure 2.2 Beta Energy Release Rate vs Elapsed Time From LOCA - Source 1 (Airborne) and Several Reactor Operating Times (from Reference 5)

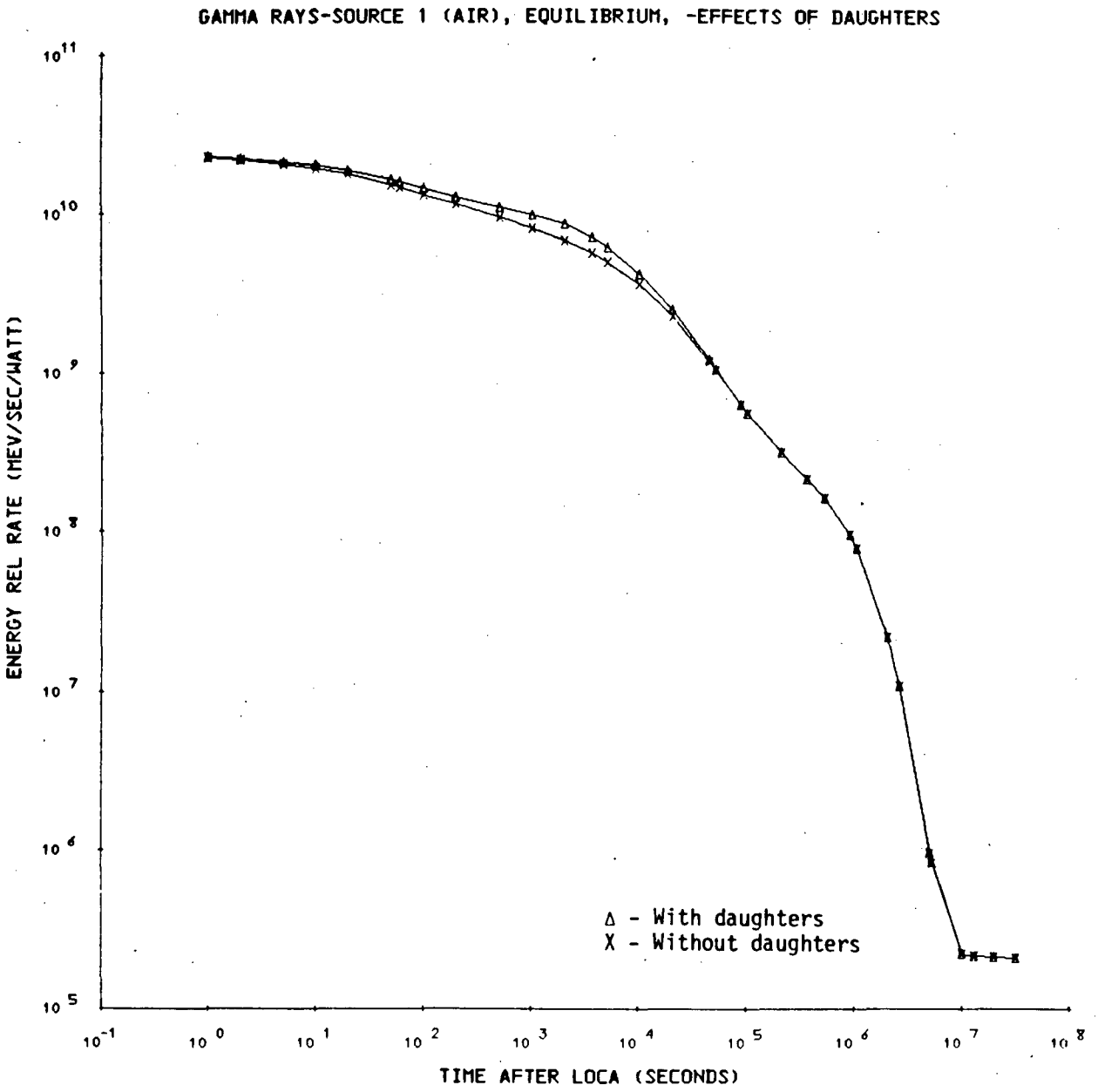

Figure 2.3 Gamma-Ray Energy Release Rate vs Elapsed Time From LOCA - Source 1 (Airborne), Daughter Product Contributions (from Reference 5)

TABLE 2.2

Percent Deviation of Selected Irradiation Times from Equilibrium Irradiations

Energy-Release Rate vs Cooling Time (from Reference 5)

SOURCE 1 (Gamma)

Cooling Time	Air			Plate Out			Water		
	5000 d	500 d	200 d	5000 d	500 d	200 d	5000 d	500 d	200 d
1 d	3.2×10^{-2}	4.8×10^{-2}	4.8×10^{-2}	1.99	2.76	4.04	1.17	1.64	2.40
4 d	<0.1	<0.1	<0.1	4.76	6.63	9.63	3.39	4.70	6.81
10 d	0.12	0.22	0.23	7.48	10.4	14.8	5.62	7.81	11.2
30 d	0.92	1.84	1.93	15.2	21.0	28.6	13.7	19.0	25.8
60 d	12.9	24.6	25.7	23.8	32.7	41.7	23.6	32.3	41.3
1 y	49.1	92.5	96.9	65.1	87.3	91.0	65.2	87.3	91.0

SOURCE 1 (Beta)

Cooling Time	Air			Plate Out			Water		
	5000 d	500 d	200 d	5000 d	500 d	200 d	5000 d	500 d	200 d
1 d	1.76	3.88	4.09	5.45	9.73	13.0	3.44	6.17	8.21
4 d	4.53	10.0	10.6	12.0	21.3	28.4	9.22	16.5	21.8
10 d	8.56	19.0	20.0	16.0	28.5	37.7	13.6	24.1	31.8
30 d	30.3	67.0	70.6	23.6	41.5	53.9	22.6	39.7	55.9
60 d	40.8	90.1	95.0	29.3	50.7	64.6	29.2	50.5	64.4
1 y	41.5	91.6	96.5	49.4	76.1	87.0	49.5	76.1	87.0

Several conclusions can be drawn from the energy-release rate calculations:

a. The length of irradiation prior to LOCA (in the range 200 d to equilibrium) does not have a significant influence on the energy-release rates until postaccident times greater than about one day; after that, differences can be significant.

b. The reactor operating power affects the fission product inventory by neutron capture transmutation of the fission products and fuel, and by depletion of the fissile isotope. For the postaccident time range of interest here and for realistic power levels and irradiation histories, these effects are not significant.

c. Several methods for treating daughters of the specified fission product types were investigated. Substantial differences in energy release rates can be obtained depending on whether or not daughters are included.

2.3 Spectra -- Source 1

In addition to energy-release rates, energy spectra of the fission products were also calculated at selected times after LOCA. The method of calculation involved folding the activities of each of the fission-product isotopes at the time of interest with the individual beta or gamma-ray spectrum of that nuclide and summing over all nuclides. The results of the spectra calculations for all sources and distribution categories are given in References 4 and 5.

An interesting result obtained from the calculations is the behavior of the average particle energy as a function of cooling time. An example of these results (for Source 1) is shown in Figure 2.4. The spectra "soften" (i.e., average energy decreases) with time, reaching a minimum in the neighborhood of 1 to 10 d, then "harden" at longer times. This behavior occurs for both gamma-ray and beta spectra. The general variation in average energy is not unexpected since it is generally true that radioactive emissions from short-lived nuclides are higher in energy than those

from long-lived nuclides; the rehardening of the spectra must be a function of the selected fission product inventory.

Other examples of spectral behavior with variation of parameters are shown in Table 2.3 and Figures 2.5 and 2.6.

The spectral shape has potential for impact on radiation qualification testing and thus the implication of changing spectrum hardness must be addressed. This is particularly true when radiation simulators that have fixed or monoenergetic spectra (like Cobalt-60) are used in qualification testing.

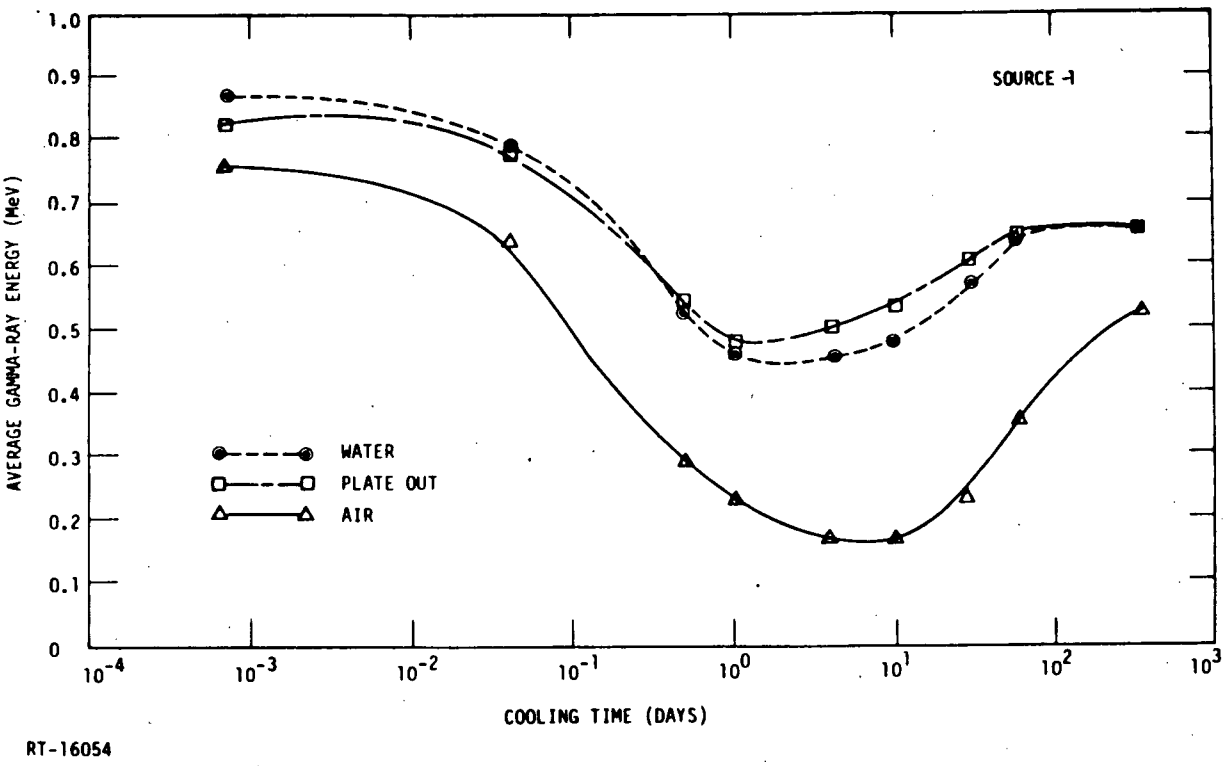

Figure 2.4 Average Gamma-Ray Energy vs Reactor Cooling Time - Source 1 (from Reference 5)

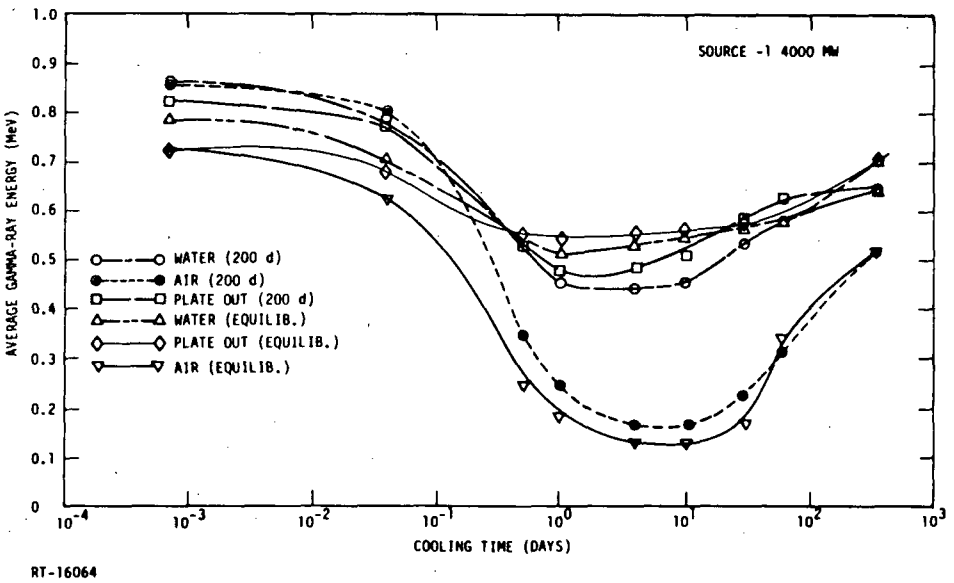

Figure 2.5 Average Gamma-Ray Energy vs Reactor Cooling Time - Source 1 and Several Reactor Operating Times (from Reference 5)

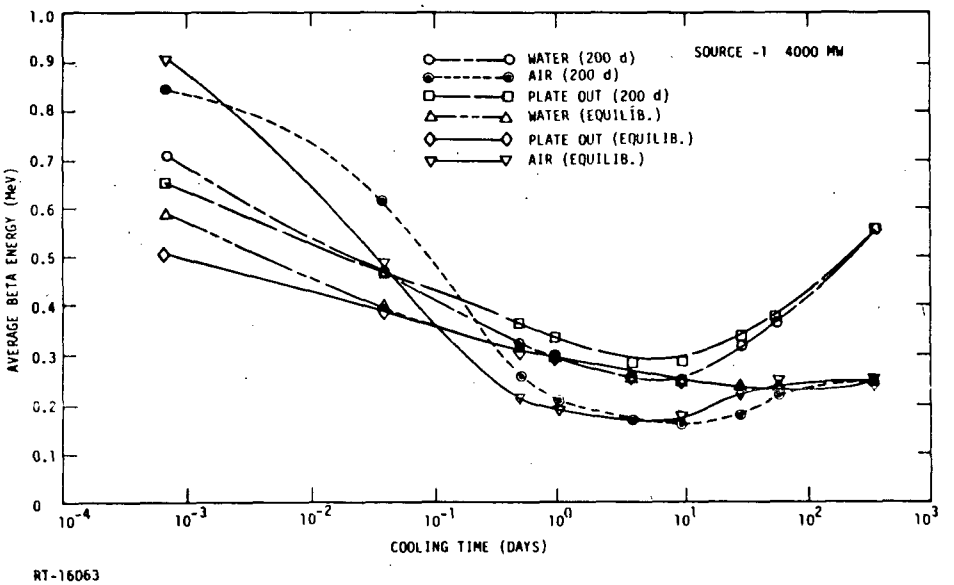

Figure 2.6 Average Beta Energy vs Reactor Cooling Time - Source 1 and Several Reactor Operating Times (from Reference 5)

TABLE 2.3

Average Particle Energy vs Cooling Time - Source 1 and Several Reactor Operating Times (from Reference 5)

Time After LOCA Initiation	Equilib.	5000 d	500 d	200 d	Equilib.	5000 d	500 d	200 d
		Source 1 (Air) γ				Source 1 (Air) β		
0	0.7095	0.7096	0.7096	0.7096	1.0066	1.0080	1.0098	1.0100
1 min	0.7556	0.7556	0.7556	0.7556	0.7866	0.7879	0.7895	0.7897
1 h	0.6361	0.6361	0.6361	0.6361	0.5609	0.5622	0.5638	0.5639
12 h	0.2864	0.2864	0.2864	0.2864	0.2652	0.2654	0.2656	0.2657
1 day	0.2248	0.2247	0.2247	0.2247	0.2102	0.2098	0.2092	0.2092
4 days	0.1638	0.1638	0.1637	0.1637	0.1656	0.1638	0.1615	0.1612
10 days	0.1640	0.1639	0.1637	0.1637	0.1678	0.1643	0.1595	0.1590
30 days	0.2297	0.2284	0.2268	0.2267	0.2158	0.2014	0.1746	0.1700
60 days	0.3567	0.3428	0.3224	0.3201	0.2441	0.2432	0.2325	0.2217
1 year	0.5252	0.5253	0.5269	0.5296	0.2456	0.2456	0.2456	0.2456
		Source 1 (Plate Out) γ				Source 1 (Plate Out) β		
0	0.8320	0.8323	0.8325	0.8327	0.7492	0.7528	0.7550	0.7570
1 min	0.8263	0.8266	0.8269	0.8271	0.6475	0.6501	0.6517	0.6530
1 h	0.7776	0.7780	0.7783	0.7785	0.4657	0.4663	0.4660	0.4659
12 h	0.5367	0.5357	0.5354	0.5343	0.3719	0.3698	0.3670	0.3648
1 day	0.4781	0.4756	0.4748	0.4727	0.3493	0.3456	0.3409	0.3373
4 days	0.5012	0.4954	0.4937	0.4887	0.3131	0.3025	0.2901	0.2796
10 days	0.5282	0.5201	0.5179	0.5110	0.3307	0.3174	0.3002	0.2849
30 days	0.6069	0.5974	0.5966	0.5881	0.3934	0.3829	0.3613	0.3375
60 days	0.6466	0.6393	0.6425	0.6370	0.4249	0.4210	0.4012	0.3712
1 year	0.6551	0.6222	0.5985	0.6398	0.4631	0.4922	0.5568	0.5473
		Source 1 (Water) γ				Source 1 (Water) β		
0	0.8917	0.8914	0.8915	0.8917	0.8307	0.8330	0.8345	0.8357
1 min	0.8658	0.8660	0.8661	0.8662	0.7063	0.7081	0.7092	0.7101
1 h	0.7876	0.7878	0.7880	0.7881	0.4628	0.4631	0.4630	0.4629
12 h	0.5267	0.5260	0.5258	0.5252	0.3592	0.3578	0.3559	0.3546
1 day	0.4568	0.4552	0.4547	0.4534	0.3357	0.3331	0.3301	0.3278
4 days	0.4552	0.4505	0.4490	0.4452	0.2825	0.2736	0.2642	0.2566
10 days	0.4728	0.4654	0.4630	0.4570	0.2964	0.2836	0.2691	0.2568
30 days	0.5705	0.5585	0.5558	0.5460	0.3772	0.3641	0.3415	0.3181
60 days	0.6408	0.6322	0.6345	0.6281	0.4230	0.4185	0.3982	0.3680
1 year	0.6551	0.6222	0.5985	0.6398	0.4631	0.4922	0.5568	0.5473

TABLE 2.3 (cont)

Time After LOCA Initiation	Equilib.	5000 d	500 d	200 d	Equilib.	5000 d	500 d	200 d
		Source 2 (Air) γ				Source 2 (Air) β		
0	0.7192	0.7192	0.7192	0.7192	0.9435	0.9468	0.9510	0.9514
1 min	0.7550	0.7550	0.7550	0.7550	0.7408	0.7438	0.7474	0.7478
1 h	0.6502	0.6502	0.6502	0.6502	0.5246	0.5273	0.5306	0.5310
12 h	0.3369	0.3369	0.3369	0.3369	0.2785	0.2792	0.2801	0.2802
1 day	0.2766	0.2766	0.2765	0.2765	0.2296	0.2291	0.2285	0.2284
4 days	0.2109	0.2107	0.2105	0.2105	0.1781	0.1743	0.1691	0.1686
10 days	0.2099	0.2095	0.2091	0.2091	0.1829	0.1762	0.1660	0.1648
30 days	0.2803	0.2782	0.2755	0.2753	0.2283	0.2205	0.1895	0.1816
60 days	0.3951	0.3784	0.3513	0.3481	0.2449	0.2444	0.2387	0.2317
1 year	0.5251	0.5251	0.5257	0.5266	0.2455	0.2456	0.2456	0.2456
		Source 2 (Plate Out) γ				Source 2 (Plate Out) β		
0	0.8397	0.8397	0.8397	0.8397	0.6820	0.6820	0.6820	0.6820
1 min	0.8331	0.8331	0.8331	0.8331	0.6049	0.6049	0.6049	0.6049
1 h	0.7870	0.7870	0.7870	0.7870	0.4389	0.4389	0.4389	0.4389
12 h	0.5141	0.5141	0.5141	0.5141	0.3411	0.3411	0.3411	0.3411
1 day	0.4286	0.4286	0.4286	0.4286	0.3146	0.3146	0.3146	0.3146
4 days	0.3716	0.3716	0.3716	0.3716	0.2155	0.2155	0.2155	0.2155
10 days	0.3528	0.3528	0.3528	0.3528	0.1959	0.1959	0.1959	0.1959
30 days	0.3698	0.3698	0.3698	0.3698	0.2025	0.2025	0.2025	0.2025
60 days	0.3801	0.3801	0.3801	0.3801	0.2075	0.2075	0.2075	0.2075
1 year	0.6750	0.6750	0.6750	0.6750	0.1993	0.1993	0.1993	0.1993
		Source 2 (Water) γ				Source 2 (Water) β		
0	0.9007	0.9007	0.9007	0.9007	0.8165	0.8165	0.8165	0.8165
1 min	0.8727	0.8727	0.8727	0.8727	0.6974	0.6974	0.6974	0.6974
1 h	0.7930	0.7930	0.7930	0.7930	0.4492	0.4492	0.4492	0.4492
12 h	0.5141	0.5141	0.5141	0.5141	0.3411	0.3411	0.3411	0.3411
1 day	0.4286	0.4286	0.4286	0.4286	0.3146	0.3146	0.3146	0.3146
4 days	0.3716	0.3716	0.3716	0.3716	0.2155	0.2155	0.2155	0.2155
10 days	0.3528	0.3528	0.3528	0.3528	0.1959	0.1959	0.1959	0.1959
30 days	0.3698	0.3698	0.3698	0.3698	0.2025	0.2025	0.2025	0.2025
60 days	0.3801	0.3801	0.3801	0.3801	0.2075	0.2075	0.2075	0.2075
1 year	0.6738	0.6738	0.6738	0.6738	0.2576	0.2576	0.2576	0.2576

2.4 Doses and Dose Rates for a Generic Containment

The conversion of the gamma and beta release signatures to dose and dose rate must account for the transport of the radiation inside the containment with its complement of internal structure. Since this calculation is completely plant specific, further simplifying assumptions were made to complete these scoping estimates. Several are discussed here; the reader should also review Reference 2.

- The containment structure was modeled as an empty cylinder with an inside radius of 1768 cm, inside height of 6355 cm, and concrete walls, 114 cm thick; total free volume is approximately 6.25 x 10^{10} cm^3 (2.2 million ft^3); the internal structure was not modeled at all. Certainly for betas, and to a first approximation for gammas, free volume is a pertinent scaling factor. While the modeled structure is most typical of a PWR containment, the scaling factors should allow approximate application to BWR structures as well.

- An additional factor is the reactor power assumed prior to the LOCA. While merely a scaling factor that can be adjusted for a specific plant, the full impact of these environments is more graphically illustrated when a "typical" power level is assumed. The calculations are presented for a 4000-MW(t) plant, approximately the 1300-MW(e) class of a nuclear power plant.

- Certain other assumptions are important in the calculation of dose and rate, but do not affect the energy-release rates and spectra:

a. Instantaneous, uniform release or deposition.
b. Engineered safety features are neglected.
c. Containment leakage is neglected.

The first assumption is particularly important in establishing the initial dose rate; the latter two may affect the total integrated dose, although typical containment leak rates are on the order of 0.1 to 0.5 volume percent per day and thus would change the total dose by 3% to 15% over a 30-d period.

The gamma dose and rate from the airborne volumetric source is shown in Figure 2.7 as a function of time after release. The initial centerline dose rate is about 3.5 Mrad/h and the dose to 30 d is about 28 Mrad. The edge and midradius dose rates are also shown; because of the penetrability of the gamma radiation, the edge dose and rate are similar in magnitude (e.g., about 2.5 Mrad/h initial dose rate).

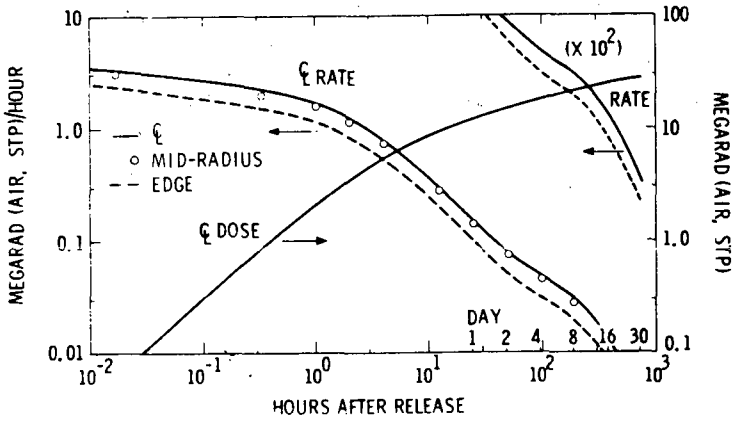

Figure 2.7 Gamma-Ray Dose/Dose Rate vs Elapsed Time From Release - Airborne Source

However, the dose and rate to a particular area of the containment is a combination of the three sources. Clearly, the airborne source and the plate-out source are additive (spatially). But the waterborne source is less spatially defined. Figure 2.8 assumes that 1/10 of the waterborne source is added to the airborne and plate-out sources. The resultant initial centerline dose rate is about 4.5 Mrad/h and the dose to 30 d is about 45 Mrad. While the airborne source is the principal dose and rate contributor everywhere in containment, the plate-out source adds significantly to the edge dose so that dose and rate are almost uniform throughout the containment in this model. The doses and rates are severe, but are a result of the assumptions that must be critically examined for specific plant applicability.

The complementary beta rates and doses are shown in Figures 2.9 and 2.10. For the airborne beta source (Figure 2.9), the initial centerline rate is greater than 50 Mrad/h (about 75 Mrad/h at 1 s) and the dose to 30 d is about 320 Mrad. The early time decay is very rapid, so that at 1 h the dose rate is about 15 Mrad/h and at 1 d about 1.7 Mrad/h. The edge dose and rate are also shown; a reasonable assumption is that the edge dose and rate are about 1/2 the centerline values since a receptor at the edge is exposed to essentially a semi-infinite volume.

As was done for the gamma sources, Figure 2.10 combines the three spatial beta sources by assuming 1/10 of the waterborne source is added to the airborne and plate-out source. The resultant initial centerline dose rate is greater than 50 Mrad/h and the dose to 30 d is about 370 Mrad. The edge dose and rate are even more significant because of the plate-out source; the initial rate exceeds 80 Mrad/h and the dose to 30 d is 5 to 6 times the centerline dose. While these are very significant doses and rates, the assumptions must be critically examined for specific plant applicability.

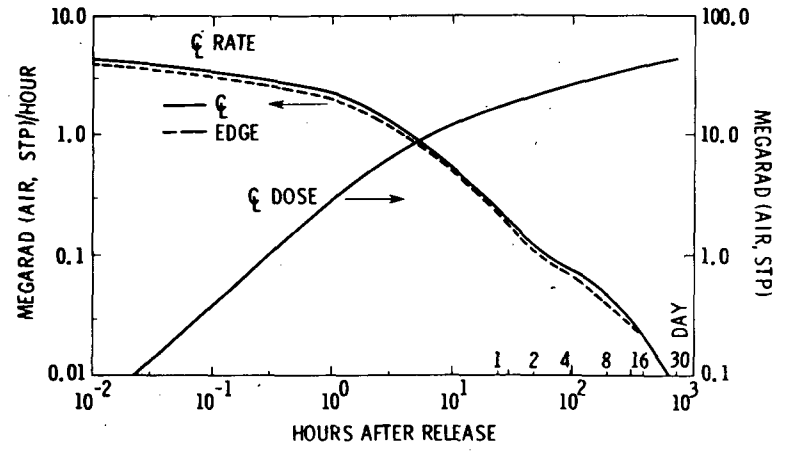

Figure 2.8 Gamma-Ray Dose/Dose Rate vs Elapsed Time From Release - Specifically Combined Airborne, Plateout, and Waterborne Sources

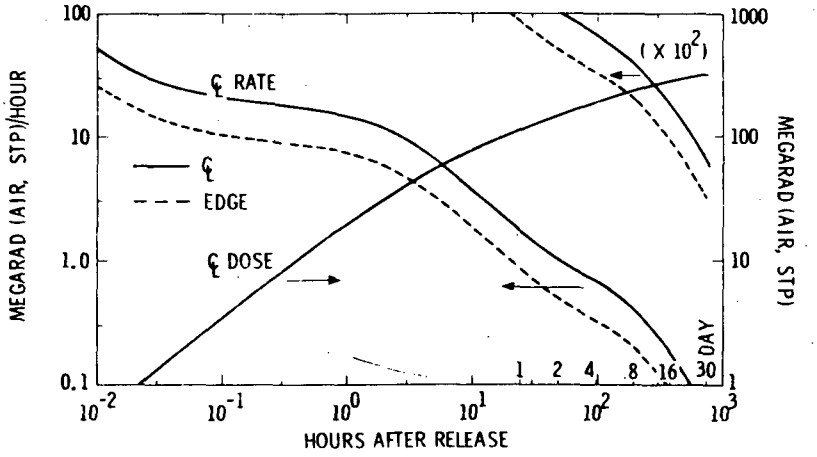

Figure 2.9 Beta Dose/Dose Rate vs Elapsed Time From Release - Airborne Source

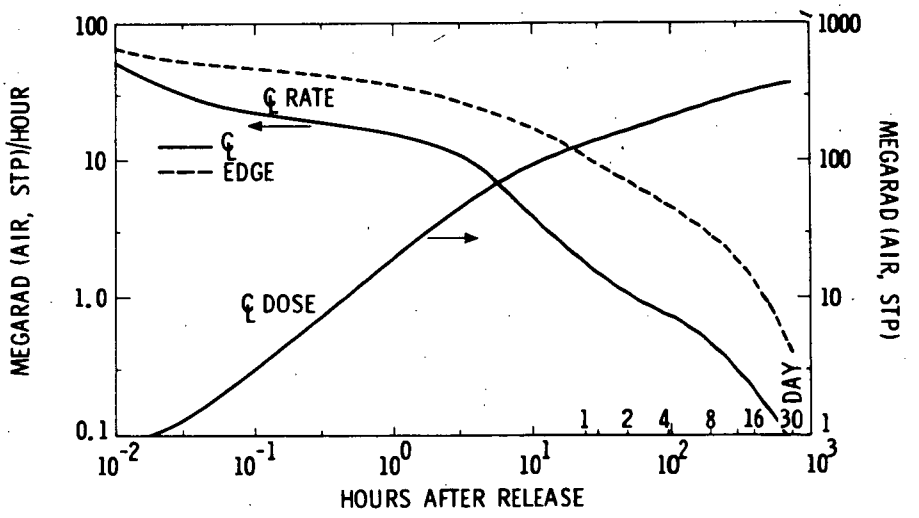

Figure 2.10 Beta Dose/Dose Rate vs Elapsed Time From Release - Specifically Combined Airborne, Plateout, and Waterborne Sources

2.5 Summary

The significant features of the LOCA-radiation signature definition can be summarized as follows:

- A (formal) definition of expectable magnitudes of the gamma and beta dose and rate for a typical containment, using the applicable Regulatory Guides. These values are further segregated according to their spatial dependence as water-borne, airborne, and plate-out sources. The implications of the spatial dependence may be significant in radiation qualification testing, and should at least be a consideration.

- A formal recognition that the beta dose and rate is significantly greater than the corresponding gamma values. Compared to the gamma contribution, betas have been shown to contribute perhaps seven times

more dose (to 30 d) and to have correspondingly greater dose rates. Both measures of radiation are very significant in radiation qualification testing.

- A definition of the LOCA-radiation sources energy spectra as a function of time following the hypothesized releases. Both the gamma and beta spectra exhibit a changing energy dependence with time. For mono- or fixed-energy simulators, the changing spectra cannot be followed. While not a clearly important test parameter, this must be a consideration in testing and will be a consideration in evaluating the adequacy of simulators. The resolved energy spectra also demonstrate an apparent sensitivity to the assumed nuclide fractionation which could be an important feature if a "new" LOCA source term were hypothesized.

- While sensitive to the assumed nuclide fractionation selected, the energy-release rates and spectra are not strongly influenced by reactor-operating parameters, such as fuel composition, power level, duration of operation, and treatment of progeny.

3. Comparative Calculations of Exposed Organics' Response to Simulator and LOCA Radiation

3.1 Depth-Dose and Charge Deposition

In an effort to evaluate the performance of simulators compared to the LOCA sources, a series of calculations of energy deposition in a modeled electric-power cable were carried out;[15] the full report is attached as Appendix A. The model used for the calculations consisted of a solid copper conductor surrounded by an elastomeric insulator (ethylene-propylene rubber) and jacket (Hypalon). Using a coupled photon-electron transport technique based on Monte Carlo methods, the energy deposition (and charge deposition) as a function of radius in the cable was calculated for the LOCA sources, ^{60}Co, and ^{137}Cs. The dimensions and materials selected as the modeled cable may be considered in the range of typical cables, but not exactly like any one manufacturer's type in particular. Similarly, the significance is not as an electrical cable, but as an exposed organic material specimen; slightly different elastomeric materials (but composed basically of CH_2) would not be expected to have much effect on the results, nor would small changes in dimensions be expected to change the conclusions.

The calculations also take advantage of the interesting spectral features of the LOCA radiation signatures. In order to establish bounds, the depth-dose calculations were limited to the extremes of the hardest spectra (1 min) and the softest spectra (4 d) (see Figures 2.4 through 2.6). Included in the various parametric calculations were effects of water thickness for waterborne beta sources, effects of an intervening steel test chamber, effects of 70-psig steam versus dry air as a surrounding medium, comparison brute-force calculations of distributed airborne sources, and the like.

Figures 3.1 through 3.4 illustrate various Source 1 depth-dose calculations as well as comparison simulator results. For scaling

purposes, note that the doses can be expressed per unit incident fluence. Since the surface area of a 10-m segment of the model cable is 7102.5 cm^2, one particle per 10-m segment represents a fluence of 1.480×10^{-4} particles/cm^2. To scale the depth-dose results presented here to a specified particle fluence (ϕ), one multiplies the doses by $\phi/1.408 \times 10^{-4}$. For example, to determine the dose for an incident fluence on the cable of 10 photons/cm^2, multiply by $10/1.408 \times 10^{-4} = 71{,}025$.

Figures 3.5 and 3.6 show selected depth-dose calculations for Source 2; these can be compared directly with Figures 3.3 and 3.4, respectively.

Another potential damage mechanism is charge buildup, illustrated in Table 3.1. Net charge deposition is defined as the number of electrons entering a zone in excess of those leaving a zone. Thus, a positive value for the net number of electrons deposited produces a net negative charge in that region. Conversely, a negative value of electrons deposited results in a positive charge. Charge deposition is to be interpreted as the instantaneous charge deposited for the various identified fission product sources. No mechanisms for leakage or other forms of dispersal of the charges have been included. The gamma-ray sources (including ^{60}Co) consistently produce a positive charge on the outer layer of the jacket (Hypalon), but on the interior of the cable no regular pattern is apparent. The beta sources, on the other hand, produce a much larger negative charge on the outermost region of the cable which falls off with decreasing radius. A much more regular behavior is observed in the copper regions. For the case of the cable surrounded by water, the charge buildup is about two orders of magnitude smaller. In a combined beta-gamma radiation field, there will be some compensation of the opposite-sign charge depositions.

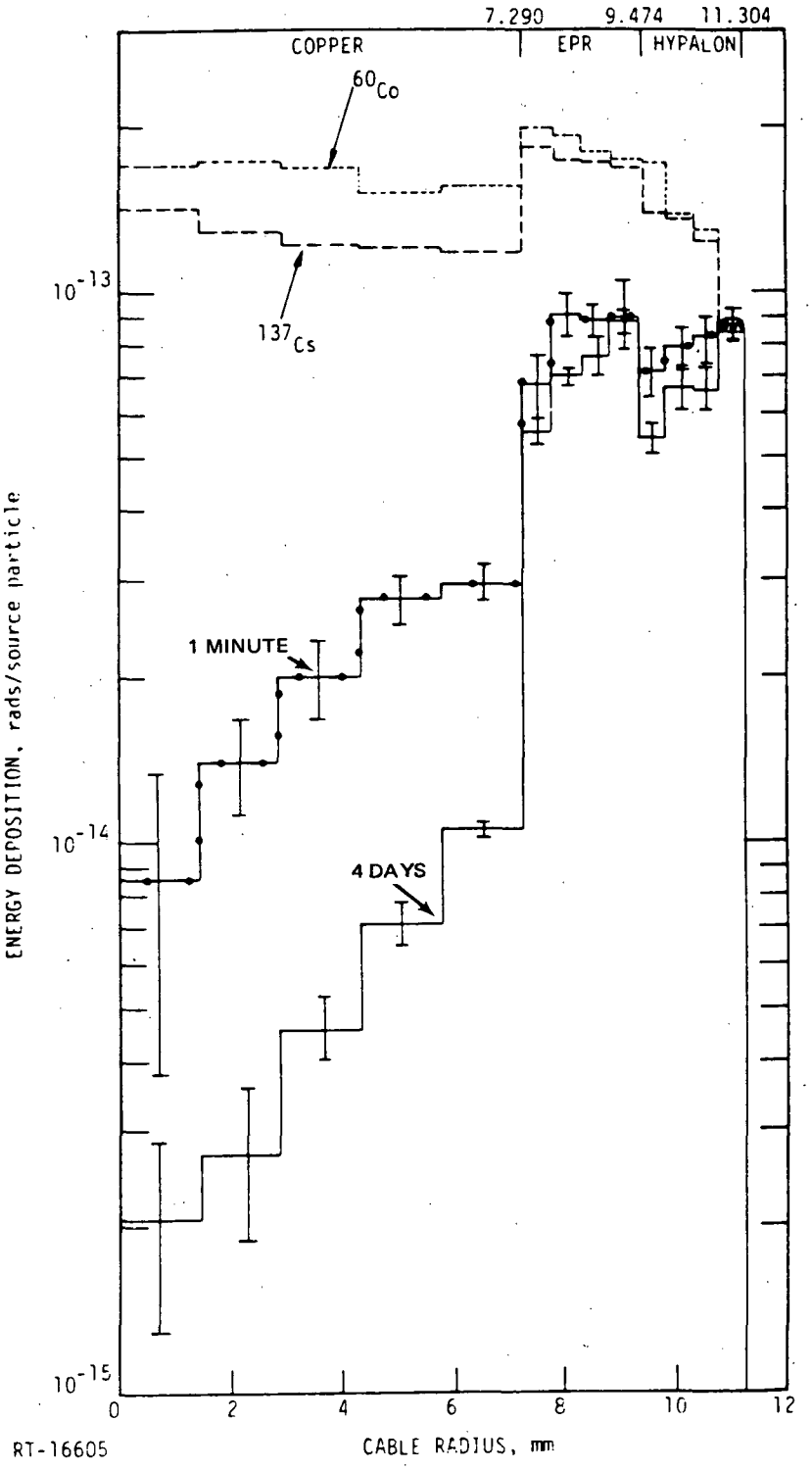

Figure 3.1 Dose vs Penetration Depth - ^{60}Co, ^{137}Cs, and Source 1 (Airborne) Gamma Rays Onto Typical Cable Configuration. The isotopic source results have been normalized at the outer zone. (from Reference 15)

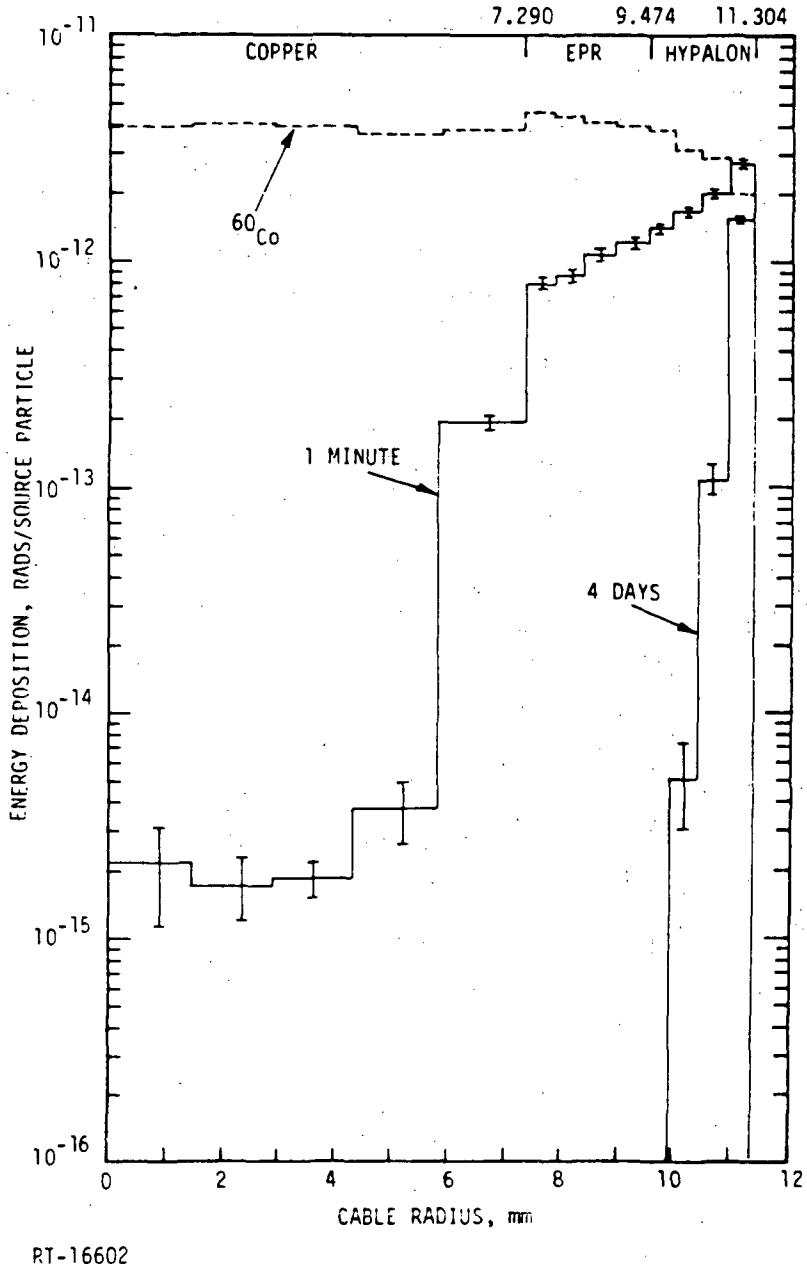

Figure 3.2 Dose vs Penetration Depth - ^{60}Co and Source 1 (Airborne) Betas Onto Typical Cable Configuration. The isotopic source results have been normalized at the outer zone. (from Reference 15)

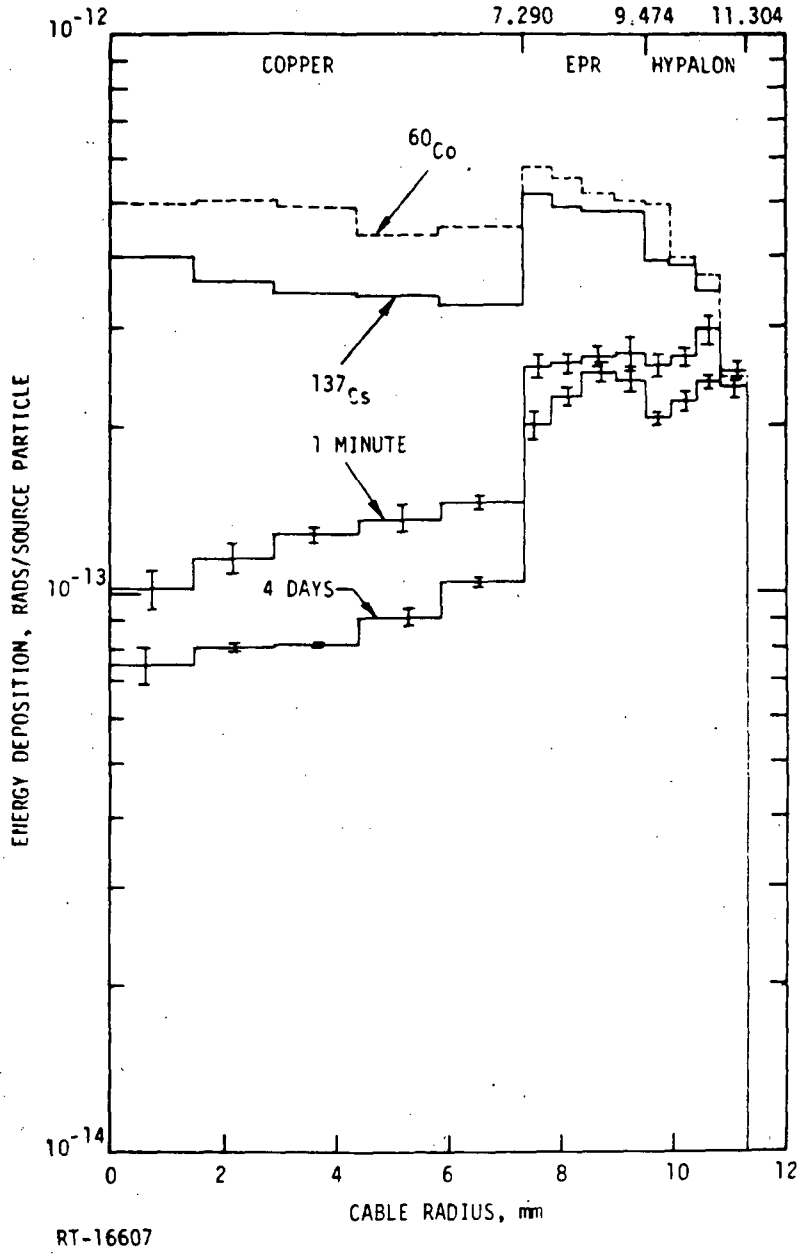

Figure 3.3 Dose vs Penetration Depth - ^{60}Co, ^{137}Cs, and Source 1 (Plateout) Gamma Rays Onto Typical Cable Configuration. The isotopic source results have been normalized at the outer zone. (from Reference 15)

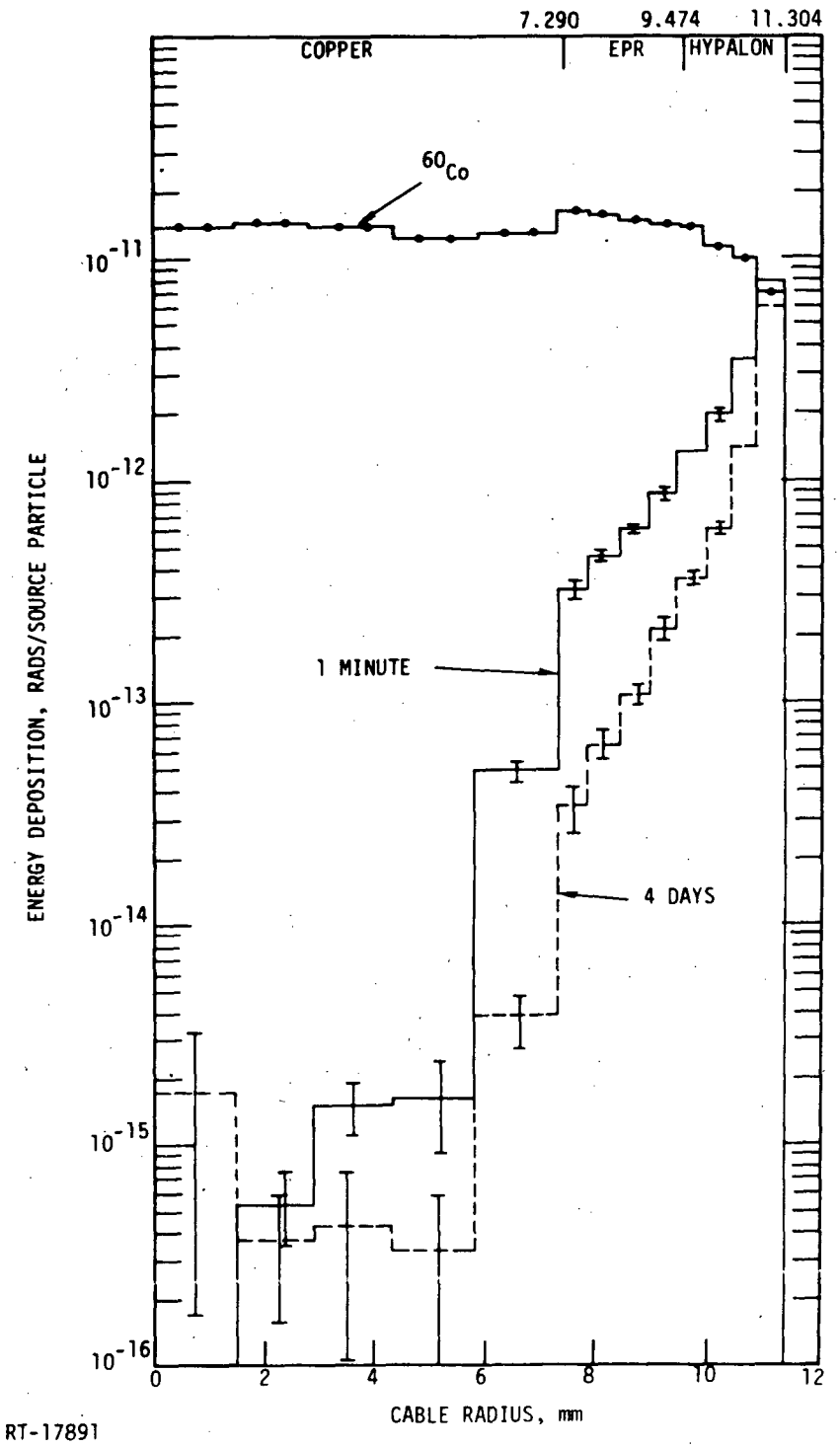

Figure 3.4 Dose vs Penetration Depth - ^{60}Co and Source 1 (Plateout) Betas Onto Typical Cable Configuration. The isotopic source results have been normalized at the outer zone. (from Reference 15)

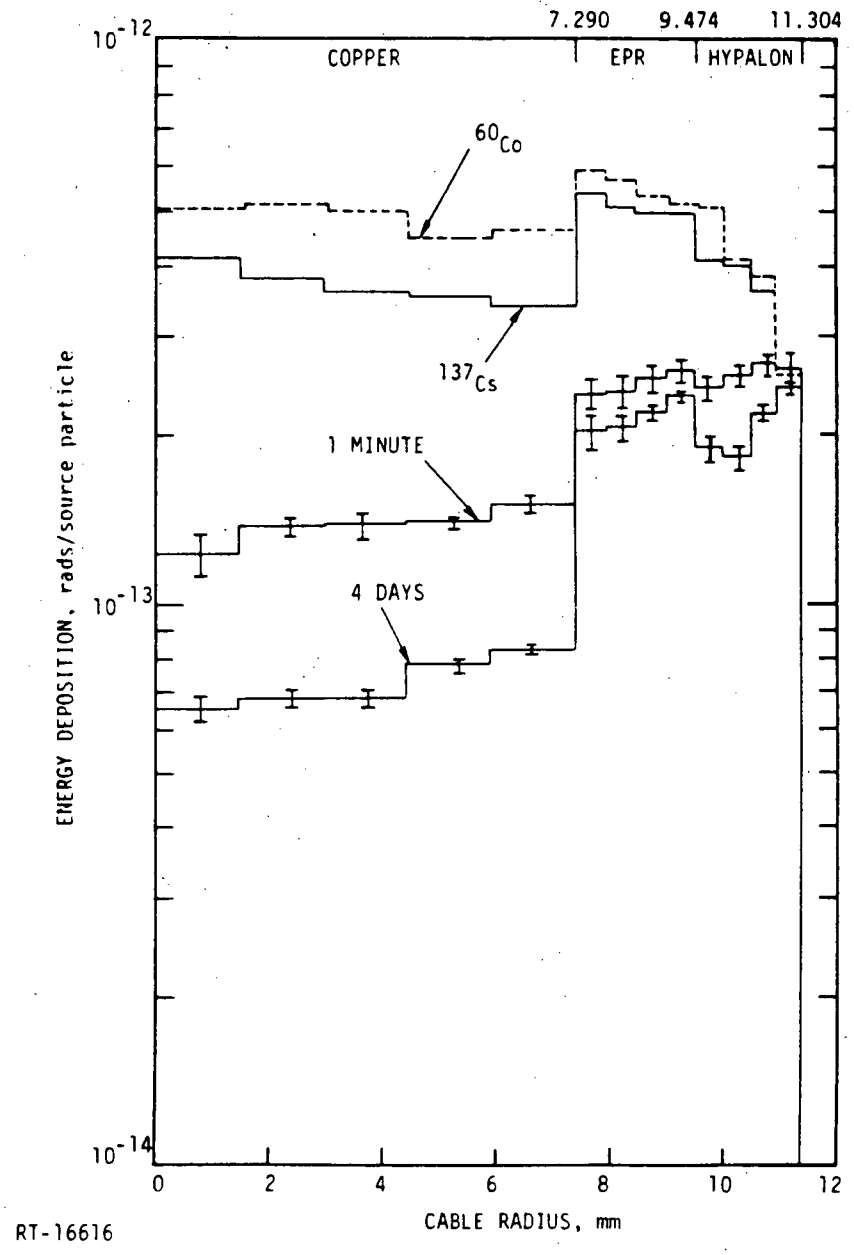

Figure 3.5 Dose vs Penetration Depth - ^{60}Co, ^{137}Cs, and Source 2 (Plateout) Gamma Rays Onto Typical Cable Configuration. The isotopic source results have been normalized at the outer zone. (from Reference 15)

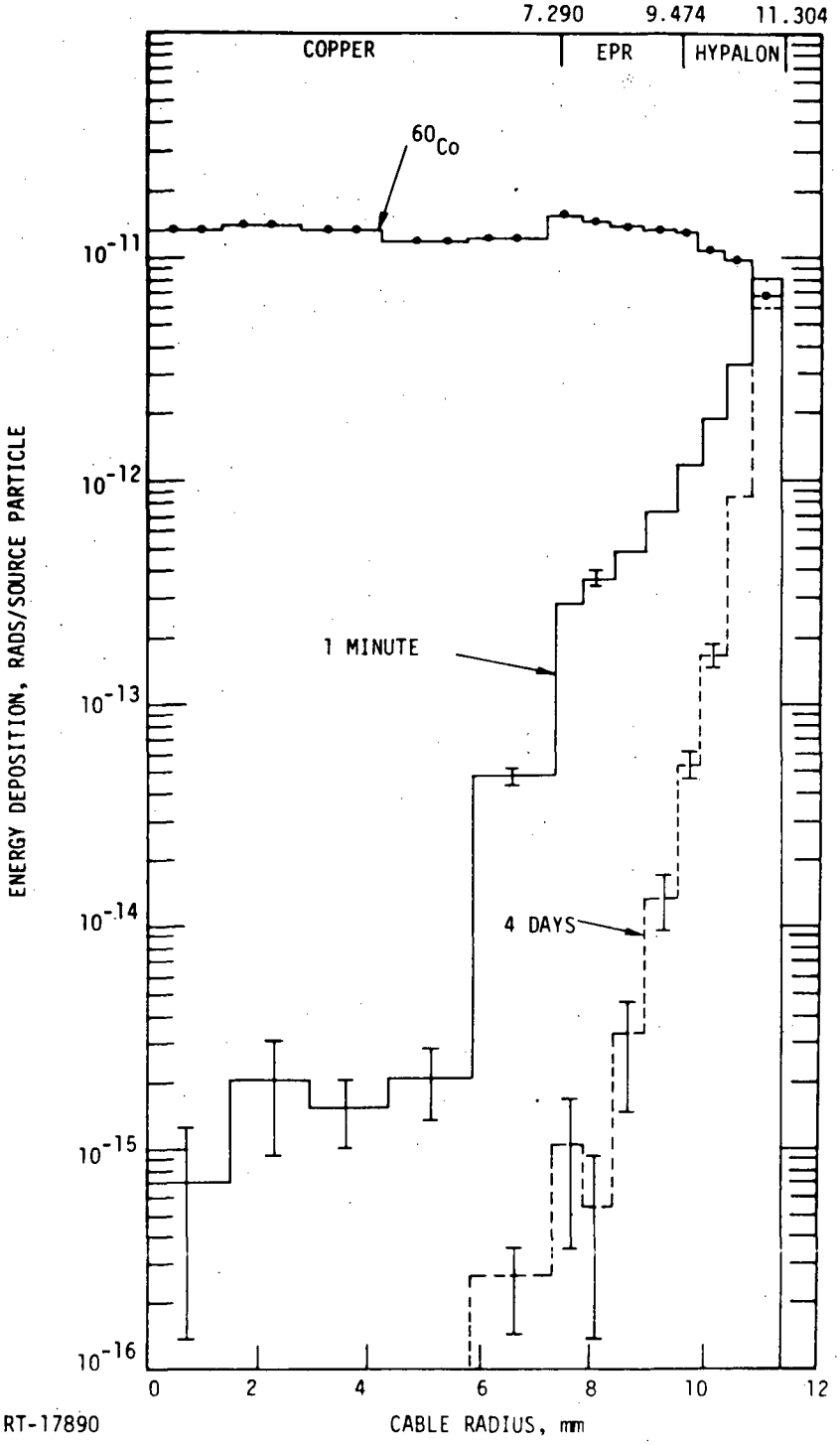

Figure 3.6 Dose vs Penetration Depth - ^{60}Co and Source 2 (Plateout) Betas Onto Typical Cable Configuration. The isotopic source results have been normalized at the outer zone. (from Reference 15)

TABLE 3.1

Charge Deposition in the Cable Configuration
(from Reference 15)

Net Electrons Deposited per 10^3 Source Gamma Rays Incident on a 10^3 cm Length of Cable

Material	Zone Outer Radius (mm)	^{60}Co	Airborne				Plate-Out				Waterborne			
			Source 1		Source 2		Source 1		Source 2		Source 1		Source 2	
			1 min	4 days	1 min	4 days	1 min	4 days	1 min	4 days	1 min	4 days	1 min	4 days
Hypalon	11.304	-5.10	-1.05	-0.30	-1.70	-0.45	-9.15	-8.15	-8.15	-5.00	-0.95	-0.85	-1.60	-0.75
"	10.847	-2.35	-0.25	0.10	-0.80	0.15	-0.55	0.25	-1.95	-0.80	-0.40	-0.15	0.35	0.05
"	10.390	0.45	-0.20	-0.05	0.20	-0.05	1.25	0.50	0.15	-0.35	0.60	0.20	-0.15	0.15
"	9.932	0.70	-0.60	0.30	0.35	0.15	0.25	0.80	-0.90	1.55	-0.30	0.10	0.15	-0.20
EPR	9.474	0.10	-0.25	-0.05	-0.10	0.15	-0.65	-1.20	0.75	-1.25	-0.10	0.10	0.25	0.35
"	8.928	-0.35	0.05	-0.25	0.15	-0.15	-1.05	0.75	-0.35	0.90	0.50	-0.10	-0.05	-0.25
"	8.382	-0.30	0.10	0.25	-0.15	-0.20	-1.05	0.25	0.05	-0.70	-0.20	0.05	-0.25	-0.10
"	7.836	0	0.30	-0.10	-0.40	0	0.95	-0.60	0.35	-0.35	-0.25	-0.25	-0.20	0.10
Copper	7.290	-0.60	0.10	0.10	0.25	0.20	0.20	0	-0.25	0.45	-0.15	-0.15	0.25	0.05
"	5.832	-0.25	-0.15	-0.10	-0.10	-0.20	0.55	0.60	0.60	0.30	0.35	0.10	0.10	0.05
"	4.374	1.50	-0.05	0.05	-0.05	0.05	-0.30	-0.30	0.10	-0.10	-0.25	-0.05	0	-0.05
"	2.916	-0.30	0.10	-0.05	0.20	-0.05	0	0.15	-0.40	0	0.05	0.05	0.05	0
"	1.458	-0.15	0.05	0	-0.05	0.05	0	-0.05	0.25	0	-0.05	0	0	0

Net Electrons Deposited per 10^3 Source Betas Incident on a 10^3 cm Length of Cable

Hypalon	11.304	-5.10	60.90	175.80	75.60	169.80	350.20	363.20	357.30	535.80	2.94	2.01	2.76	8.09
"	10.847	-2.35	29.00	10.70	29.30	11.90	114.50	116.70	119.60	65.50	1.34	0.40	0.88	1.08
"	10.390	0.45	22.60	0.60	22.70	2.00	60.50	61.33	56.50	11.50	0.84	0.15	0.40	0.27
"	9.932	0.70	17.30	0	17.10	0.20	34.90	39.00	34.00	3.40	0.46	0.05	0.24	0.02
EPR	9.474	0.10	14.20	0	14.90	0.10	19.80	17.33	17.90	0.60	0.33	0.06	0.11	0.01
"	8.928	-0.35	12.30	0	9.80	0	9.70	12.00	9.30	0.20	0.19	-0.01	0.03	0.01
"	8.382	-0.30	9.10	0	7.20	0	7.10	4.33	7.70	-0.10	0.11	0.02	0.03	0
"	7.836	0	8.20	0	5.20	0	4.80	3.33	3.20	0.10	0.13	0.02	0.02	0
Copper	7.290	-0.60	26.40	0	16.10	0	9.10	10.33	8.20	0	0.26	0	0.01	0
"	5.832	-0.25	0.50	0	0	0	0.10	0	0.10	0	0	0	0	0
"	4.374	1.50	0	0	0	0	0.10	0	0	0	0	0	0	0
"	2.916	-0.30	0	0	0	0	-0.10	0	0	0	0	0	0	0
"	1.458	-0.15	0	0	0	0	0	0	0	0	0	0	0	0

3.2 Summary

The interpretation of the depth-dose calculations in terms of establishing simulator adequacy is not straightforward. Reasonable matching of the dose profile in the cable by the simulator source would be sufficient to guarantee its adequacy. However, a failure to produce equivalent depth versus dose does not necessarily mean that the simulator is inadequate; it is necessary to determine the mechanism of failure of the cable in the LOCA radiation field, and then ascertain whether or not this damage mechanism is sufficiently stressed by the simulator. A plausible argument is that the ^{60}Co or ^{137}Cs sources produce a more conservative situation since, if they are normalized at the surface, they always produce more dose in the inner regions of the cable than do the LOCA sources. Thus, according to this argument, if the cable survives the ^{60}Co irradiation test, it will survive the LOCA radiation environment since the latter will deposit a smaller dose in the interior. In order for this argument to be valid it is necessary that the degradation of the cable be directly related to total dose. It is not clear that the problem is as simple as that. For example, charge buildup and dielectric breakdown are dependent upon the dose gradient in the cable. Other failures such as heating and gas evolution from the breakdown of polymeric materials and differential mechanical stress could also depend upon the dose gradient.

4. Damage Mechanisms Identified and Prioritized

4.1 Concerns in Adequacy Evaluations

As indicated previously, simulator adequacy is assured if its radiation signature adequately matches the LOCA-radiation signature. However, the previous discussion in Chapters 2 and 3 indicates, in general, that is not the case. Finally, the true indicator of adequacy is that the damage mechanisms and damage be duplicated in the test item.

To identify these radiation damage mechanisms, the staff of the IRT Corporation was asked to consider the possible mechanisms and to discuss their relative importance; their full report[16] is attached as Appendix B. Concurrently, Sandia staff, expert in radiation effects in polymers, separately evaluated the possible mechanisms and critiqued the IRT report.

Before proceeding to the discussion of damage mechanisms, it is important to narrow attention to the pertinent features of radiation qualification and simulator adequacy.

First, it will be a priori concluded that gamma simulators are inherently adequate (dose rate will be discussed later) to simulate the gamma accident and the ambient-radiation signature, when taken as a separate entity. The various figures in Chapter 3 illustrate the nearly identical relative depth-dose profiles on which this conclusion is based. Thus, for the ambient (i.e., aging) environments when only gammas are present,[18,19] gamma simulators are adequate; aging environments will not be further discussed in this report. Similarly, the gamma-accident signature is adequately addressed using gamma simulators.

Second, just because gamma simulators are adequate for the gamma accident-radiation signature taken as a separate environment, that does

not endorse or justify the typical sequential qualification program where the radiation (accident and ambient) profile is separately applied. Discussion of possible combined-environments effects will be included in succeeding sections; an example may be radiation heating added to the already elevated temperature from the direct LOCA heat releases.

Third, even when taken singly, adequate gamma-profile simulation must include both a spectral and a magnitude consideration. The data, shown in Chapter 3, indicates that spectra are reasonably accommodated. Some other data[20] demonstrate dose-rate effects in certain elastomeric materials, but these would seem to be relatively insignificant so long as the simulator rate is within an order of magnitude or so of the rate to be simulated. (With justifying data, the range of dose rate may be significantly extendable, which is imperative for accelerated aging techniques.)

Fourth, concern for adequate beta simulation can be reduced to concern for induced heating (and/or heating rate) if beta penetrability is not a concern. That is to say, for "shielded" equipment, beta radiation is adequately simulated by adequate heating of the "shielded" equipment by any radiation simulator (or other heating-simulator device). (But consideration should be given to secondary radiations, bremsstrahlung, from beta interactions with materials.)

Very simplistically then, the adequacy of a radiation simulator hinges on the beta-radiation damage-simulation adequacy.

4.2 IRT Study Summary[16]

The IRT study identified three major damage mechanisms which are generally related to radiation damage:

- Charge buildup, discharge and electrical changes
- Temperature changes due to dose rate
- Mechanical/chemical change due to total dose.

In discussing the effects of these mechanisms, the information in Figure 4.1 served as bases. Further, it was assumed that the surrounding environment was at an elevated temperature (143°C, approximately 60 psia)

somewhat typical of the LOCA condition. The summary discussion is presented here; additional detail is supplied in the subsequent chapters.

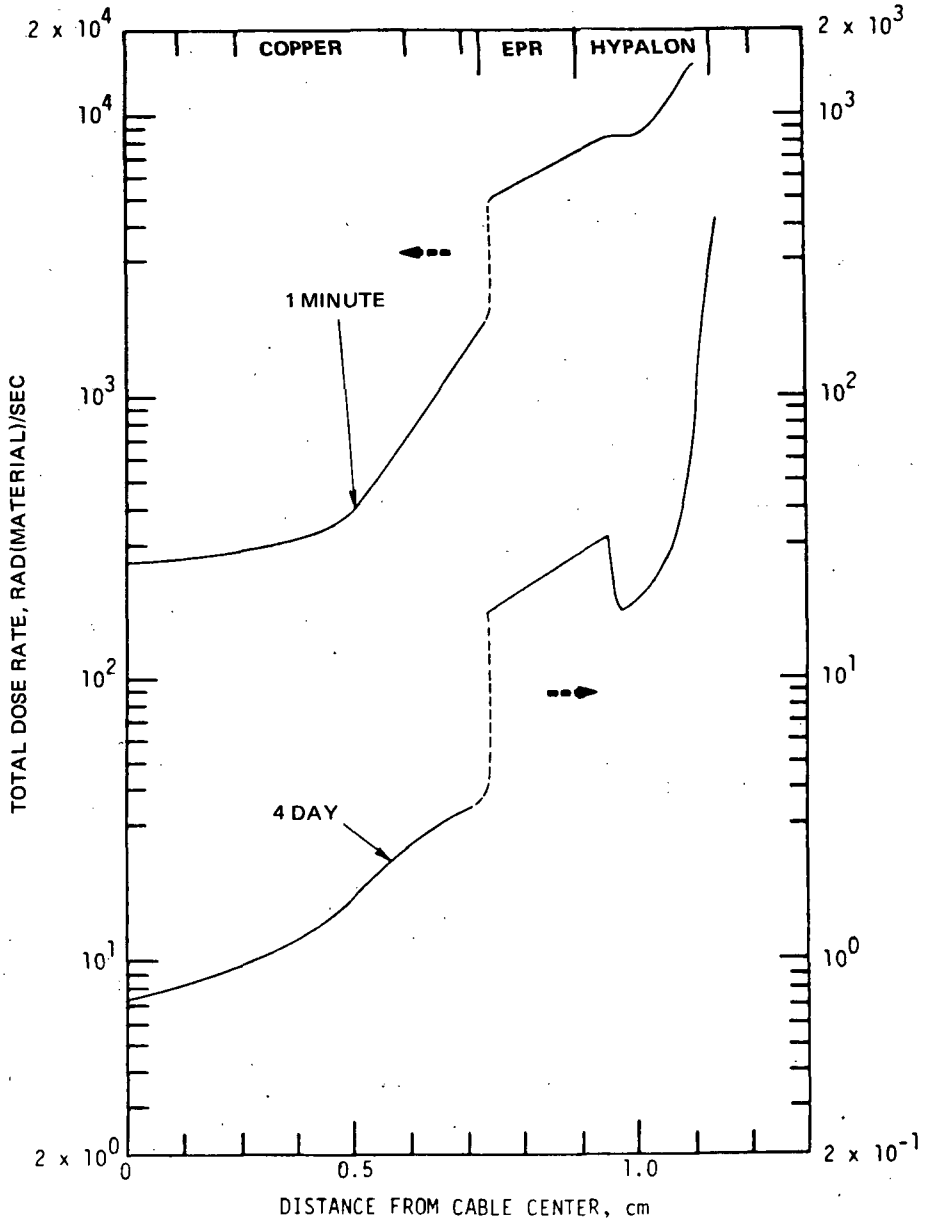

Figure 4.1. Dose Rate vs Penetration Depth - Combined LOCA Radiation Environment, 1-min and 4-d Following LOCA

"The trapped charge in the insulator is largely a consequence of the nonuniform dose deposited in the cable. The mechanism that applies here is that the secondary emission leaving a volume element is not balanced by secondary emission from adjacent points because the adjacent points are not receiving the same primary radiation. The gamma-source simulators do not show such a strong attenuation as does the true LOCA source so they will not properly simulate the trapped charge and any resultant noise spikes. The amplitude of noise pulses built up by breakdown in the cable depends almost completely on the exact details of the cable termination. If the termination is either a small resistive load or a large capacitive load, then the noise spikes will not be large. However, because radiation-induced leakage currents are judged to be inconsequential, we suggest that the LOCA environment is adequately simulated by ^{60}Co as long as average doses are matched.

"The ^{60}Co and ^{137}Cs simulation-radiation sources do not reproduce the true LOCA attenuation into the cable so that the temperature profiles established by these simulators will not accurately reproduce the true LOCA profiles. In particular, the simulation fields are not attenuated in the cable as is the true LOCA spectrum. Thus, the simulator will deposit too much power in the copper and inner portions of the Hypalon compared with the power deposited into the outer surface. If the simulation is performed so that the total doses are equivalent, then the simulator will exaggerate the heating of the inner insulator region. This is the inverse of the case of electrical effects generated by trapped charges where the simulator understresses the effect.

"The most serious problems that will occur with the cable are chemical and mechanical deterioration which are expected to occur after a few hours to a day in LOCA environment. Impact strength and elongation changes by 50% within 10 h. In order to properly evaluate these effects, the expected vibrational and bending stresses should be included in the specification of the LOCA environment."

4.3 Sandia Study Summary[17]

The work of Harrah[17] identified one other potential damage (or failure) mechanism that is a result of the strong radial dependence of the depth-dose profile. The mechanism involves the shrinkage of a material relative to its remaining elongation and is illustrated in Figure 4.2. If the surface of an elastomer suffers shrinkage on the order of the remaining elongation, it is plausible that surface crazing or cracking could occur. If the dose (and elongation and shrinkage) are nearly equal across the material, it is unlikely that cracking would occur because of the absence of a differential stress; hence, the mechanism is a direct result of a steep depth-dose profile in the material. (Further complications could occur as illustrated by the temperature dependence in the figure.)

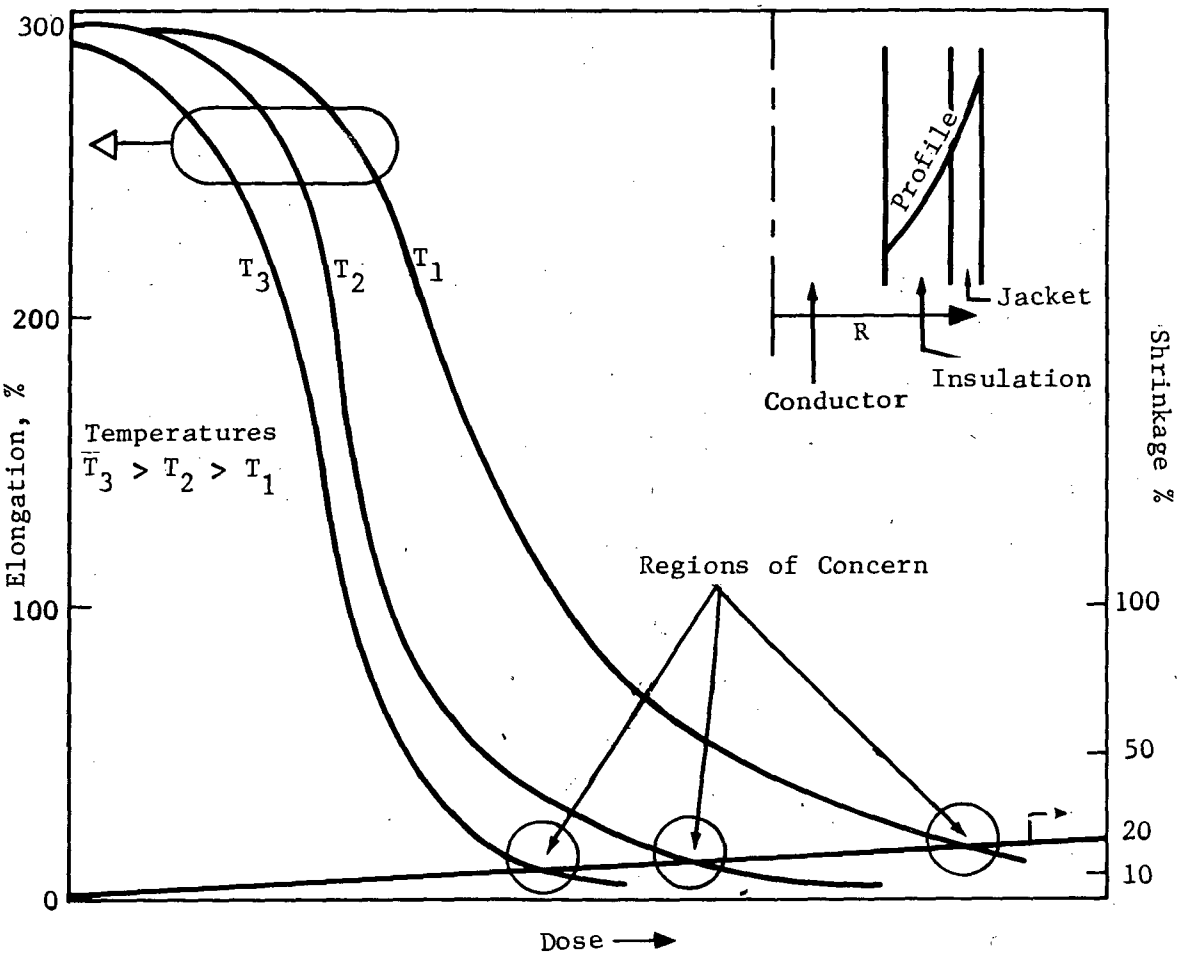

Figure 4.2 Material Elongation/Shrinkage Change vs Integrated Dose - Illustrative Example for an Organic Material

4.4 Relative Importance of Damage Mechanisms Relative to Simulator Adequacy

All four mechanisms will be discussed in Chapters 5 through 8, but they can be immediately assessed as to their relative importance.

Charged particle distribution is a direct function of depth-dose profiles and beta radiation. Charge breakdown and noise pulses depend specifically on the elastomeric material and/or the cable terminations. Generalized conclusions may be difficult to obtain.

Temperature changes in material may be sufficient to be a concern. Here the beta radiation can be viewed as a total heat source, since the depth-dose features are relatively unimportant. In the same regard, the simulator may be relatively unimportant as long as the heat source is duplicated (where important).

Total chemical and mechanical changes in materials are not a strong function of the radiation source as long as the total damage is duplicated as appropriate.

The singularly important mechanism may be the differential stress caused by the actual radiation environments that can not, in general, be duplicated by existing gamma-radiation simulators. Chapter 8 will examine the available supporting data and estimate the importance of the damage mechanism and of its accurate simulation.

4.5 Other Damage Mechanisms

It is impossible to be inclusive of all possible damage mechanisms or to suggest adequate simulation techniques for all occasions. Some of these mechanisms are a result of the specific functioning and design of the equipment. For example, electronic assemblies may be more or less susceptible to the radiation signatures by their design or choice of components. It is not possible to examine all specifics in this study.

Other potential damage mechanisms have also been suggested. Secondary emissions induced by beta interactions may be an important consideration even when the primary betas do not penetrate. Here an example might be the bremsstrahlung superimposed on the internal sensing/transmitting elements of a transmitter when the primary betas are stopped by the metal case of the housing. Certainly this added contribution (theoretical energy conversion can range to 10 percent or more) must be accounted for, but it might be logical to account for this by summing with the gamma-accident rate and dose.

Surface (and bulk) conductivity changes might also be important in some practical application. But again, the location of such sensitive equipment would be internal to a housing (in general) and not exposed to primary beta radiation. Thus while the effect may be real, simulation is not first-order dependent on the beta component.

The purpose of this section is to recognize that other unique or specific damage mechanisms or simulation considerations exist. Others, not specifically identified in this report, probably exist as well. That is just one reason that it is impossible to endorse any simulator for every application. Simulators must be intelligently used in an overall qualification program.

5. Radiation-Induced Electrical Signals in Cables

5.1 Background

Radiation-induced signals in cables are primarily the result of ionization-induced conductivity changes in the cable insulation and the ultimate release of trapped charge in the insulation material. Ionization of atoms in the insulation will occur when one or more orbital electrons is removed, leaving a positively charged ion and one or more free electrons. Ionization may be produced in the case of a LOCA-radiation environment through either source-electron/target-electron collisions or photon-electron collisions and subsequent secondary-electron/target-electron interactions. In the simulator environment, ionization most likely will occur through the source-photon/target-electron, secondary-electron/target-electron, processes. Significant charge trapping is the result, generally, of nonuniform energy dissipation (either photon or electron) in an insulating material.

Simulation of the LOCA-radiation environment is complicated by the presence of a large electron component not usually present in typical isotopic irradiation facilities. It is generally accurate to state that the presence of a large electron component in the radiation field can result in charge-/energy-deposition profiles in materials whose magnitude is extremely dependent on penetration depth into the material. Herein, apparently, lies the main concern about the adequacy of isotopic simulators to reproduce the electrical effects of a LOCA-radiation exposure.

The typical LOCA sources expected, presented in Table 2.1 and based on conditions set forth in Reference 9, are given again in Table 5.1. Composition and quantity of radiation emitters potentially available for release is dependent on the reactor-operating history and elapsed time from the hypothesized excursion. Regardless of the nature of the excursion, once the reactor primary system has been breached, fission

products available for release are considered to be instantaneously released and uniformly dispersed. A consequence of uniform material dispersion is that any source "self-absorption" is minimized. This means that the preponderence of electrons emitted in fission-product decay and normally absorbed in the fuel and cladding must be added to the decay-product gamma-source term for purposes of estimating damage to safety systems and components.

TABLE 5.1

LOCA Sources Specification (Reference 9)

Source 1 (Containment heat-removal systems, etc)	Airborne	100% noble gases, 25% iodines
	Plateout	25% iodines, 1% solids
	Waterborne	50% halogens, 1% solids
Source 2 (Other safety-related electrical systems)	Airborne	10% noble gases (except ^{85}Kr) 30% ^{85}Kr, 5% iodines
	Plateout	5% iodines
	Waterborne	10% halogens

The LOCA electron and photon spectra are varying functions with time; however, it was demonstrated in Chapter 2 that spectra existing at about 1 min and 4 d reasonably bracket the hardest and softest spectra associated with a LOCA source. In Table 5.2 are listed average and peak energies for both electron and photon spectra at both 1 min and 4 d following a postulated LOCA.[5] Depending on the elapsed time from the onset of a LOCA, electron to photon dose ratio (rad/rad) is on the order of 10/1 to 100/1.

Many gamma-irradiation facilities doing materials testing, instrument calibration, basic research, and the like, use ^{60}Co. Therefore, for purposes of comparison, we will assume a typical (LOCA) simulator would be ^{60}Co configured in the conventional fashion; i.e., some sort of an array

of source ^{60}Co pencils. As is well known, ^{60}Co decays by beta emission which is in coincidence with a cascade of photons at 1.17 and 1.33 MeV. End-point energy of the decay-beta particle is about 0.3 MeV and, thus, will not contribute to the radiation field external to the source pencils.

TABLE 5.2

Source 1 Airborne Spectra Parameters
(Reference 5)

Elapsed Time	E (MeV)	E_{max} (MeV)
Gamma Spectra		
1 min	0.72	5.0
4 d	0.16	0.75
Beta Spectra		
1 min	0.75	3.4
4 d	0.17	0.60

The electron spectrum generated by scattering of photons in a medium may be estimated on the basis of photon cross sections for the medium (Reference 21). In Table 5.3 are tabulated electron and photon spectra for ^{60}Co and a medium of CH_2 composition. The photon data are uncollided values; the rationale is that scattering in the source and medium would have little effect on line broadening of the two cobalt (gamma) lines.

Examination of Tables 5.2 and 5.3 shows that the ^{60}Co spectra, in CH_2, are comparable to the LOCA 1-min spectra but are considerably harder than the LOCA 4-d spectra. In the range of energies listed in Tables 5.2 and 5.3, energy loss by electrons will be through ionization and excitation; hence, energy-deposition mechanism by both LOCA and the isotopic simulators are identical. In the case of the isotopic simulator, once a state of electron equilibrium in the scattering/absorbing medium is established, energy loss by recoil electrons through ionization and excitation processes will be compensated for by photon energy loss to electrons

by Compton scattering. The range[22] of a maximum energy ^{60}Co recoil electron in CH_2 is about 0.465 g/cm^2, approximately equal to the distance required to establish electron equilibrium in the CH_2. The thickness of insulation and jacket on a typical power cable (of interest here) just happens to be approximately 0.450 g/cm^2 which is about equal to the range of maximum energy recoil electron in CH_2 and also is the thickness of material necessary to establish a characteristic electron spectrum. At this penetration depth, free electron density and electron trapping become somewhat constant with deeper penetration. As material thickness is increased, energy deposition also increases until a state of electron equilibrium is achieved. At this point energy deposition/density/trapping versus depth of penetration should remain constant provided the incident photon beam remains essentially unattenuated. Thus, the energy/charge profile in the typical cable insulation and sheath exposed to the ^{60}Co isotopic source should be a monotone, increasing function with penetration.

TABLE 5.3

^{60}Co Spectra - Medium CH_2

Gamma Spectrum	
$\bar{E}$ (MeV)	E_{max} (MeV)
1.25	1.33
Electron Spectrum	
0.58 MeV	1.12 MeV

The LOCA source energy/charge depositions differ from the isotope deposition profiles in that a state of electronic equilibrium is never achieved. For the 1-min source, maximum electron energy is about 5 MeV and the ratio of electron to photon power is in the range of (10-100)/1. Since the range of the electrons approaches 2.4 g/cm^2, this means primary

(source) electrons dominate energy/charge deposition and, since no internal (material) source of high energy secondaries is available, charge/energy deposition is expected to decrease monotonically with increasing penetration. The 4-d source is characterized by both lower energy photon and electron spectra. The range[22] of the maximum energy electron is about 0.21 g/cm^2; hence, the primary electron component should be dissipated in the outermost cable sheath. The relatively soft primary photon spectrum assures that attentuation of the photon beam will occur with penetration into the cable materials. Attenuation of the primary photon (recoil electron) beam along with complete removal of the primary electron beam (in the outer sheath) assures that the general shape of the 4-d deposition profile is similar to but lower in magnitude than the 1-min spectrum.

In summary it may be stated that as far as basic energy transfer mechanisms are concerned, the LOCA spectrum and the ^{60}Co spectrum transfer energy to the test material via the same processes: ionization and excitation. The LOCA sources are always rapidly attentuated with penetration into materials, whereas ^{60}Co exposures will result in minimum attentuation of primary source particles.

To this point we have inferred, inductively, the general shape of the trapped charge and free electron distributions existing in insulating materials exposed to both LOCA and ^{60}Co radiation environments. However, in order to evaluate the severity of radiation-induced signals in cables, accurate estimates of absolute charge deposition along with energy deposition profiles (induced conductivity change is proportional to dose rate) are required. Deposition/charge profiles were calculated[15] using sources listed in Table 5.1 for 1-min and 4-d postrelease times. Additional calculations based on ^{60}Co and ^{137}Cs source terms were also made. The energy/charge deposition profiles were calculated in all instances, using the coupled electron-photon Monte Carlo transport code SANDYL.[23]

Deposition calculation results are presented in Figures 5.1 and 5.2. The results in Figure 5.1 have been normalized on the basis of LOCA electron and photon dose rate calculated by Bonzon.[2] Deposition profile data for ^{60}Co are given in Figure 5.2 for two conditions. In the first

instance, the calculation considers the deposition in a cable configuration under free field conditions and, in the second, deposition in a cable shielded by 1/4-in. steel as might occur during testing in an autoclave chamber. In Table 5.4 the respective charge deposition results are tabulated.

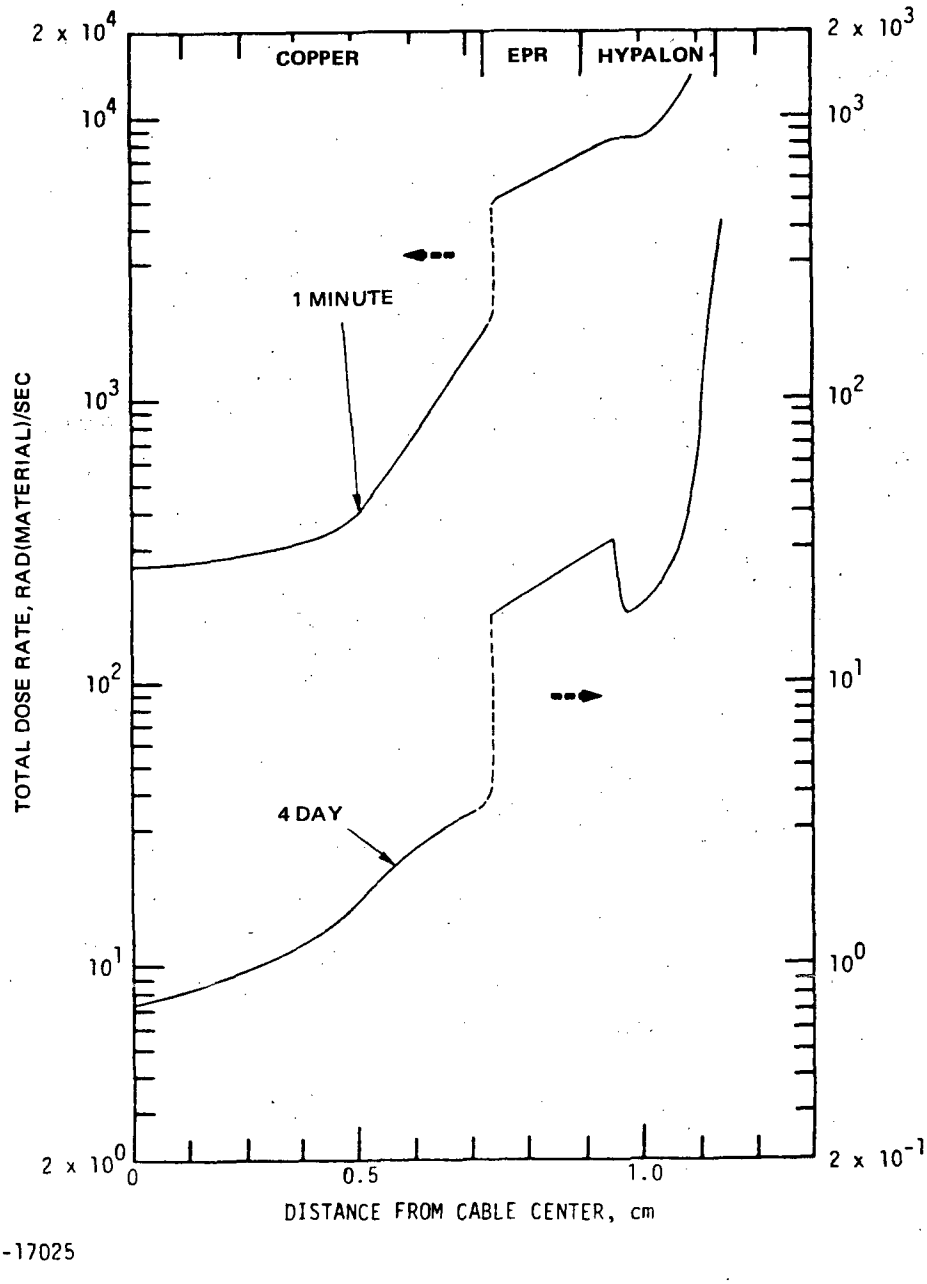

Figure 5.1 Dose Rate vs Penetration Depth - Combined LOCA Radiation Environment, 1-min and 4-d Following LOCA (from Reference 15)

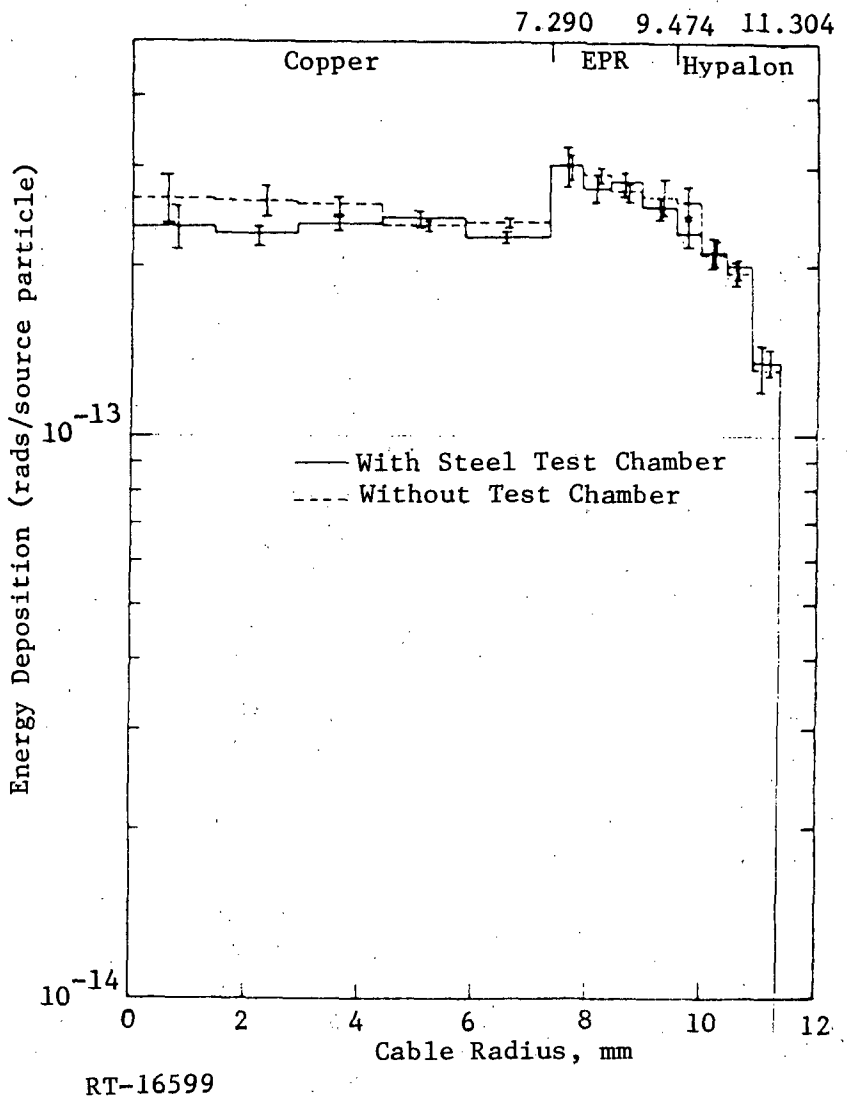

Figure 5.2 Dose vs Penetration Depth - ^{60}Co Onto Typical Cable Configuration, With and Without Intervening Iron Liner (from Reference 15)

TABLE 5.4

Charge Deposition in the Cable Configuration
(from Reference 15)

Net Electrons Deposited per 10^3 Source Gamma Rays Incident on a 10^3 cm Length of Cable

Material	Zone Outer Radius (mm)	^{60}Co	Airborne				Plate-Out				Waterborne			
			Source 1		Source 2		Source 1		Source 2		Source 1		Source 2	
			1 min	4 days	1 min	4 days	1 min	4 days	1 min	4 days	1 min	4 days	1 min	4 days
Hypalon	11.304	-5.10	-1.05	-0.30	-1.70	-0.45	-9.15	-8.15	-8.15	-5.00	-0.95	-0.85	-1.60	-0.75
"	10.847	-2.35	-0.25	0.10	-0.80	0.15	-0.55	0.25	-1.95	-0.80	-0.40	-0.15	0.35	0.05
"	10.390	0.45	-0.20	-0.05	0.20	-0.05	1.25	0.50	0.15	-0.35	0.60	0.20	-0.15	0.15
"	9.932	0.70	-0.60	0.30	0.35	0.15	0.25	0.80	-0.90	1.55	-0.30	0.10	0.15	-0.20
EPR	9.474	0.10	-0.25	-0.05	-0.10	0.15	-0.65	-1.20	0.75	-1.25	-0.10	0.10	0.25	0.35
"	8.928	-0.35	0.05	-0.25	0.15	-0.15	-1.05	0.75	-0.35	0.90	0.50	-0.10	-0.05	-0.25
"	8.382	-0.30	0.10	0.25	-0.15	-0.20	-1.05	0.25	0.05	-0.70	-0.20	0.05	-0.25	-0.10
"	7.836	0	0.30	-0.10	-0.40	0	0.95	-0.60	0.35	-0.35	-0.25	-0.25	-0.20	0.10
Copper	7.290	-0.60	0.10	0.10	0.25	0.20	0.20	0	-0.25	0.45	-0.15	-0.15	0.25	0.05
"	5.832	-0.25	-0.15	-0.10	-0.10	-0.20	0.55	0.60	0.60	0.30	0.35	0.10	0.10	0.05
"	4.374	1.50	-0.05	0.05	-0.05	0.05	-0.30	-0.30	0.10	-0.10	-0.25	-0.05	0	-0.05
"	2.916	-0.30	0.10	-0.05	0.20	-0.05	0	0.15	-0.40	0	0.05	0.05	0.05	0
"	1.458	-0.15	0.05	0	-0.05	0.05	0	-0.05	0.25	0	-0.05	0	0	0
Net Electrons Deposited per 10^3 Source Betas Incident on a 10^3 cm Length of Cable														
Hypalon	11.304	-5.10	60.90	175.80	75.60	169.80	350.20	363.20	357.30	535.80	2.94	2.01	2.76	8.09
"	10.847	-2.35	29.00	10.70	29.30	11.90	114.50	116.70	119.60	65.50	1.34	0.40	0.88	1.08
"	10.390	0.45	22.60	0.60	22.70	2.00	60.50	61.33	56.50	11.50	0.84	0.15	0.40	0.27
"	9.932	0.70	17.30	0	17.10	0.20	34.90	39.00	34.00	3.40	0.46	0.05	0.24	0.02
EPR	9.474	0.10	14.20	0	14.90	0.10	19.80	17.33	17.90	0.60	0.33	0.06	0.11	0.01
"	8.928	-0.35	12.30	0	9.80	0	9.70	12.00	9.30	0.20	0.19	-0.01	0.03	0.01
"	8.382	-0.30	9.10	0	7.20	0	7.10	4.33	7.70	-0.10	0.11	0.02	0.03	0
"	7.836	0	8.20	0	5.20	0	4.80	3.33	3.20	0.10	0.13	0.02	0.02	0
Copper	7.290	-0.60	26.40	0	16.10	0	9.10	10.33	8.20	0	0.26	0	0.01	0
"	5.832	-0.25	0.50	0	0	0	0.10	0	0.10	0	0	0	0	0
"	4.374	1.50	0	0	0	0	0.10	0	0	0	0	0	0	0
"	2.916	-0.30	0	0	0	0	-0.10	0	0	0	0	0	0	0
"	1.458	-0.15	0	0	0	0	0	0	0	0	0	0	0	0

5.2 Radiation-Induced Disturbances

The problem of radiation-induced disturbances in cables was analyzed by IRT.[16] The IRT analyses estimated (a) cable conductivity changes resulting from a LOCA radiation and temperature environment, (b) the consequences of the conductivity change, and (c) the effects of charge trapping in cable insulation.

Dielectric and conductivity calculations were based on the dose rates estimated to be present in the cable as a result of the "1 min" LOCA-radiation environment (Figure 5.1 and Table 5.5). Effects of such conductivity changes were analyzed on the basis of a shunt resistance. The effects of charge trapping (Table 5.4) that were considered were (a) electric field enhancement, (b) possible I^2R dielectric heating, and (c) noise spikes resulting from instantaneous charge release.

Using the conductivity value, based on the "1 min" LOCA, the IRT calculations estimate a shunt resistance in the range of 70 to 7 megohms would result depending, of course, on the value of cable length used in the calculation.

Charge trapping calculations estimate an initial electric field enhancement on the order of 10^{-8} V/cm. Release of trapped charge is based on the assumption that charge buildup proceeds until dielectric breakdown occurs. Based on the above assumption, it is estimated that currents on the order of 1 A/cm of failed cable could be induced.

The assumption that charge buildup proceeds until instantaneous insulation breakdown occurs allows for estimating the absolute maximum radiation induced noise spike that may be expected. An additional, more realistic estimate of the effect of charge trapping has been obtained wherein charge mobility was considered to be a function of cable conductance and the charge induced voltage gradient occurring in the cable insulation. Charge distribution within the cable insulation was based on the one minute (LOCA) beta dose rate and its companion electron distribution within the cable.

Using these assumptions it is calculated that the charge distribution associated with the maximum anticipated dose rate would result in a maximum voltage gradient across the cable of about 1200 volts per centimeter. Since typical cable dielectric strength is on the order of 10^6 volts per centimeter, it is highly unlikely that noise pulses on the order of those predicted above or that insulation breakdown could occur in cables exposed to LOCA radiation environments.

5.3 Conclusions

Based on the IRT calculation, LOCA radiation-conductivity changes and electric-field buildup should have negligible effect on an electric cable's function. In the case of noise-spike generation due to charge release, currents on the order of 1 A/cm may be induced. Currents of this magnitude would have little effect on power cables. In the case of signal leads, however, cable termination would need to be specified; e.g., high impedence terminations result in a large induced-voltage pulse. However, based on the continuous charge drain calculations described in Section 5.2, it is not likely that a charge necessary to generate a one ampere current would be trapped in the exposed cable. In general, then a LOCA-radiation environment would not significantly alter electric signals or power transmission in exposed insulated electric cables.

In order to assess the adequacy of an isotopic simulator, the average dose rates calculated for the LOCA-radiation environment and those estimated for a ^{60}Co simulator are shown in Table 5.5. The simulator results are based on the results in Figure 5.2 and the assumption of a ^{60}Co source strength capable of delivering a dose rate of 5 Mrad/h.

It may be observed that such a source would be capable of delivering (at an extended time) any specified LOCA integrated-absorbed dose to any region that may be considered particularly susceptible to radiation induced damage. Note that the simulator dose rate in the dielectric components is less than those LOCA one-minute dose rates. Since the IRT[16] analyses of radiation induced electrical disturbances in cables were based

in part on the LOCA one-minute values of absorbed dose rates and were demonstrated to be of negligible consequence, it may be concluded that simulator induced electrical disturbances/damage in cables would also be of little consequence.

TABLE 5.5

LOCA Conditions
Average Dose Rates - rads(mtl)/s

Elapsed Time From LOCA	Cable Regions		
	Copper	EPR	Hypalon
1 min	5.9 + 2	6.4 + 3	1.1 + 4
4 d	1.9	2.6 + 1	1.0 + 2
^{60}Co Capabilities - rads(mtl)/s - (5 Mrad/h source)			
	3.8 + 3	4.5 + 3	3.0 + 3

NOTE: 5.9 + 2, read as 5.9×10^2

6. Bulk Temperature Effects

6.1 Background

In Section 5.1 both LOCA and hypothetical isotopic (simulator) radiation sources were defined on the basis of phenomenology and calculations. Since the source description necessary for cable degradation analysis will suffice for material bulk temperature effects as well, only the appropriate data are presented again here.

Table 6.1 lists averaged values of energy deposition[16] in the three zones of a typical cable configuration. Also in the table are comparable dose rates for two isotopic simulators - a ^{60}Co source delivering 1 rad/s and another delivering 5 Mrad/h (1400 rad/s). Normalization discussed earlier is based on the averaged dose distribution across the Hypalon region.

6.2 IRT Heat Flow and Temperature Estimates - LOCA Source

Heat flow and temperature (changes) resulting from LOCA radiation-energy deposition were estimated by IRT[16] for the generic cable. The source terms used were the 1-min values given in Table 6.1. Heat flow across the insulator and sheath were estimated using the one-dimensional conduction equation. Using these approximations it was estimated that a total temperature difference of about 8°C would be required to conduct the deposited energy from the cable to the atmosphere. In the event of poor transfer at the cable/air interface, conduction was assumed to proceed inward and then through the copper conductor. In this instance a temperature rise between 10° and 100°C was predicted. Since these predictions approach the maximum allowable temperature (above a superimposed LOCA thermal temperature) for certain insulation materials, the study argued that alternate heat-flow paths would probably restrict the insulator temperature to acceptable limits by heat transfer to the

atmosphere in addition to circulation along the central conductor. Reference 16 presents no numerical results for isotope simulation.

TABLE 6.1

Dose-Rate Deposition Estimate - LOCA and ^{60}Co Sources

LOCA Dose Depositions - rads(mtl)/s

Elapsed Time From LOCA	Cable Regions		
	Copper	EPR	Hypalon
1 min	5.9 + 2	6.4 + 3	1.1 + 4
4 d	1.9	2.6 + 1	1.0 + 2
^{60}Co Dose Depositions - rads(mtl)/s - 1 rad/s Source			
	2.75	3.20	2.20
^{60}Co Dose Deposition - rads(mtl)/s - 5 Mrad/h Source			
	3.80 + 3	4.5 + 3	3.00 + 3

NOTE: In the case of the LOCA tabulation, primary electron and photon contributions have been summed.

NOTE: The 5 Mrad/h isotope source choice is arbitrary but not unreasonable. Typical planar (one directional field) ^{60}Co sources are capable of producing exposures on the order of 2 to 3 Mrad/h.

6.3 Some Sandia Estimates - Simulator Source

Since the IRT[16] analysis included no calculation of the thermal effects of a simulator exposure, the following simulator heating estimates are included for the purpose of comparison.

Instantaneous temperature rises were estimated for the three-region cable assuming the LOCA radiation field for the 1-min and 4-d intensities and for a hypothetical ^{60}Co irradiator configured for a 5 Mrad/h maximum dose rate. Instantaneous temperature rise, based on room temperature heat capacities[24] are given in Table 6.2.

TABLE 6.2

Instantaneous Temperature Rates - °C/s

Source	Cable Regions		
	Copper	EPR	Hypalon
^{60}Co - 5 Mrad/h	9.7 - 2	2.2 - 2	1.4 - 2
LOCA - 1 min	1.5 - 2	3.1 - 2	5.3 - 2
LOCA - 4 d	5.0 - 5	1.2 - 4	4.8 - 4

It is observed from Table 6.2 (and assuming that the cable is in equilibrium with its external environment) that heat flow for the cobalt exposure would be, initially at least, in the reverse direction to that for cable exposed to LOCA environments. Temperature differences necessary for energy transport by conduction across the several cable boundaries were estimated in a manner similar to that used in Reference 16.

Using the conduction equation for concentric cylinders and the values of thermal conductivity listed in the reference, it is estimated that a temperature difference of 7°C and 9°C, across the EPR and Hypalon, respectively, would be required to balance the energy input from the ^{60}Co configured for a 5 Mrad/h dose rate. Transfer of this energy to the surroundings is accomplished by convection and radiation. Energy transfer from the outer cable sheath to the surrounding environment is estimated by an expression of the form:

$$q = (h_c + h_r) \times A \times (T_s - T)$$

where h_c and h_r are, respectively, convective and radiative heat-transfer coefficients, A is a unit of surface area, T_s is the cable surface temperature, and T is the ambient temperature. h_c was estimated using methods presented in Reference 25, while h_r was obtained using Reference 26. Under conditions of maximum simulator energy input (5 Mrad/h), an equilibrium value of $(T_s - T)$ 65°C is obtained. Working backwards through the cable, a temperature of 81°C above ambient would be required in the EPR if an equilibrium energy-transfer condition were to exist.

Ultimate temperatures achieved in the various cable regions will depend upon specification of the ambient environment. Obviously, thermal damage to the cable insulation and sheath will occur should that ambient specification be too large. Reduction of the simulator dose rate by an appropriate value (an option usually available on well-designed simulators) would reduce the cable temperature to within acceptable temperature limits.

We observe that although temperature gradients resulting from ^{60}Co exposures probably do not simulate those due to a LOCA exposure (assuming the temperature profile tracks with the energy-deposition profiles), adjustment of the ^{60}Co dose rate will allow for maintaining cable temperatures below maximum rating during any simulator-radiation exposure -- a result in accordance with IRT predictions[16] for a LOCA exposure.

In Figures 6.1 and 6.2 polymer temperatures as a function of simulator dose rate have been plotted. Figure 6.1 is a plot of outer surface (Hypalon) temperature as a function of dose rate; temperature plotted is Hypalon surface temperature versus environment temperature. As may be observed (and was discussed earlier), reduction in dose rate is an effective method of lowering surface-environment temperature differential. Figure 6.2 plots temperature differential across the EPR and Hypalon regions as a function of simulator dose rate; temperature behavior is as would be expected. Although these calculations were specifically for a ^{60}Co simulator, the character of the plotted data should be comparable for other isotopic source environments --lowering of surface-environment temperature lowers the temperature differentials in the sample interior.

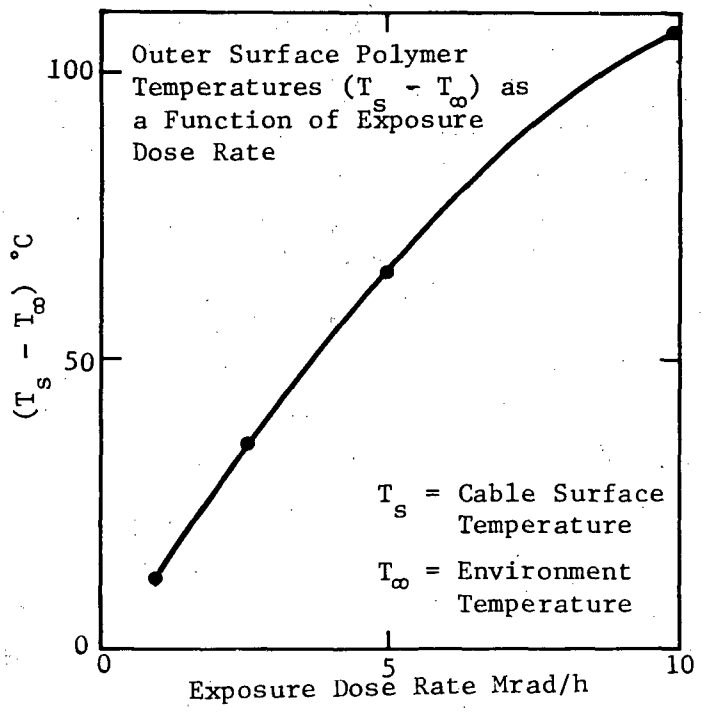

Figure 6.1 Outer Surface Polymer Temperature vs Exposure Dose Rate

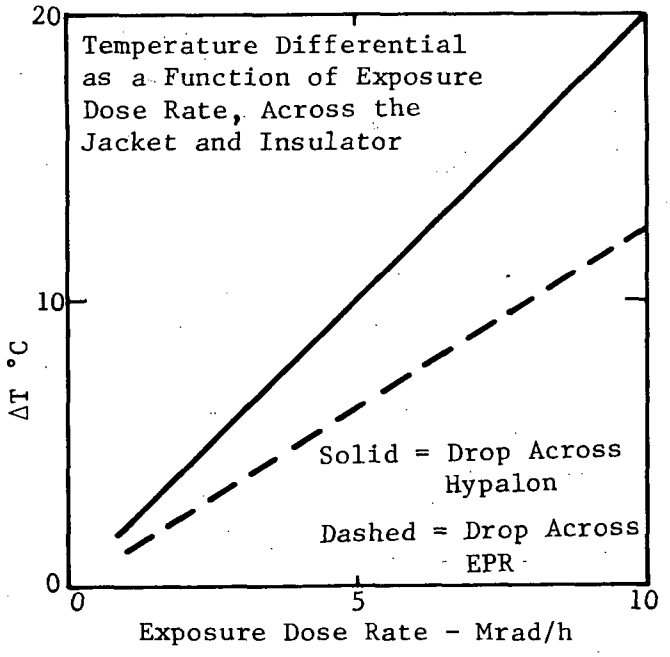

Figure 6.2 Temperature Differential Across Cable Jacket and Insulation vs Exposure Dose Rate

6.4 Conclusions

Radiation-induced temperature rise in polymeric materials were considered for two radiation sources -- a LOCA-radiation environment and a hypothetical ^{60}Co simulator. The one minute LOCA studies were performed by IRT[16] for two cases. In both studies it was assumed that thermal equilibrium had been established in the cable. Considered first was the case where the cable was in good thermal contact with its environment. In this instance thermal equilibrium could be maintained, by radial conduction to the environment, with a thermal gradient of but a few degrees. In the case of poor thermal contact it was estimated that gradients on the order of 100°C might be required to maintain thermal equilibrium. The IRT report concluded that actual conditions would bridge these two extremes and that service temperatures of the insulating and sheathing components would not be exceeded.

Sandia calculations were based on a ^{60}Co simulator capable of rates on the order of 5 Mrad/h - a rate between the LOCA 1-min and 4-d rates. The results predict that because of differences in energy deposition, heat flow would (initially at least) be in opposite directions for the exposures. These calculations predict that simulator-radiation-induced heating of cable configurations can be held to tolerable operating temperatures and simultaneously deliver a dose to materials on the order of a LOCA-radiation deposited dose.

In summary we conclude that one-minute LOCA radiation environments probably will not result in cable temperatures in excess of specified service temperatures. Similarly it may be stated that a suitably designed ^{60}Co simulator will deliver prescribed radiation absorbed doses to cable components while not exceeding the service temperatures of the various cable materials.

7. Bulk Polymer Degradation

7.1 Integrated Radiation Dose Effects

Bulk polymer degradation is, primarily, the result of radiation induced ionization. Effects to polymers exposed to ionizing radiation may be:

a. Radical (or ion) production
b. Molecular chain cleavage
c. Molecular chain cross linkage, and
d. Gas evolution

LOCA radiation effects to bulk polymeric materials were investigated by IRT (analytically) on the basis of total integrated absorbed dose.[16] The IRT analysis is based, primarily, on polymer degradation resulting from chain cross linking and unsaturation. Yield parameters (G-values) required for the analysis were based on those given in the literature.

The IRT calculations for Hypalon and ethylene-propylene may be summarized as follows:

a. Hypalon

(1) 90 Mrads (10 h) - onset of deterioration
(2) 300 Mrads (1 to 2 d) - serious loss of stability

b. Ethylene Propylene Rubber

(1) 100 Mrads (1 to 2 d) - 20% loss in tensile strength
(2) 500 Mrads (5 to 10 d) - 50% loss in tensile strength

The above estimates are based on a combination of the 1-min and 4-d LOCA source estimates.

7.2 Dose-Rate and Oxygen Effects

Although the dose-rate and oxygen effects reported here are the results of an investigation into the feasibility of accelerated polymer aging tests, the results can well have a bearing on the simulation of a LOCA environment.

The results of this study[27] are both experimental and theoretical in nature. In essence, the premise of this study was that radiation damage to a polymeric material, polyethylene in the study, was due primarily to the interactions of radiation produced radicals, in the polymer, with oxygen present in the materials. The rationale, here, being that the presence of oxygen in the neighborhood of the active species (radicals) enhanced molecular chain cleavage with resultant suppression of the cross-linking reaction. For the particular applications of this study molecular cleavage was considered to be more detrimental than cross-linking.

While holding total integrated dose constant, this study examined polymer degradation as a function of dose rate, oxygen pressure, and polymer sample thickness. Polymer degradation was based on reduced gel formation (inhibited cross-linking) with variation of the above parameters.

The theory predicted and experiments confirmed that polymer degradation (inhibited gel formation) varied directly with the square root of environment oxygen pressure and in an inverse manner with the square root of the dose rate for a given polymer thickness and integrated radiation dose. Since integrated dose was held constant, dose rate dependence of polymer damage was a function of oxygen diffusion time into the interior of the polymer sample.

7.3 Conclusions

We have reported the results of two studies on the radiation induced degradation of polymeric materials. The first, by IRT[16], was theoretical in nature and examined the effects of a LOCA radiation environment on

polymer performance. The second study was concerned with simulating the long term aging effects of polymers; this study was both experimental and theoretical.

The IRT study demonstrated that significant polymer degradation, in a LOCA environment, would occur for exposure times between 10 hours and 8 days. The second study demonstrated that a correlation between radiation dose rate, oxygen concentration, etc., and a polymer damage parameter could be established.

Based on the first study, typical LOCA dose rates, to Hypalon for example, would range somewhere between 10^4 and 10^2 rads/sec (see Table 5.5). Reference to Table 5.5 indicates that the typical simulator is, on the average, able to deliver a dose rate comparable to the LOCA dose rate.

10

The results in Section 7.2 show that under certain conditions and for a specific material that a predictable relationship between polymer damage and the polymer environment exists. The specific results of the study cannot be generalized to all polymer materials and environments. The study does indicate that given a specific polymer and environment, that environment and its effects could be adequately simulated by an appropriately designed simulator experiment.

To sum up, it is considered that, based on these studies, the effects of a LOCA environment on bulk polymer materials could be reasonably well simulated with judiciously designed simulator experiments.

8. Differential Mechanical Stress in Insulating Materials

8.1 Background

In Sections 7.1 and 7.2, effects to bulk polymers were discussed. In those sections, neither deposition profile nor methods of monitoring polymer degradation were considered. In considering differential stress effects, energy deposition distributions are of basic importance. In view of that importance, some aspects of energy-deposition distributions will be reviewed (e.g., effects of source energy distribution and particle makeup).

Methods of monitoring polymer degradation become important in considering possible stress effects since the parameter used to monitor degradation may proceed at a much more rapid rate (with dose/dose rate) then the parameter responsible for internal stress generation.

Polymer degradation, as a result of exposure to a simulated LOCA environment, has been based on changes in the polymer elasticity.[20] Elasticity change has proved to be a particularly sensitive and easily measurable parameter. Much degradation data, in the form of change in ultimate elongation, has been accumulated for several polymers exposed to a variety of environments.

Stress generation has been attributed to differential shrinkage in elastomeric material as a result of nonuniform energy deposition in the sample. It now becomes clear that if loss in elasticity proceeds at a more rapid rate than shrinkage, then (due to loss in elasticity) the polymer material may for all intents and purposes become useless as an insulating material well before appreciable shrinkage has occurred.

8.2 Energy Deposition and Polymer Degradation

Isotopic-source irradiation of polymeric materials will deliver a relatively uniform energy deposition into the polymer. On the other hand, a LOCA exposure delivers a nonuniform temperature distribution that correlates with the dose distribution. The result of a LOCA exposure on a macroscopic scale is a nonuniform material-degradation profile that is a decreasing function with penetration in any material layer of a sample.

The difference in cable energy deposition profiles for cables irradiated under LOCA and simulator conditions are presented in Figures 5.1 and 5.2 respectively. From the figures it is apparent that a cable configuration exposed to a LOCA environment will exhibit a deposition pattern that is highly spatially dependent. By comparison simulator irradiated cable samples will exhibit almost negligible spatial dose dependence. Hence simulation dose based on the surface dose to a LOCA irradiated specimen would certainly overstress most regions of the sample. Initially, such a procedure to greatly overstress most zones in the cable configuration, when compared to a LOCA exposure, would appear to be a conservative approach to testing. However, if it is postulated that polymer degradation is accompanied by material dimensional change, then the above statement about conservative simulator overtesting is probably not true.

A uniformly irradiated cable would undergo uniform dimensional change. On the other hand, a LOCA or nonuniformly irradiated cable would contain regions of unequal dimensional change. Hence nonuniformity in dimensional changes could give rise to circumferential and/or radial stresses with resultant mechanical damage. Thus, if the above postulation concerning dimensional changes is true and the change is appreciable compared to other effects, then uniform overstress of the cable sample would not represent a conservative or valid test.

8.3 Polymer Degradation - Elongation/Shrinkage Experiments

Elongation/shrinkage experiments were performed by Gillen,[28] using several typical safety-related cable samples. The elongation/shrinkage

changes were induced in all cases by an accelerated aging technique at elevated temperatures. Multiple samples were used in all experiments.

The results for these thermally aged cable polymers[28] are given in Figures 8.1 and 8.2. The results plotted are fractions of initial elongation versus aging time for the various materials aged at several temperatures. In most tests aging was continued until the samples were almost totally degraded. Also, plotted in Figures 8.1 and 8.2 are shrinkage data for each sample. Data presented in this instance are fractions of initial length versus aging time. In all instances, open symbols represent elongation data while matching closed symbols are representative of shrinkage data. As may be seen from the data, shrinkage of most samples was insignificant -- the maximum observed shrinkage was about 5%. It is also interesting that the preponderance of cable shrinkage occurred early (in time) in the aging experiments. From the thermal-aging data of Gillen it may be observed that changes in sample dimension remain slight up to the point where severe degradation occurs.

8.4 Polymer Degradation - Elongation/Density-Change Experiments

The elongation/density-change experiments investigated the effects to polymers similar in composition to those used in the thermal-aging experiments reported in Section 8.3. The elongation/density-change effects were radiation-induced with a ^{60}Co irradiator. The irradiations were performed under ambient conditions (i.e., at room temperature and in an air atmosphere).

Data from these experiments include changes in elongation versus radiation (integrated) exposure and shrinkage data in the form of density changes versus dose. In Figures 8.3 and 8.4 are presented the radiation elongation and shrinkage data.[29,30] Presented in the figures are fractional parameter changes versus exposure dose. Again the open symbols represent elongation data and the respective closed symbols represent density data.

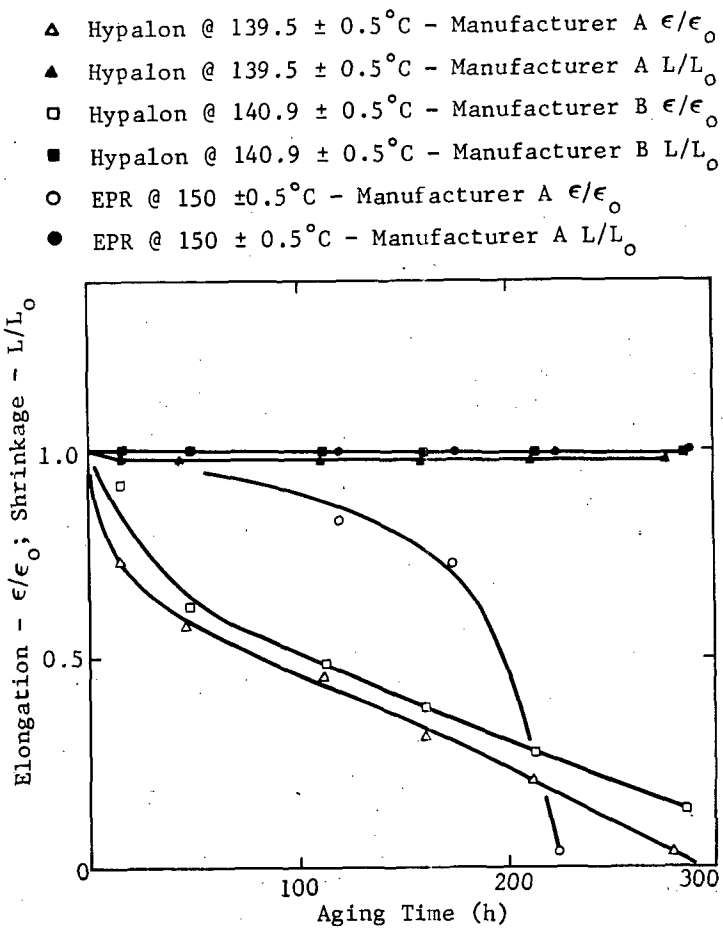

Figure 8.1 Polymer Aging vs Aging Time - Aging Thermally Accelerated

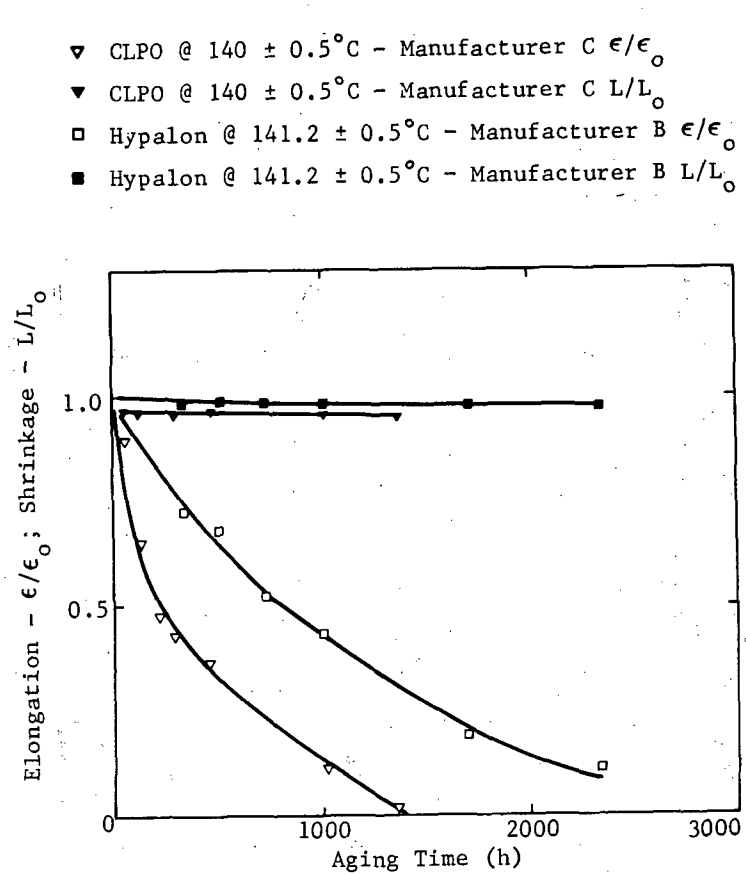

Figure 8.2 Polymer Aging vs Aging Time - Aging Thermally Accelerated

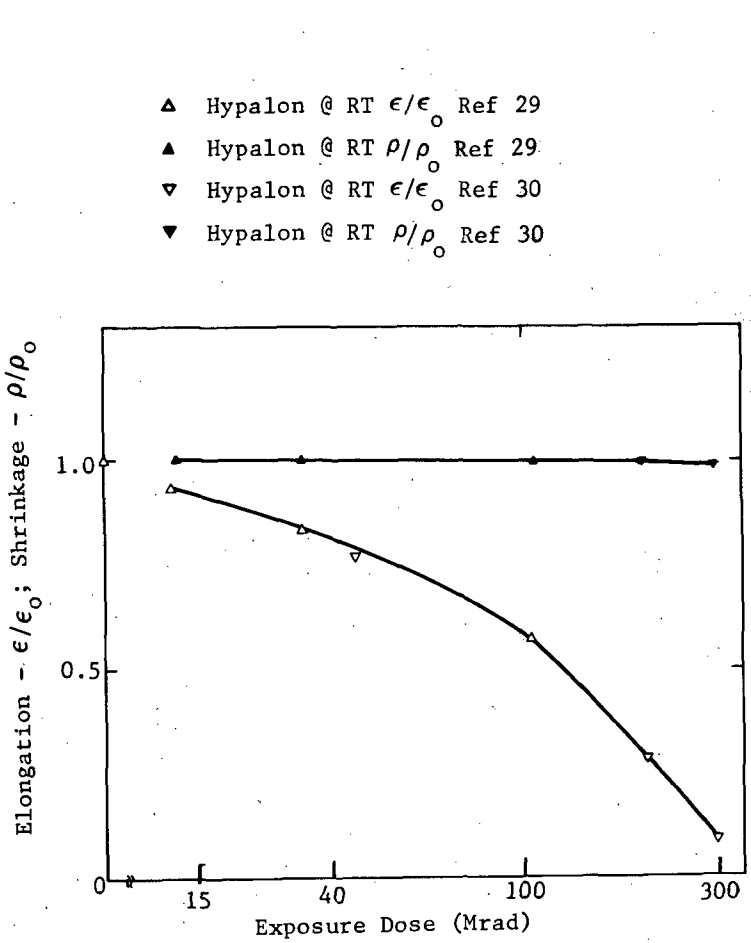

Figure 8.3 Polymer Aging vs Aging Time - Aging Radiation Accelerated

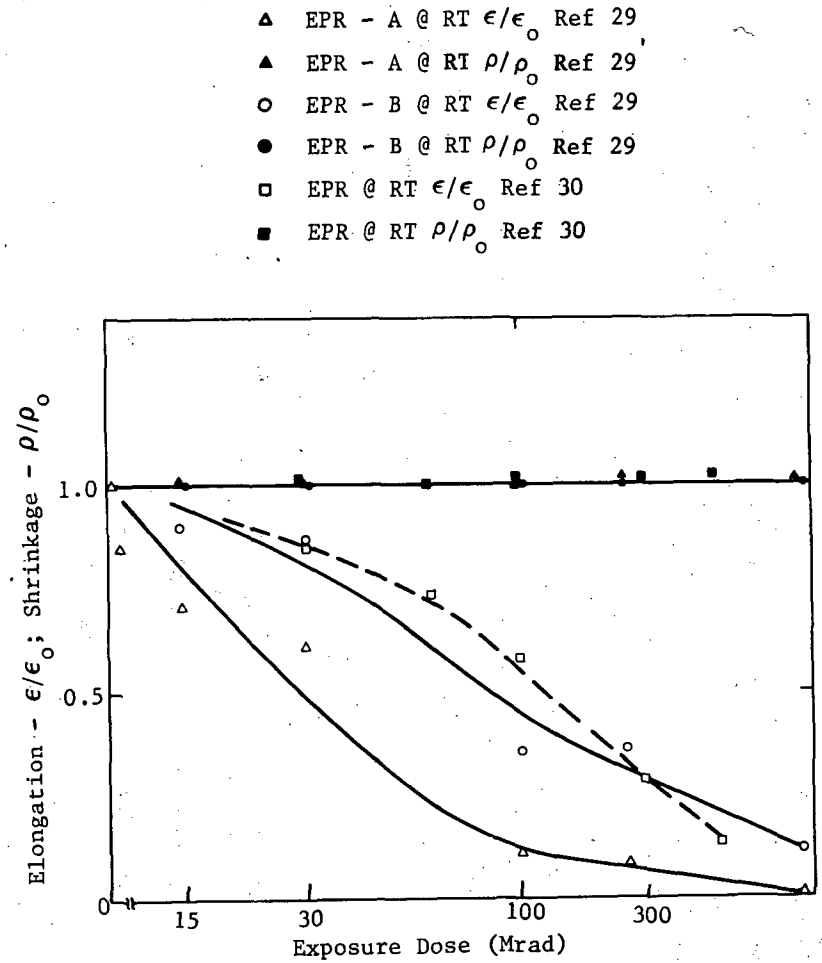

Figure 8.4 Polymer Aging vs Aging Time - Aging Radiation Accelerated

As may be observed, the polymer densities were little affected by the radiation aging even to the point of complete loss of sample elasticity. Lack of density change may be interpreted as absence of significant sample dimensional change.

8.5 Other Considerations

One further item of interest in the realm of simulator adequacy is that of radiation-induced temperature rise of simulator versus LOCA-exposed samples. All other things being equal, the ultimate temperature rise in a given irradiated sample will be dependent on the energy deposition rate. Simulator capability to achieve early time LOCA rates does not exist. It is just possible that early time LOCA exposures could result in a combined temperature-radiation aging condition not normally present in a simulator-irradiation test. Although the combined effects may be small, such effects could probably be compensated for. Gillen[27] has demonstrated that a functional relationship between thermal- and radiation-induced aging exists for several polymeric materials. This relationship shows that over a certain range the effect of temperature fluctuations on aging could be accounted for by adjustment of dose rate and vice versa. Establishing such relationships for cable polymers would then allow compensation to be made for any elevated temperatures occurring during a LOCA exposure and not present during a simulator exposure.

8.6 Conclusions

Polymer tensile elongation is an easily measured parameter that is extremely sensitive to radiation or thermally-induced stress. Since loss of tensile elongation is a major cause of polymer failure, monitoring of tensile elongation changes of radiation or thermally-stressed material represents a particularly sensitive measure of polymer performance; there is concern that other physical changes in stressed polymeric materials (dimensional/density or material shrinkage) would be particularly sensitive to the LOCA environment. Major contributors to polymer failure were considered in Figures 8.3 and 8.4. The results of the studies summarized in Figures 8.3 and 8.4 show that, in materials stressed both thermally and

by radiation, failures due to loss in elasticity could be expected before any appreciable material dimensional changes. In the case of combined radiation/thermal stress of polymers, recent studies strongly suggest that simulator environments could be adequately compensated for so that the proper LOCA effect could be reasonably duplicated.

It is concluded that:

a. Polymer tensile elongation change is a valid monitor for material performance

b. Loss of elasticity is a major contributor to mechanical failure of polymeric materials - dimensional change contributing little, if any, to that failure. Hence, differential-mechanical stress failure is not a practical failure mechanism

c. Exact simulation of a LOCA radiation/thermal stress is not required to reproduce the LOCA radiation/thermal-stress-induced changes.

9. Summary and Conclusions

The standard gamma-radiation simulators can adequately duplicate the damage mechanisms and damage in safety-related equipment that result from the postulated nuclear-plant ambient and accident radiation environments. The conclusion can be no stronger than that because the simulators must be intelligently used in an overall qualification program that implies combinations of environments, magnitudes, secondary radiations (e.g., bremsstrahlung), functioning, and other considerations.

Other specialized simulators, which strive to more closely achieve the LOCA-radiation signature, are equally adequate with similar provisos. However, there seems to be no reason to select one simulator over another.

One recommendation is to overstress the equipment/material everywhere to greater total dose than expected from the combined LOCA-radiation signature; dose rates should also approximate the expected (combined) rates. However, other logical data-based techniques (e.g., averaged dose and rates) may also be acceptable.

In summary, we have seen no evidence of unique damage mechanisms in exposed organic materials that demand unique radiation-simulation techniques; neither can radiation be arbitrarily applied to the test item without consideration of the complete qualification program.

Nevertheless, this study should not terminate because not all aspects of simulator adequacy evaluation are complete. A few areas requiring additional attention can be suggested:

- Equivalence of beta/gamma and or neutron/gamma (for aging environments) ratios in bulk degradation. That is, are peak doses/rates appropriate, or are averaged values acceptable?

- Charge breakdown resulting in transient noise and/or permanent damage may be important in selected equipment.

- Secondary emissions, magnitudes and effects, may be a consideration.

- Simulator adequacy evaluations should be extended to more complex and specific equipment items.

REFERENCES

1. IEEE Standard for Qualifying Class 1E Equipment for Nuclear Power Generating Stations, IEEE Std. 323-1974., the Institute of Electrical and Electronics Engineers, Inc., 1974.

2. L. L. Bonzon, Radiation Signature Following the Hypothesized LOCA, SAND76-0740 (NUREG76-6521), (Albuquerque: Sandia Laboratories, revised October 1977).

3. L. L. Bonzon, "In-Containment Radiation Environments Following the Hypothesized LOCA (LWR)", Transactions of the American Nuclear Society, pp 601-602, TANSAO, 23, 1976.

4. L. L. Bonzon, N. A. Lurie, D. H. Houston, and J. A. Naber, Definition of Loss-of-Coolant Accident Radiation Source, SAND78-0090 (Albuquerque: Sandia Laboratories, February 1978).

5. L. L. Bonzon, N. A. Lurie, D. H. Houston, and J. A. Naber, Definition of Loss-of-Coolant Accident Radiation Source: Summary and Conclusions, SAND78-0091 (Albuquerque: Sandia Laboratories, May 1978).

6. N. A. Lurie, J. A. Naber, and L. L. Bonzon, The Hypothesized LOCA Radiation Signature and the Problem of Simulator Adequacy, ENS/ANS International Topical Meeting on Nuclear Power Reactor Safety, October 1978, Brussels, Belgium; also, SAND78-0348/IRT 8167-005 (Albuquerque: Sandia Laboratories, 1978).

7. L. L. Bonzon, K. T. Gillen, and E. A. Salazar, Qualification Testing Evaluation Program, Quarterly Report, October-December 1978, SAND79-0761, NUREG/CR-0813 (Albuquerque: Sandia Laboratories, June 1979).

8. Qualification of Class 1E Equipment for Nuclear Plants, Regulatory Guide 1.89, September 23, 1974.

9. Qualification of Safety-Related Electric Equipment for Nuclear Power Plants, U.S. Nuclear Regulatory Commission, Regulatory Guide 1.89, Rev. 1 (Draft, November 1, 1976).

10. N. A. Lurie, "Best-Estimate LOCA Radiation Signature; Phase 1, Suggested Accident Scenario and Source Definition," IRT 0056-001. Prepared for Sandia Laboratories, June 1978. (This report intended for internal Sandia use only, to be published in full as a Sandia topical report.)

11. N. A. Lurie, "Best-Estimate LOCA Radiation Signature; Phases 2 through 4: Calculated Energy Release Rates, Spectra, and Energy Deposition Profiles," IRT 0056-005. Prepared for Sandia Laboratories, June 1979. (This report intended for internal Sandia use only, to be published in fall as a Sandia topical report.)

12. L. L. Bonzon and N. A. Lurie, Best-Estimate LOCA Radiation Signature, SAND79-2143, NUREG/CR-1237 (Albuquerque: Sandia Laboratories, January 1980).

13. R. A. Lorenz, J. L. Collins, and A. D. Malinauskas, Fission Product Source Terms for the LWR Loss-of-Coolant Accidents; Summary Report, ORNL/NUREG/TM-206, Oak Ridge National Laboratory (1978).

14. N. A. Lurie, J. A. Naber, and L. L. Bonzon, Adequacy of Radiation Sources for Qualification of Class 1E Reactor Components, IRT 8167-003/ SAND78-0161A, Transactions of the American Nuclear Society, Vol 28, 1978 (Albuquerque: Sandia Laboratories, 1978).

15. N. A. Lurie, Calculations to Support Evaluation of Test Sources for Radiation Qualification of Class 1E Equipment, IRT 8167-010(B), IRT Corporation, April 1979. Included as Appendix A of this report.

16. J. F. Colwell, B. C. Passenheim and N. A. Lurie, Evaluation of Radiation Damage Mechanisms in a Reactor Power Cable in a Loss-of-Coolant Accident, IRT 0056-002A, IRT Corporation, August, 1978. Included as Appendix B of this report.

17. Private communication, L. A. Harrah to L. L. Bonzon, August 21, 1978, "Co-60 Simulation of LOCA Exposure".

18. J. Sejvar, "Normal Operating Radiation Levels in PWR Plants", Transactions of the American Nuclear Society, pp 605-606, TANSAO, 23, 1976.

19. Work of United Engineers and Constructors, Inc; summarized in Qualification Testing Evaluation Program, Quarterly Report, April-June 1978, SAND78-1452 (Albuquerque: Sandia Laboratories).

20. K. T. Gillen and E. A. Salazar, Aging of Nuclear Power Plants Safety Cables, ENS/ANS International Topical Meeting on Nuclear Power Reactor Safety, October 1978, Brussels, Belgium; also, SAND-0344 (Albuquerque: Sandia Laboratories).

21. F. H. Attix and W. C. Roesch eds., Radiation Dosimetry - Volume 1 (New York: Academic Press, 1968).

22. "Studies in Penetration of Charged Particles in Matter", Report No. 39, National Academy of Sciences - National Research Council, 1964.

23. Sandyl: A Computer Program for Calculating Combined Photon-Electron Transport in Complex Systems, SLL 74-0012 (Albuquerque: Sandia Laboratories, May 1974).

24. K. C. Weast, ed., Handbook of Chemistry and Physics - 50th Edition (Cleveland: The Chemical Rubber Co., 1969).

25. W. H. McAdams, Heat Transmission (New York: McGraw-Hill Book Co., 1954).

26. W. H. Giedt, Principles of Engineering Heat Transfer (New York: D. Van Nostrand Co. Inc., 1957).

27. Seguchi, T., Hashimoto, S., Kawakami, W., and Kurijama, E., Radiation Damage of Polymer Materials I. Simulation Studies on Distribution of Oxygen Concentration in Polymer Film Under Irradiation in Oxygen, JAERI-M7315, October 1977.

28. Private communication, K. T. Gillen, April 1979.

29. Fujita, H., Obuchi, H., Okade, M., Mio, K., and Terasaki, I., "Radiation Resistance of Rubber and Plastic Cables", Dainichi Nippon Densen Johio, #48, 1971.

30. Kakuta, T., Wakayama, N., and Kawakami, T., Gamma Irradiation Test of Wire and Cable Insulations and Electronic Materials, JAPFNR-172, August 1974.

APPENDIX A

Calculations to Support Evaluation of Test Sources for Radiation Qualification of Class 1E Equipment

IRT 8167-010(B)

April 9, 1979

IRT 8167-010(B)

CALCULATIONS TO SUPPORT EVALUATION OF TEST SOURCES FOR RADIATION QUALIFICATION OF CLASS 1E EQUIPMENT

FINAL REPORT - Phases 5 and 6

N. A. Lurie

This report documents part of the Qualification Testing Evaluation (QTE) Program (A 1051-8) being conducted by Sandia Laboratories for the United States Nuclear Regulatory Commission under DOE Contract AT(29-1)-789.

Prepared for

SANDIA LABORATORIES
Albuquerque, New Mexico

Under

Contract 07-3272

April 9, 1979

IRT
Corporation

Instrumentation
Research
Technology

7650 Convoy Court • P.O. Box 80817
San Diego, California 92138

714 / 565-7171
Telex: 69-5412

(This page intentionally left blank)

TABLE OF CONTENTS

LIST OF FIGURES

1. INTRODUCTION

Phases 5 and 6 of the present program are devoted to consideration of energy deposition in a model reactor component. The objective of this work is to establish the basic data required to assess the validity of various radiation simulators for duplicating the damage in reactor Class 1E equipment resulting from a loss-of-coolant accident (LOCA). The definition of the LOCA source terms as specified by U.S.N.R.C. Regulatory Guide 1.89 (Ref 1) was considered in Phases 2 and 3 of the program (Ref 2). Those energy spectra were used as starting points in the present calculations.

The reactor component considered for this initial comparison was a power cable. Energy deposited by the beta and gamma-ray fields as defined in Phases 2 and 3 are to serve as benchmarks for comparison with the simulator results. Simulators used for qualification testing come in many forms including ^{60}Co and ^{137}Cs isotope sources, bremsstrahlung and electrons from linear accelerators (Linacs), and spent fuel assemblies. By far the most common testing is by ^{60}Co irradiation. The energy deposition in terms of dose versus depth for the LOCA sources and for ^{60}Co will provide part of the data necessary to formulate judgments as to the validity of ^{60}Co as a test source.

Previous work on this problem (Refs 3,4) was preliminary and qualitative in nature. The present work was intended as a careful quantitative study to provide the calculational data necessary to allow meaningful conclusions to be drawn about the adequacy of simulator sources.

In the sections that follow a description is given of the mathematical model used for the cable including the approximations and assumptions made. Discussion is also given of the source-cable geometry. Proper configuration of the source is a very important aspect of proper modeling. Section 3 discusses the methods employed for carrying out the calculations and the inherent approximations; some special treatments of the sources were required to make the calculations tractable. In Section 4 the sources selected for study are summarized, from the many previously calculated. This is followed by the results for the LOCA sources. Section 5 includes the same information for the simulator sources. Finally, some comparisons and discussion are presented in Section 6 along with our conclusions and recommendations for additional work in Section 7.

(This page intentionally left blank)

2. CABLE MODEL

2.1 PHYSICAL PROPERTIES

There are many types and manufacturers of cable used in nuclear power plants. The type selected for study here is a 600V power cable consisting of a copper core with elastomer insulator and jacket. Discussions with several manufacturers were held to collect data on their "typical" 600V cables. Not surprisingly, it was found that the dimensions and material compositions varied widely. Thus, the model selected may be considered in the range of typical cables, but not exactly like any one manufacturer's type in particular. Other, slightly different elastomeric materials (but composed basically of CH_2) would not be expected to have much effect on the results, nor would small changes in dimensions be expected to change the conclusions. It is difficult, however, to generalize without doing model sensitivity calculations wherein these model parameters are varied systematically. In the discussion of results (Section 6) a few comments are given about the expected sensitivity of the model.

The dimensions and material properties of the model are shown in Figure 1. Only an unshielded cable was studied. Each region of the cable was subdivided into annular zones of uniform thickness for calculations of depth versus dose. For most cases four or five zones were used for each region.

2.2 DAMAGE MECHANISMS

The question of ultimate interest is to what extent a given radiation field will affect the properties or operating characteristics of a material or component. In many instances, experience has shown that the degradation is directly related to the total energy deposited or absorbed dose. Thus, the usual analysis of radiation effects involves determination of the (nonequilibrium) dose to the critical regions of the component. In many complex systems such as electrical or electronic equipment this simple approach may not be adequate. The controlling damage mechanisms may involve phenomena that are not simply related to the energy deposition. Therefore, any measure of simulator performance must use as a basis the best estimate of the

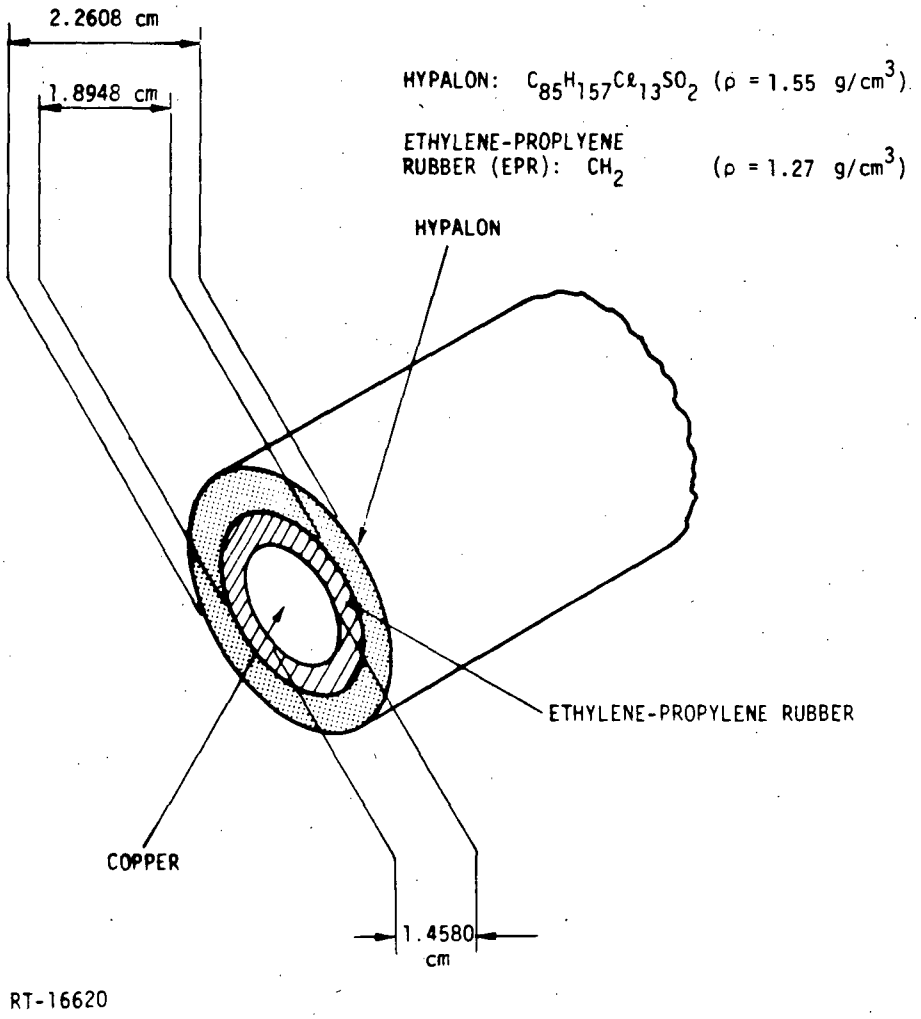

Figure 1. Model of the reactor power cable

controlling damage mechanism, whether it is energy deposited or some other quantity appropriate to the component of interest.

A detailed evaluation of the damage mechanisms for reactor components is a complex analysis problem that is beyond the scope of this project. Even for the case of a reactor power cable there are many physical interaction phenomena that must be considered (Ref 5). The type of calculations presented here that will support such an assessment are the energy deposition profiles, that is, the dose versus radial depth in the cable. We also attempted to calculate net charge deposition as a function of radial depth.

2.3 SOURCE-CABLE CONFIGURATION

Regulatory Guide 1.89 (Ref 1) calls for three distribution categories (airborne, plate-out, waterborne) for each of two LOCA sources. For purposes of studying their interactions in the cable, each of the three distribution categories requires a different source configuration. The airborne source was taken to consist of a uniform distribution of point sources in air plus 70 psig saturated steam. A few calculations were also done with dry air (i.e., no steam) to evaluate the sensitivity of this parameter. The waterborne source was assumed to consist of sources uniformly distributed in the water. The plate-out source was uniformly distributed on the surface of the cable.

The latter geometry presents no calculational difficulty. The spatially extended source distributions, however, are not efficiently treated by direct Monte Carlo transport methods. The reason for this is that the cable subtends a very small solid angle; in other words, the probability that a source particle sampled from the air will hit the cable is too small to get statistically meaningful results in a reasonable time. Consequently, an approximate technique was used to map the distributed airborne and waterborne sources into a practical configuration. The details of this procedure are described in subsection 3.2.

(This page intentionally left blank)

3. METHODS OF CALCULATION

Detailed descriptions of the calculational methods employed in this work to calculate the energy deposition are given in the subsections that follow. Treatment of the distributed source problem is also described.

3.1 TRANSPORT METHODS

All of the calculations of depth versus dose reported here were carried out using the code SANDYL (Ref 6). It is the most general and widely recognized coupled photon-electron transport code presently available. It has served as the industry standard for several years. Extensive experience with this code has demonstrated its capabilities for a wide variety of transport problems (Ref 7).

SANDYL is a FORTRAN code for computing photon-electron transport and deposition in complex systems by the Monte Carlo method. The code was developed at Sandia Livermore Laboratories (Ref 6). It is based on a photon transport code from Lawrence Livermore Laboratory (SORS) (Ref 8), and the electron transport codes of Berger (Refs 9,10). Like many transport codes, SANDYL uses the physical approach which consists of random sampling and simulation of individual histories which are used to construct the solution to the physical problem. A transport equation is never explicitly written and solved. The only information needed to simulate a history is the probabilistic description of all events which may occur at each point in the history. The random, probabilistic nature of particle/radiation interaction with matter renders Monte Carlo methods particularly well suited to problems of particle/radiation transport. The necessary information in this case includes a description of the geometrical boundaries of the different regions through which transport occurs, the material composition of each region, and the cross sections (differential in energy and direction) of the constituent isotopes.

A simulation consists of generating a large number of particle histories one at a time, with primary particles starting at the source, and secondaries starting at their generation points along the trajectories. As the particles traverse the different regions

of the system, the contributions to the quantities of interest are tallied following each collision to generate the desired information. The average of these quantities for a number of primary, and their induced secondary, particle histories represents a statistical approximation of the solution.

Photon histories are generated by tracing their trajectories from collision to collision. At each point of photon-medium interaction the type of interactions, secondaries and the new photon energy, direction, and distance to the next collision are determined on the basis of probability distributions characteristic of the medium composition. Photon collisions can result in photoelectric absorption, Compton scattering, or pair production. Secondary photons include bremsstrahlung, fluorescence, and annihilation radiation.

Electrons are treated in a slightly different manner because, as a result of being electrically charged, they suffer a much larger number of collisions. The method used for electron transport is known as condensed-history Monte Carlo (Ref 10). Accordingly, an electron history is generated by following the trajectory in spatial steps of pre-computed length, so that the electron energy and direction at each point may depend on a number of different collisions which may have occurred in the previous step. Therefore, electron energies and directions are determined on the basis of multiple scattering distributions. Within a step, secondary photons and electrons are generated according to the corresponding probability distributions. Electron interactions include electron-electron collisions, bremsstrahlung radiation, and medium polarization. Secondary electrons which are followed include knock-on, pair, Auger, Compton, and photoelectric electrons.

Three-dimensional geometries with a high degree of complexity can be treated. The problem geometry is divided into zones of homogeneous atomic composition bounded by planes and quadrics. Options are available for splitting or biasing to improve the statistical uncertainty in certain problems. The code calculates flux or energy deposition (dose or spectrum) in any desired zones as well as net charge deposited. Photon and electron transport are followed in an energy range from 1 keV to 1 GeV or higher.

3.2 SOURCE DISTRIBUTIONS

The source configurations specified for the airborne and waterborne cases are spatially distributed, isotropic sources surrounding the cable. As noted earlier, spatially

extended sources present a problem for Monte-Carlo-type calculations because the region of interest is small compared to the dimensions of the source. In this problem the cable radius is about 1 cm whereas the source consists of point sources uniformly distributed in the containment with dimensions of the order of 25 m (radius). For gamma rays in air there is little attenuation, and sources at distant points can contribute to the energy deposition in the cable. The attenuation in water is considerably greater and thus smaller source regions can be considered. The most energetic betas in this work (~6 MeV) have a range in air of ~25 m; their range in water, however, is only about 3 cm.

In this study we have used an approximate method to obtain the distributions of radiation, both in energy and angle, incident on the surface of the cable. This permits conventional Monte Carlo methods to be used with maximum efficiency to calculate the depth-dose profiles of interest. We have assumed that the energy and annular distributions are not coupled so that each may be approximated independently.

3.2.1 Spatial Distributions

The sources are taken to be uniformly distributed in an annular region surrounding the cable (see Figure 2). The high symmetry of the problem means that only sources in a sector of the annulus need be considered. Furthermore, if the cable is taken to be infinitely long so that end effects can be ignored, the polar angles are uniformly distributed between $\pm\pi/2$, and the problem may be reduced to a two dimensional problem. Symmetry further allows us to collapse the two dimensional sector to a line AB where the density of points on the line increases with radius like the area of the sector, that is, like (r^2-R^2).

A Monte Carlo technique was utilized to calculate the angular distribution of particles striking the surface of the cable. The method may be described as follows: The source position was randomly selected along the line AB where the density of sources increases with radius. The probability that a particle emitted at the chosen distance from the cable strikes the cable (ignoring attenuation and scattering in the medium) was calculated in the following way. Only particles emitted into a cone defined by the cable can hit it. A particle from within the cone was selected at random and its angle of incidence on the surface of the cable (with respect to the surface normal) was computed. The computed angle was stored with a weight equal to the solid angle, (the probability of a hit) and the whole process was repeated. In this way a

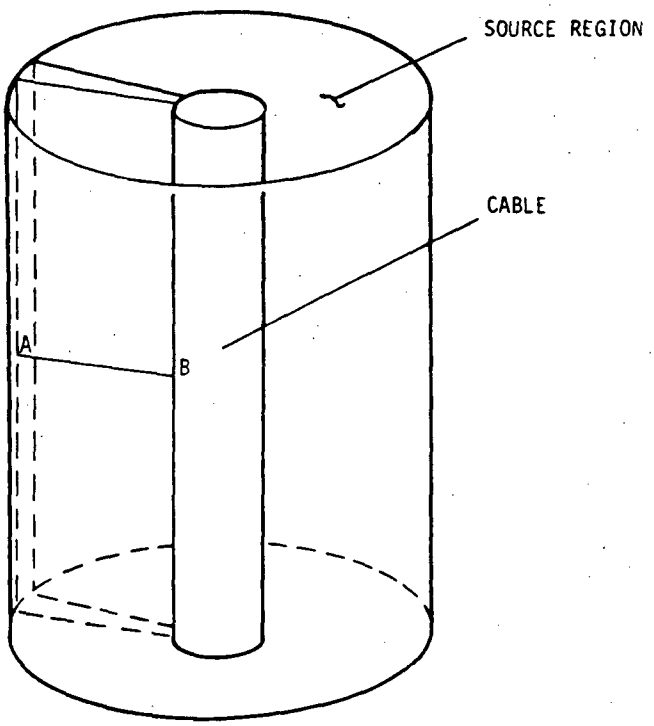

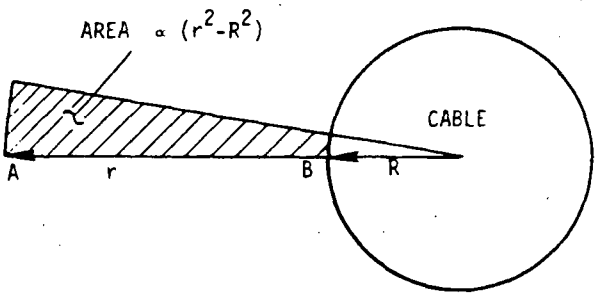

TWO-DIMENSIONAL GEOMETRY

RT-16619

Figure 2. Source-cable geometry

distribution of normal angles was generated which corresponds to the case of the spatially distributed source with no attenuation or scattering in the medium.

The results of such calculations for the cases where the source annulus is 2.5 m radius and 25 m radius are shown in Figure 3. The 25 m dimension corresponds roughly to the radius of the containment of a commercial light water power plant, and also the range of a 6 MeV beta particle in air. The 2.5 m dimension is taken as an effective thickness of the gamma-ray source in water. Less than 0.1 percent of all gamma rays beyond 2.5 m would reach the cable for the waterborne sources used here.

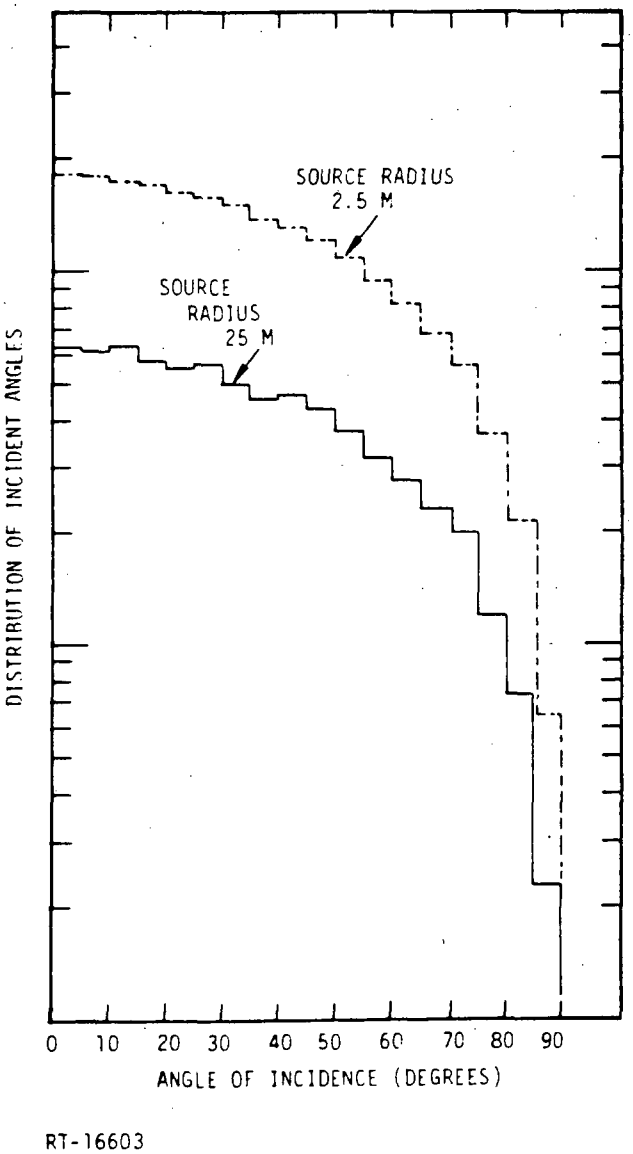

Figure 3. Distribution of incident angles (with respect to surface normal) on cables

The shapes of the angular distributions are virtually identical for these two cases and correspond to a cosine distribution. It was found that for any size of annular source region large compared to the cable radius, the incident angular distribution of particles has the cosine shape. When the thickness of the source region is of the order of the cable radius or less, a departure from the cosine shape was observed (the distribution becomes flatter).

Although it is not necessary, it was convenient for the subsequent depth-dose calculations to transform the calculated distribution of incident angles into a distribution from a fixed point source at a specified distance from the cable, Figure 4 defines the angles. We call $N(\alpha)$ the calculated distribution of normal angles, α, from the distributed source. We desire to express this in terms of the angles ϕ measured with respect to a point source at a specified distance. The transformation is given by

$$N(\phi) = N(\alpha) \frac{d+R}{R} \frac{\cos \phi}{\cos \alpha} ,$$

where the angles are related by

$$\sin \alpha = \frac{d+R}{R} \sin \phi .$$

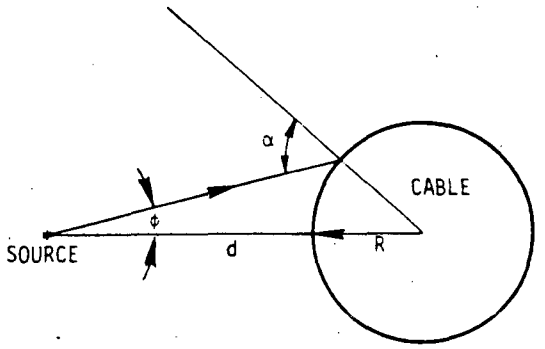

RT-16618

Figure 4. Relationship between distributions with respect to surface normal and with respect to a point source

If $N(\alpha)$ is a cosine distribution, as was apparently determined by the Monte Carlo calculations,

$$N(\alpha) = C \cos \alpha \quad ,$$

where C is a constant which depends on the size of the source region. Thus,

$$N(\phi) = C \frac{d+R}{R} \cos \phi \quad ,$$

where ϕ can assume values from 0 to $\sin^{-1}\left(\frac{R}{d+R}\right)$. Thus, the source azimuthal angles at distance d from the cable may be selected according to the distribution $N(\phi)$, and the resulting particles which strike the cable will do so with an angular distribution identical to that which is obtained from an extended spatial distribution of isotropic point sources. For the three dimensional problem, the azimuthal angle is combined with the polar angle (sampled from a uniform distribution between $\pm\pi/2$) to yield the direction cosines of a source particle.

3.2.2 Energy Distributions

The energy spectrum of particles incident on the cable from a spatially extended source will differ from the fission product source spectrum because of energy loss due to scattering and attenuation in the surrounding medium. The extent to which the source spectrum is perturbed depends upon the nature of the medium (especially the density) and the size of the region considered. To account for such spectral changes the following calculations were made. Each fission product source was uniformly distributed in a simple model of the reactor containment consisting of a large cylinder of air plus steam or water surrounded by concrete. The flux energy spectra at various radii in the containment were calculated to determine the radial variation of the spectra. For this purpose only the spectral shapes are of interest.

The calculational procedure used was to distribute the source throughout the containment volume and sample the particle spectrum crossing successively smaller, imaginary, concentric cylinders. The radii were reduced until the statistical uncertainty became unacceptably large. For the case of gamma rays in air, computations were done at 9 radii between 200 cm and 25 m.

It was found that the airborne source spectrum is somewhat perturbed by the interactions in the air-steam mixture and with the concrete wall. However, the radial variation of the spectrum is very slight. In general, the structure of the original source

spectra are smoothed. A few examples of the results are shown in Figure 5 for the case of Source 1 gamma rays at 1 minute (see Section 4.1 for a description of the sources used in this study). The slow radial variation of the shape of the perturbed spectra shown in Figure 5 suggests that the energy spectrum at the cable would not be very different wherever the cable is located in the containment (ignoring internal structure), except perhaps near the wall. Thus, the perturbed spectrum at the radius of 200 cm (the smallest feasible for these calculations) was used as the source term for the depth-dose calculations in the cable. Similar results obtained for the other gamma-ray sources in air.

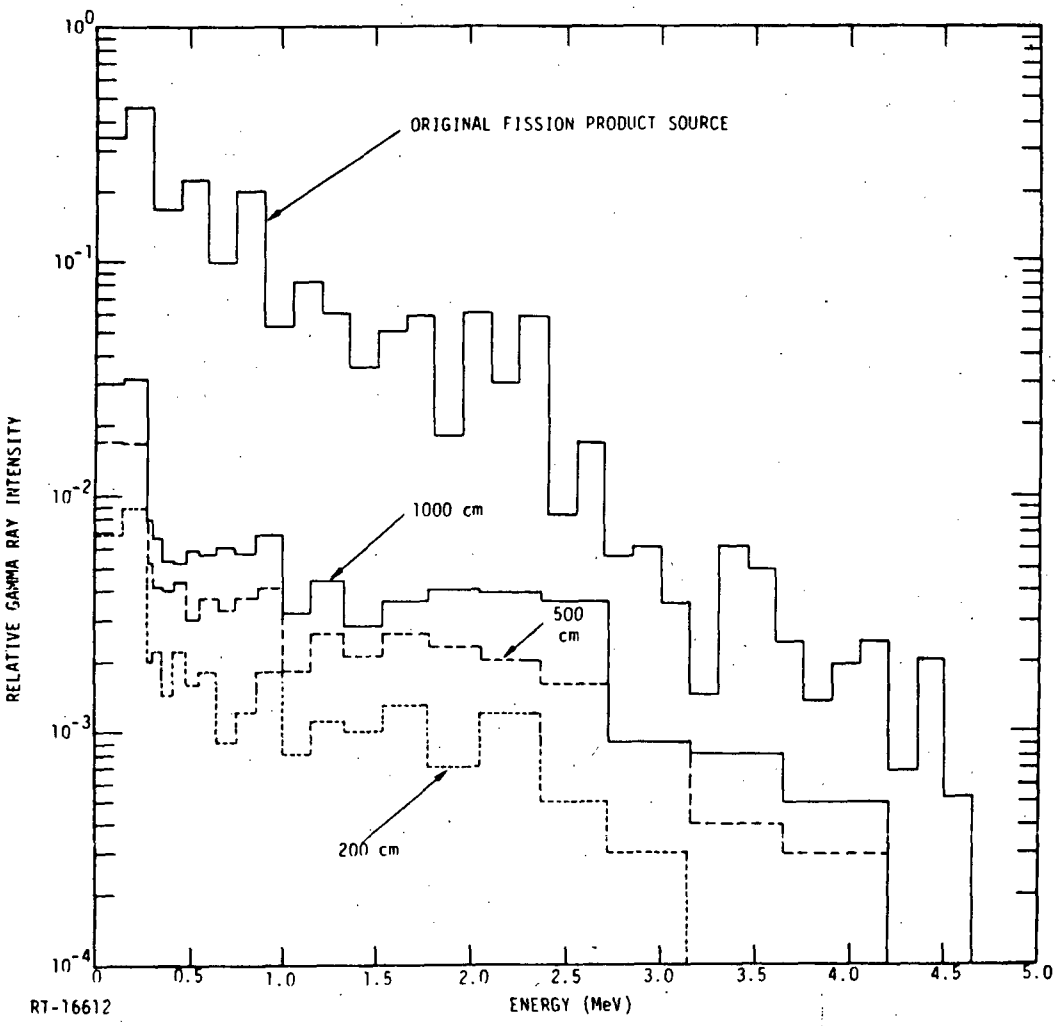

Figure 5. Original and perturbed gamma-ray spectra at various radii (1000 cm, 500 cm and 200 cm). The starting spectrum (labeled "fission product source") corresponds to airborne gamma rays at 1 minute. Only the shapes of spectra are significant for the present purposes.

The same type of procedure was used for the beta sources in air and for the gamma ray sources in water. Of course, the limited ranges of the latter sources permitted much smaller cylindrical regions to be used. At the same time, the perturbations to the original spectra are significantly greater. Figure 6 shows the original and perturbed spectra for waterborne gamma rays at several radii including the radius corresponding to the outer surface of the cable. Note that there is a much more significant softening of the spectrum due to interactions in the water.

An example of the air and steam attenuation on the beta system is displayed in Figure 7. As with the gamma rays, the shape of the spectrum is not rapidly varying with radial position in the containment. The perturbed spectra at the surface of the cable were used for subsequent depth-dose calculations.

For the case of beta particles in water, the range is sufficiently small for the most energetic betas (~3 cm) that normal Monte Carlo procedures can be utilized without approximation.

3.3 DOSE ENHANCEMENT

Several years ago it was observed that photon energy deposition profiles near the interface of materials of different atomic number showed significant enhancement (Ref 11). The physical explanation of this phenomenon is that secondary electrons originating in the high atomic number material are deposited in the adjacent low atomic number material producing a dose that far exceeds the energy deposited by direct photon interactions. The effect is sensitive to many parameters including direction and energy of the incident photon beam and the atomic numbers of the materials. The importance of the phenomenon lies in the fact that dose enhancements of two orders of magnitude or more can be obtained.

Since its discovery there has been extensive study of dose enhancement effects particularly as they relate to electronic devices. Much study has been devoted to developing methods to accurately predict the doses near interfaces (Ref 12). By and large this has been successful, with both analytical and Monte Carlo codes shown to be satisfactory for most purposes. The key to properly accounting for dose enhancement is proper treatment of all secondary radiation transport and energy deposition processes. The code that has proved to be the most effective, and thus used as a benchmark for comparisons with other simpler codes, is SANDYL. Thus, for the work reported here, carried out exclusively with SANDYL, the phenomenon of dose enhancement is correctly included in the energy deposition results.

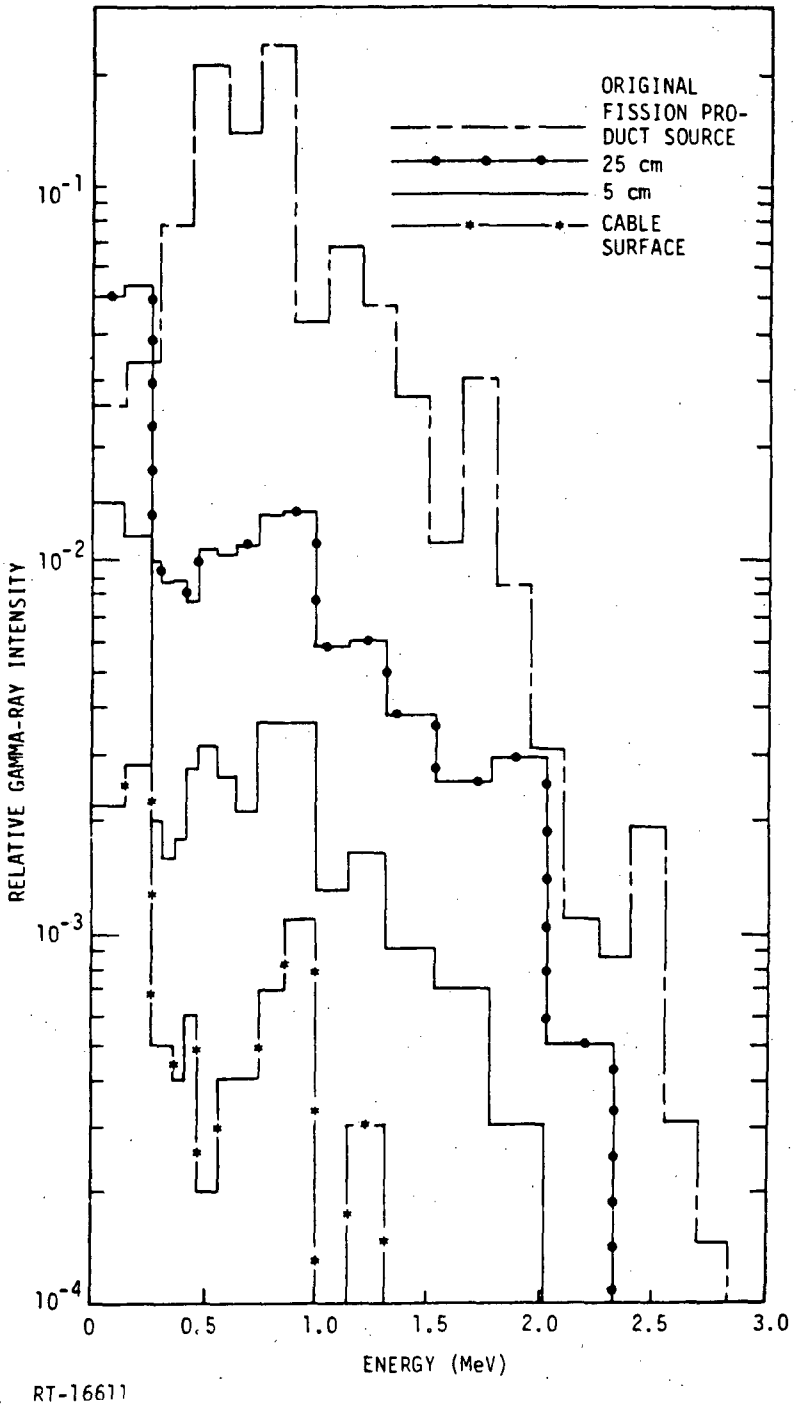

Figure 6. Original and perturbed waterborne gamma ray spectra (Source 1 at 1 minute) at various radii.

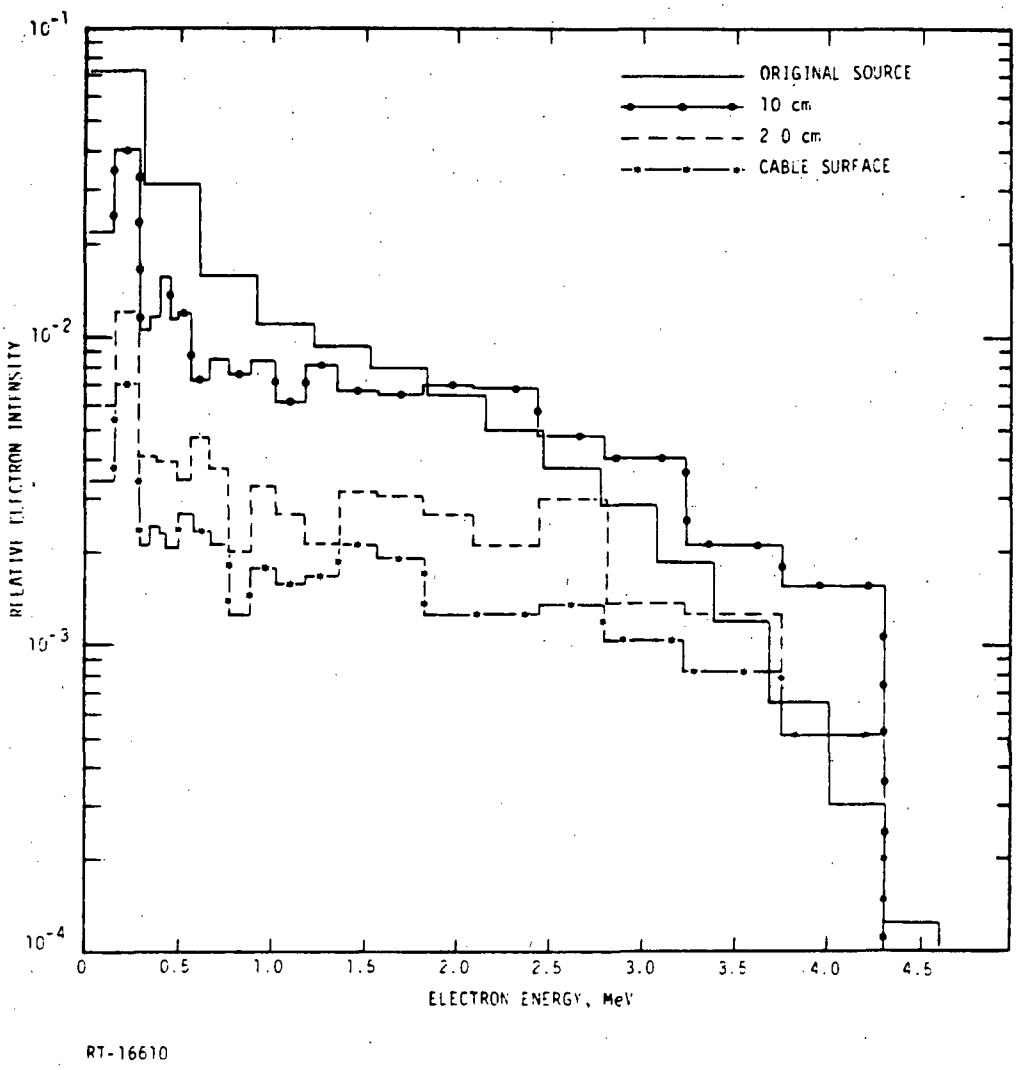

Figure 7. Original and perturbed airborne beta spectra (Source 1 at 1 minute) at various radii

3.4 UNCERTAINTIES

There are several types of uncertainty associated with the calculations of energy and charge deposition reported here. The easiest to understand is the statistical uncertainty associated with the Monte Carlo sampling processes. It is obtained by repeating the calculations with identical numbers of histories, and computing the standard deviation of the mean of the distribution of values of the quantity tallied. For the calculations reported here ten samples were used to determine the mean and standard deviation.

Error bars representing the one standard deviation uncertainties are shown on all depth-dose calculations. For nearly all the calculations with gamma ray sources the uncertainties are less than 10 percent with most regions being less than 5 percent. The exceptions are the few innermost regions of the copper where uncertainties become as high as 30 percent in some cases. For the beta sources the large attenuation in the outer region means that very little energy reaches the interior of the cable. Consequently, for the beta calculations the uncertainties in the energy deposition in the copper, where the fluence has dropped by three orders of magnitude or more, are sometimes ±50 percent or more. It is possible that biasing techniques could be used to improve this situation, but they were not utilized in this study. However, it is very unlikely that any of the conclusions reached would be altered by improvements in the accuracy of the dose at the interior of the cable.

A more vaporous contribution to the uncertainty of the results has to do with the modeling and computational methods employed. These are very difficult to estimate. Sometimes, a rough idea of the magnitude of this error can be obtained by sensitivity analysis, the procedure by which one determines how sensitive a calculated result is to alterations of the model or changes in an approximation. A serious limitation to this approach is that often the most significant approximations are the result of inherent limitations of the calculational tools and cannot be eliminated. In a few cases model sensitivity was investigated in this study. For example, the use of approximate methods to handle the spatially extended sources resulted from the inability of the calculational procedures to handle this type of source efficiently. An effort to understand qualitatively the uncertainty introduced by this approximation was made by performing a "brute-force" calculation. This consisted of a dose versus depth calculation for the cable with an exact treatment of the airborne (i.e., a uniform spatial distribution of isotropic point sources) rather than using the perturbed sources developed here.

In order to get any results with the "brute-force" model it was necessary to reduce the size of the air-steam region surrounding the cable from a thickness of 25 m to 2 m. For thicknesses larger than 2 m the solid angle subtended by the cable is too small to get useful information without excessive use of computer time. This, of course, introduces an additional approximation and complicates the interpretation of the results. A discussion of these results is given in subsection 6.2.

Suggestions for additional work along these lines are described in subsection 7.3. However, no quantitative assessment of the magnitude of the modeling errors has been included, and the error bars shown on the figures represent only the statistical part of the uncertainty.

4. RESULTS FOR LOCA SOURCES

4.1 SOURCE SELECTION

Selections from the source spectra calculated in Phase 3 were made for the depth-dose studies in the model cable. The low power (1 watt) results for an equilibrium irradiation for Sources 1 and 2 which included all daughters but did not include capture and depletion effects were used. Cooling times which produced the hardest (i.e., highest average energy) and softest spectra were selected in order to study the bounding conditions. The hardest spectrum occurs at the shortest cooling time. As a matter of practicality, the very short cooling times are not expected to be accurate since a significant number of nuclides which contribute to the energy release at short times do not have spectral data in the library. Therefore, the one-minute cooling time data were selected for the hard spectrum. The softest spectrum (i.e., lowest average energy) occurs between 1 and 10 days depending on the type of source; the 4-day results were selected. Thus, for each source and each distribution category depth-dose calculations were carried out at two times for betas and gammas. For convenience, the spectra used for the calculations reported in the next section are reproduced from Reference 2 in Tables 1 through 3.

4.2 DEPTH-DOSE CALCULATIONS

Results of the depth-dose calculations in the model cable are given in Figures 8 through 20 for the airborne, plate-out, and waterborne sources at 1 minute and 4 days cooling. The results are expressed in rads (1 rad = 10^{-2} Gy) per source particle incident on a ten-meter length of cable, where the source particles have been sampled from the input (perturbed) spectral distributions. For most of the calculations 2×10^4 histories were tracked for each source. For scaling purposes note that the doses can be expressed per unit incident fluence. Since the surface area of a ten-meter segment of the model cable is 7102.5 cm^2, one particle per ten-meter segment represents a fluence of 1.408×10^{-4} particles/cm^2. To scale the depth-dose results presented here to a specified particle fluence, ϕ, one multiplies the doses by $\phi/1.408 \times 10^{-4}$. For example,

AIRBORNE SOURCE SPECTRA

EQUILIBRIUM, 1-WATT, PURE U-235
(NUMBER/SEC)

GROUP NO.	UPPER EDGE ENERGY (MEV)	SOURCE 1 GAMMAS 1 MINUTE	SOURCE 1 GAMMAS 4 DAYS	SOURCE 1 BETAS 1 MINUTE	SOURCE 1 BETAS 4 DAYS	SOURCE 2 GAMMAS 1 MINUTE	SOURCE 2 GAMMAS 4 DAYS	SOURCE 2 BETAS 1 MINUTE	SOURCE 2 BETAS 4 DAYS
1	.15	3,374+09	9,355+08			3,441+08	8,196+07		
2	.30	4,654+09	4,313+07	6,377+09	1,156+09	5,452+08	5,539+06	7,778+08	1,481+08
3	.45	1,674+09	2,382+08			2,174+08	3,979+07		
4	.60	2,274+09	3,642+07	2,794+09	5,289+07	3,030+08	6,141+06	3,782+08	1,297+07
5	.75	9,907+08	2,663+07			1,595+08	4,449+06		
6	.90	2,010+09	2,387+06	1,456+09	3,802+06	3,417+08	3,982+05	1,913+08	8,399+05
7	1.05	5,332+08	5,450+05			7,303+07	7,649+02		
8	1.20	8,207+08	1,975+05	1,017+09	7,998+05	1,135+08	3,301+04	1,213+08	1,703+05
9	1.35	5,972+08	1,427+06			9,857+07	2,384+05		
10	1.50	3,491+08	3,362+03	8,650+08	1,031+04	4,582+07	5,613+02	9,580+07	2,056+03
11	1.65	5,022+08	1,892+04			5,514+07	1,650+03		
12	1.80	6,764+08	7,410+03	9,397+08	9,085+01	7,980+07	1,238+03	7,978+07	1,299+01
13	1.95	1,810+08	3,123+02			2,266+07	5,216+01		
14	2.10	6,145+08	2,625+02	9,982+08	2,124+01	6,312+07	8,386+01	6,385+07	2,697+00
15	2.25	2,980+08	7,039-02			3,012+07	5,881-03		
16	2.40	5,818+08	1,427+02	8,605+08	2,834+00	6,018+07	1,193+01	8,888+07	3,111-01
17	2.55	8,326+07	5,816+02			1,023+07	4,864+01		
18	2.70	1,669+08	3,085-03	9,524+08	8,718-01	1,790+07	2,577-04	3,743+07	5,048-02
19	2.85	5,589+07	3,384-04			5,588+06	2,827-05		
20	3.00	6,111+07	1,126+01	9,641+08	1,255-02	6,796+06	9,414-01	2,810+07	1,343-03
21	3.15	3,568+07	3,753+00			3,566+06	3,138-01		
22	3.30	1,448+07	3,827-04	1,846+08	2,868-03	1,448+06	3,197-05	1,963+07	3,069-04
23	3.45	6,159+07	9,631-08			6,156+06	8,046-09		
24	3.60	4,930+07	2,000-04	1,158+08	2,422-03	4,927+06	1,671-05	1,231+07	2,592-04
25	3.75	2,449+07	3,704-06			2,447+06	3,094-07		
26	3.90	1,341+07	2,058-17	6,356+07	1,953-03	1,341+06	1,720-18	6,760+06	2,089-04
27	4.05	1,966+07	1,975-05			1,965+06	1,650-06		
28	4.20	2,442+07		3,000+07	1,450-03	2,440+06		3,203+06	1,551-04
29	4.35	6,776+06				6,772+05			
30	4.50	2,042+07		1,268+07	9,491-04	2,041+06		1,354+06	1,015-04
31	4.65	5,274+06				5,271+05			
32	4.80	4,733+05		6,183+06	5,022-04	4,730+04		6,494+05	5,373-05
33	4.95	4,847+04				4,848+03			
34	5.10	8,364+05		2,965+06	1,682-04	8,360+04		3,039+05	1,800-05
35	5.25	2,217+06				2,216+05			
36	5.40	1,409+06		1,459+06	1,247-05	1,408+05		1,495+05	1,334-06
37	5.70			4,326+05				6,523+04	
38	6.00			2,353+05				2,431+04	
39	6.30			3,837+04				3,958+03	
40	6.60			5,066+02				5,086+01	
41	6.90			2,938+02				2,949+01	
42	7.20			1,312+02				1,317+01	
43	7.50			2,939+01				2,951+00	

TABLE 1

PLATE-OUT SOURCE SPECTRA

EQUILIBRIUM, 1-WATT, PURE U-235
(NUMBER/SEC)

GROUP NO.	UPPER EDGE ENERGY (MEV)	SOURCE 1 GAMMAS 1 MINUTE	SOURCE 1 GAMMAS 4 DAYS	SOURCE 1 BETAS 1 MINUTE	SOURCE 1 BETAS 4 DAYS	SOURCE 2 GAMMAS 1 MINUTE	SOURCE 2 GAMMAS 4 DAYS	SOURCE 2 BETAS 1 MINUTE	SOURCE 2 BETAS 4 DAYS
1	.15	1.877+08	5.927+07			1.397+07	5.354+06		
2	.30	2.777+08	2.137+07	1.337+09	3.350+08	3.430+07	2.722+06	1.863+08	3.307+07
3	.45	4.851+08	1.417+08			7.744+07	2.797+07		
4	.60	8.832+08	4.303+07	9.140+08	7.993+07	1.523+08	4.196+06	1.391+08	6.755+06
5	.75	7.657+08	5.166+07			1.219+08	3.127+06		
6	.90	1.545+09	4.405+07	5.799+08	2.815+07	2.834+08	2.795+05	8.552+07	7.887+05
7	1.05	2.950+08	2.933+06			3.975+07	4.352+02		
8	1.20	3.456+08	5.882+05	3.030+08	1.438+07	6.331+07	2.320+04	4.006+07	1.871+05
9	1.35	4.262+08	1.082+06			7.831+07	1.676+05		
10	1.50	1.678+08	7.376+05	1.639+08	7.126+06	2.201+07	3.943+02	1.866+07	2.103+03
11	1.65	8.207+07	1.808+07			9.964+06	9.728+01		
12	1.80	1.346+08	1.796+04	1.077+08	4.245+06	2.458+07	8.701+02	1.149+07	7.207+00
13	1.95	5.615+07	9.482+04			9.206+06	3.665+01		
14	2.10	2.382+07	1.317+05	7.414+07	2.443+06	3.434+06	3.083+01	7.897+06	9.375-01
15	2.25	1.491+07	1.657+05			6.716+05	9.452-08		
16	2.40	2.693+07	1.625+05	5.141+07	1.163+06	4.089+06	1.612-02	5.524+06	1.731-02
17	2.55	2.520+07	5.856+05			3.854+06	6.573-02		
18	2.70	2.004+07	3.108+01	3.791+07	5.151+05	2.461+06	6.317-21	4.278+06	6.670-09
19	2.85	2.885+06	5.979+01			3.586+03	4.594-21		
20	3.00	8.502+06	1.126+04	2.786+07	1.102+05	1.387+06	1.272-03	3.294+06	1.076-09
21	3.15	1.386+06	3.745+03			1.307+03	4.240-04		
22	3.30	6.005+05	2.959-01	1.934+07	1.441+04	7.568+02	2.642-21	2.294+06	2.120-21
23	3.45	2.921+06	2.959-01			1.191+03	3.905-21		
24	3.60	3.216+06	1.609-11	1.217+07	1.580+03	5.804+02		1.417+06	1.382-21
25	3.75	9.952+05	3.753-13			1.965+02			
26	3.90	5.523+05	8.421-15	6.996+06	3.655+00	1.738+02		7.884+05	7.509-22
27	4.05	7.692+04				1.290+02			
28	4.20	1.780+06		3.660+06	1.849-02	5.316+01		3.981+05	3.115-22
29	4.35	4.106+05				2.836+01			
30	4.50	1.357+06		1.722+06	1.679-10	3.709+01		1.685+05	
31	4.65	3.724+05				5.890+01			
32	4.80	1.587+04		7.957+05	8.882-11	8.726+00		5.960+04	
33	4.95	3.948+03				8.726+00			
34	5.10	6.366+04		3.235+05	2.976-11	8.726+00		1.302+04	
35	5.25	1.699+05							
36	5.40	1.080+05		1.481+05	2.205-12			6.376+03	
37	5.55	2.490+04							
38	5.70	8.870+00		6.950+04				3.570+03	
39	5.85	1.380+00							
40	6.00	3.220+00		2.836+04				1.429+03	
41	6.30			6.333+03				2.195+02	
42	6.60			1.344+03					
43	6.90			5.677+02					
44	7.20			1.152+02					
45	7.50			2.551+00					

TABLE 2

TABLE 3

WATERBORNE SOURCE SPECTRA

EQUILIBRIUM, 1-WATT, PURE U-235
(NUMBER/SEC)

GROUP NO.	UPPER EDGE ENERGY (MEV)	SOURCE 1 GAMMAS 1 MINUTE	SOURCE 1 GAMMAS 4 DAYS	SOURCE 1 BETAS 1 MINUTE	SOURCE 1 BETAS 4 DAYS	SOURCE 2 GAMMAS 1 MINUTE	SOURCE 2 GAMMAS 4 DAYS	SOURCE 2 BETAS 1 MINUTE	SOURCE 2 BETAS 4 DAYS
1	.15	2,591+08	8,600+07			2,846+07	1,071+07		
2	.30	4,529+08	3,487+07	2.355+09	5,034+08	6,952+07	5,445+06	3,913+08	6,615+07
3	.45	8,806+08	2,798+08			1,567+08	5,593+07		
4	.60	1,653+09	6,394+07	1,704+09	1,142+08	3,065+08	8,392+06	2,980+08	1,351+07
5	.75	1,423+09	6,744+07			2,535+08	6,255+06		
6	.90	3,064+09	4,583+07	1,098+09	3,190+07	5,873+08	5,591+05	1,897+08	1,577+06
7	1.05	8,092+08	2,963+06			8,272+07	8,706+02		
8	1.20	6,670+08	6,668+05	5,867+08	1,517+07	1,277+08	4,641+04	9,692+07	3,742+05
9	1.35	8,357+08	1,911+06			1,603+08	3,352+05		
10	1.50	4,366+08	7,466+05	3,304+08	7,042+06	7,554+07	7,886+02	5,194+07	4,207+03
11	1.65	1,911+08	1,825+07			3,170+07	1,946+02		
12	1.80	2,626+08	2,239+04	2,253+08	4,188+06	5,021+07	1,740+03	3,497+07	1,443+01
13	1.95	1,276+08	9,590+04			2,346+07	7,331+01		
14	2.10	5,042+07	1,331+05	1,581+08	2,410+06	8,748+06	6,166+01	2,464+07	1,882+00
15	2.25	2,050+07	1,673+05			1,800+06	5,877-06		
16	2.40	5,496+07	1,640+05	1,090+08	1,148+06	9,692+06	3,224-02	1,701+07	3,698-02
17	2.55	5,493+07	5,911+05			9,790+06	1,315-01		
18	2.70	4,172+07	3,137+01	8,112+07	5,082+05	6,791+06	2,008-07	1,290+07	3,570-04
19	2.85	2,059+07	6,036+01			3,514+06	2,203-08		
20	3.00	1,762+07	1,137+04	6,306+07	1,088+05	3,209+06	2,545-03	1,031+07	2,038-06
21	3.15	5,396+06	3,781+03			7,976+05	8,481-04		
22	3.30	4,120+06	2,987-01	4,719+07	1,421+04	6,987+05	2,491-08	7,839+06	3,780-07
23	3.45	7,651+06	2,988-01			9,421+05	1,080-11		
24	3.60	3,444+06	6,363-08	3,315+07	1,559+03	5,021+04	1,302-08	5,585+06	3,175-07
25	3.75	1,108+06	1,179-09			2,386+04	2,411-10		
26	3.90	6,152+05	8,501-15	2,234+07	3,606+00	1,342+04	1,149-21	3,831+06	2,556-07
27	4.05	1,061+07	6,286-09			2,087+06	1,286-09		
28	4.20	1,675+07		1,471+07	1,825-02	2,967+06		2,586+06	1,898-07
29	4.35	4,420+05				6,807+03			
30	4.50	1,484+06		9,468+06	6,492-07	2,708+04		1,699+06	1,242-07
31	4.65	4,045+05				6,937+03			
32	4.80	1,777+04		6,213+06	3,435-07	4,079+02		1,129+06	6,573-08
33	4.95	3,966+03				1,780+01			
34	5.10	6,885+04		4,044+06	1,151-07	1,126+03		7,467+05	2,202-08
35	5.25	1,843+05				3,105+03			
36	5.40	1,172+05		2,515+06	8,528-09	1,974+03		4,730+05	1,632-09
37	5.55	5,021+06				9,896+05			
38	5.70			1,326+06				2,513+05	
39	6.00			5,341+05				1,011+05	
40	6.30			2,111+05				4,057+04	
41	6.60			1,207+05				2,353+04	
42	6.90			5,506+04				1,082+04	
43	7.20			1,343+04				2,623+03	
44	7.50			2,232+02				4,347+01	

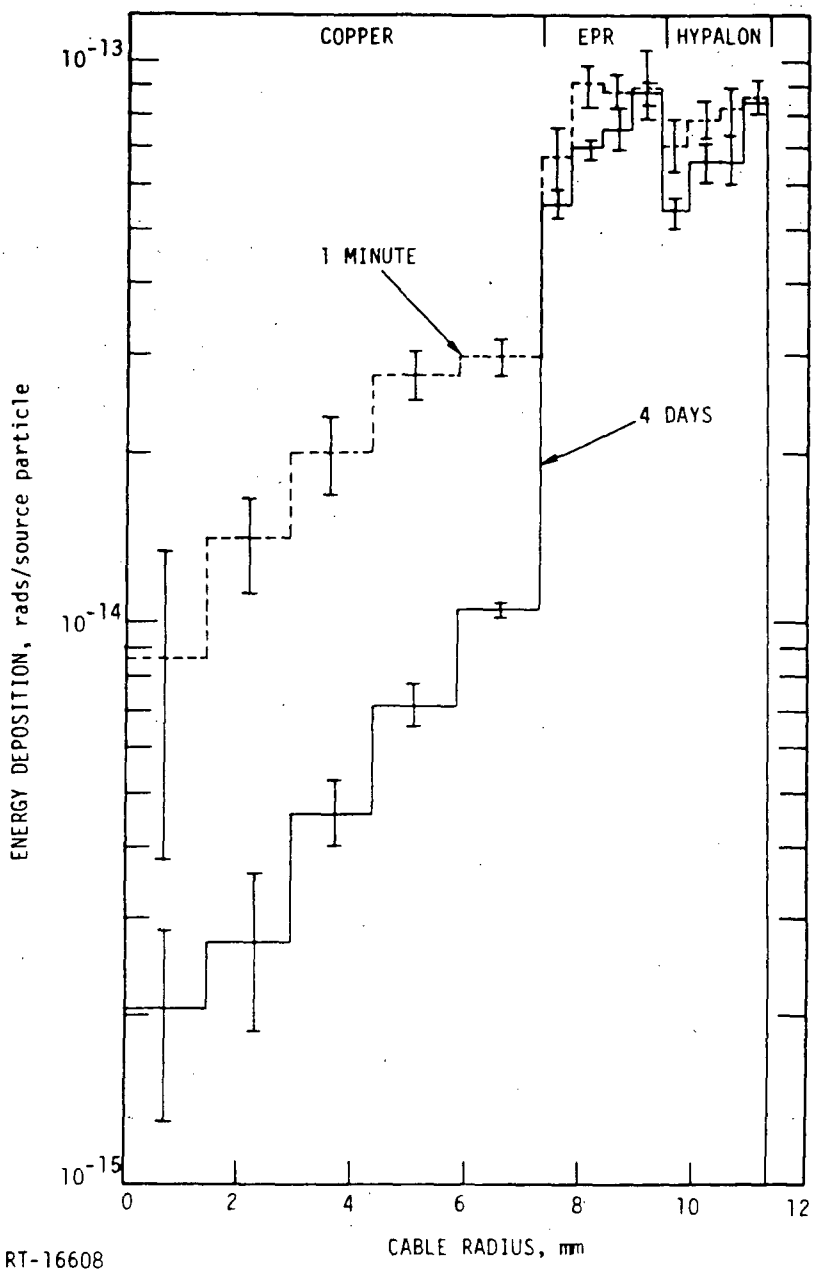

Figure 8. Depth-dose calculations for airborne gamma rays on the cable (Source 1 at 1 minute and at 4 days)

to determine the dose for an incident fluence on the cable of 10 photons/cm^2, multiply by $10/1.408 \times 10^{-4} = 71025$.

It may be seen that the largest dose is in the jacket and insulation materials. For the gamma ray sources the dose in the conductor is 5 to 10 times smaller than in the insulator and jacket. For the beta sources the dose is two or more orders of magnitude less in the conductor than at the surface. The airborne gamma-ray source calculations

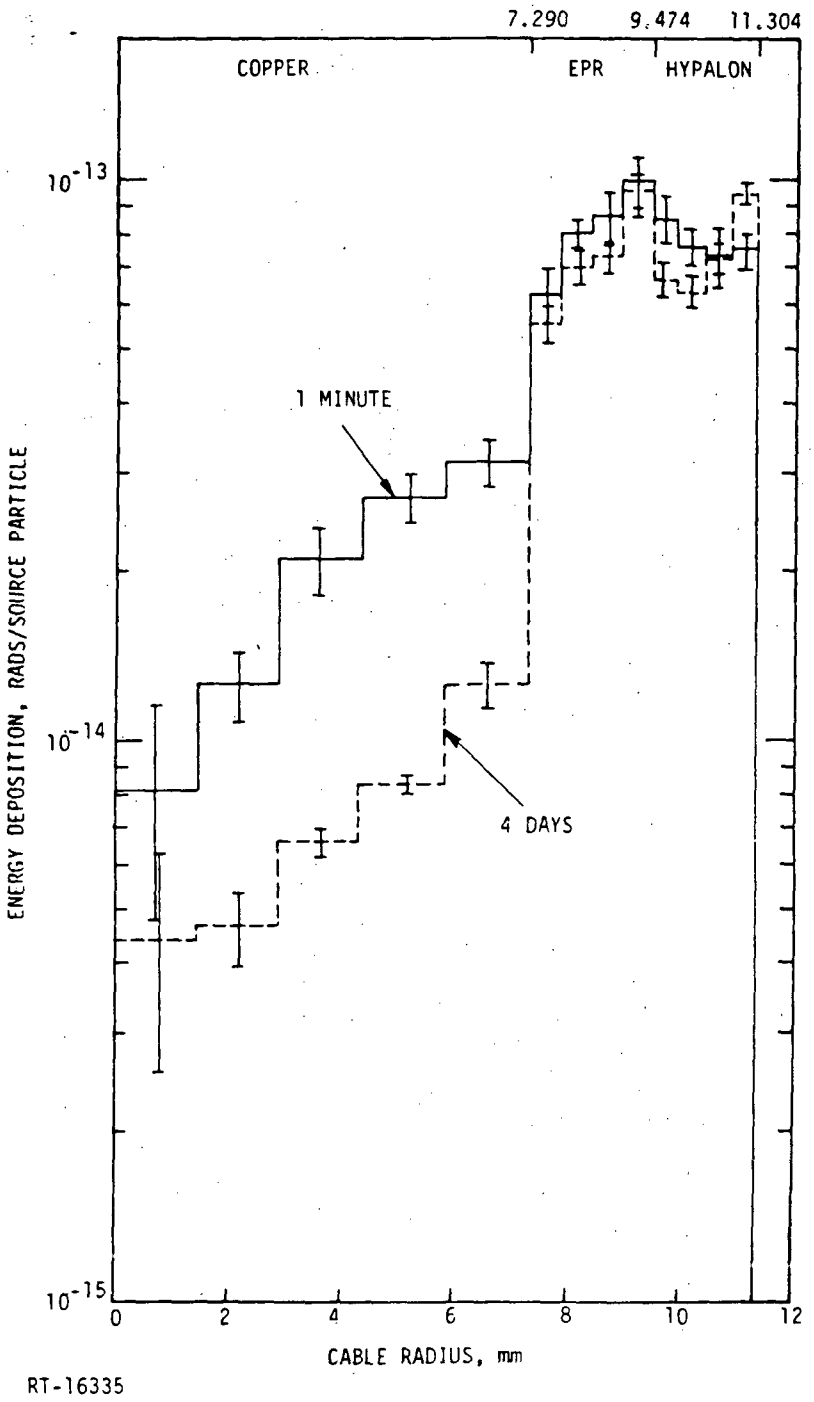

Figure 9. Depth-dose calculations for airborne gamma rays on the cable (Source 2)

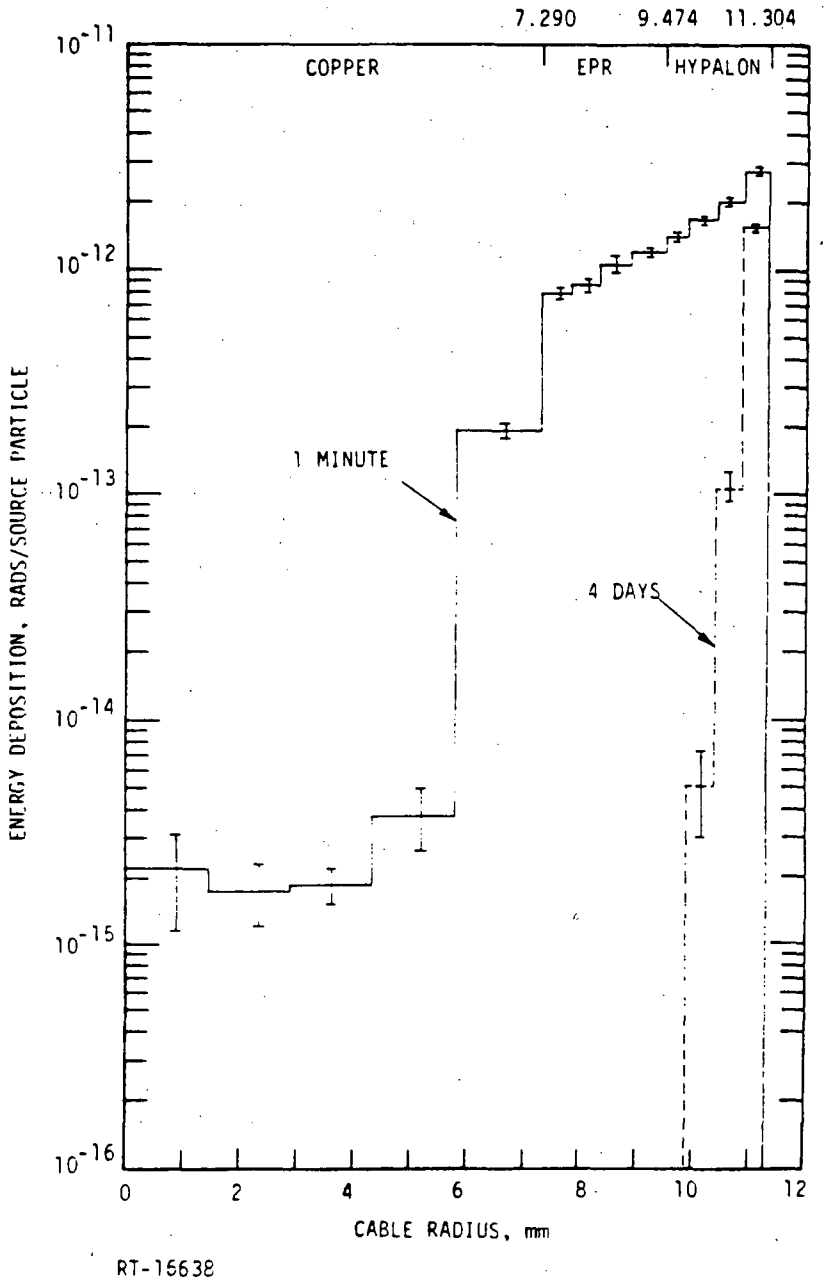

Figure 10. Depth-dose calculations for airborne betas on cable (Source 1)

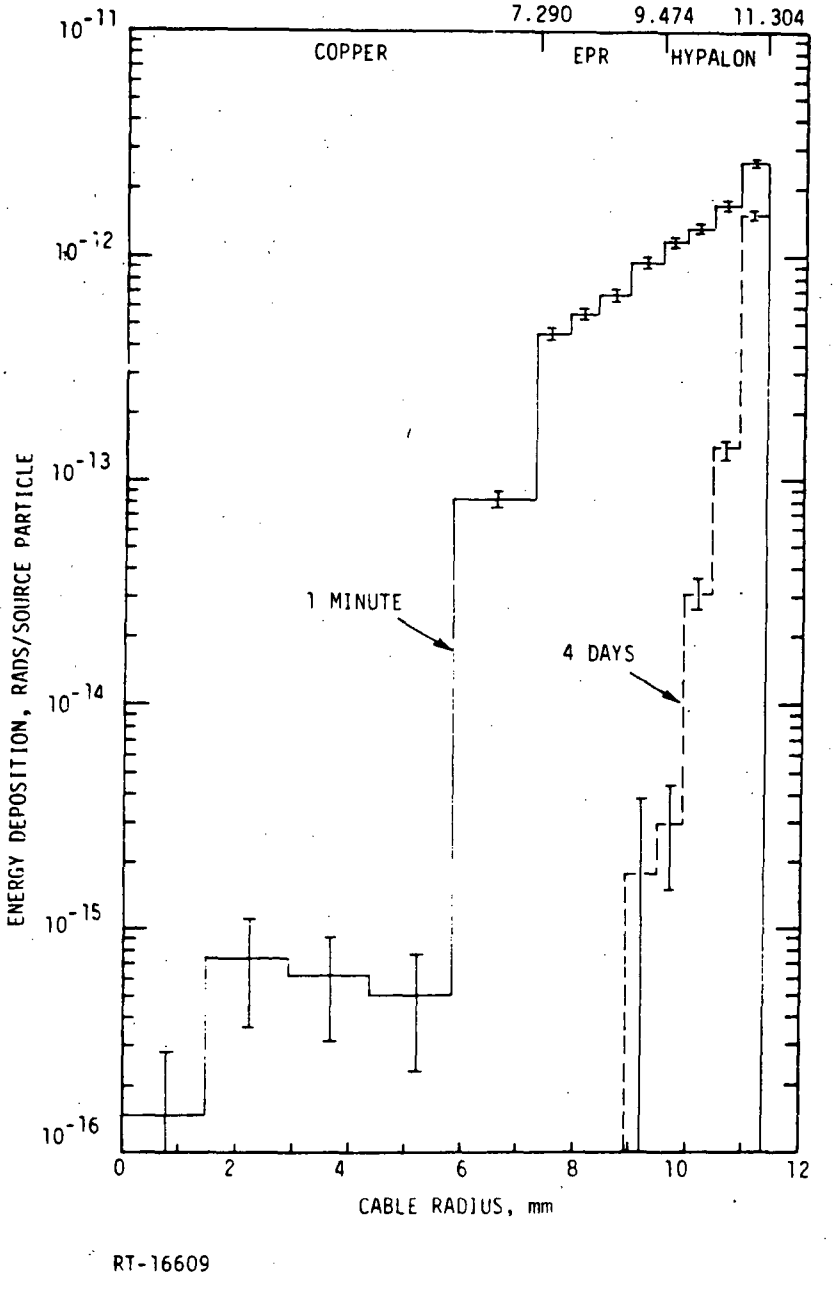

Figure 11. Depth-dose calculations for airborne betas on cable (Source 2)

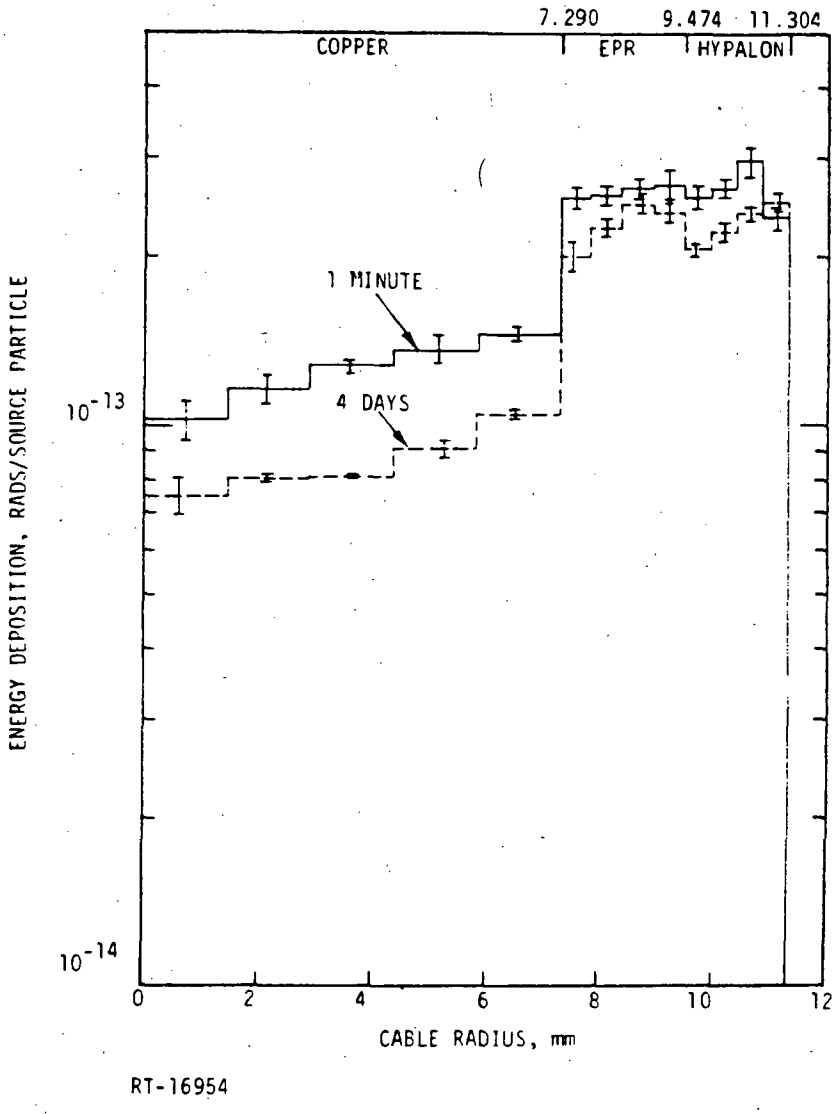

Figure 12. Depth-dose calculations for plate-out gamma-ray sources on cable (Source 1)

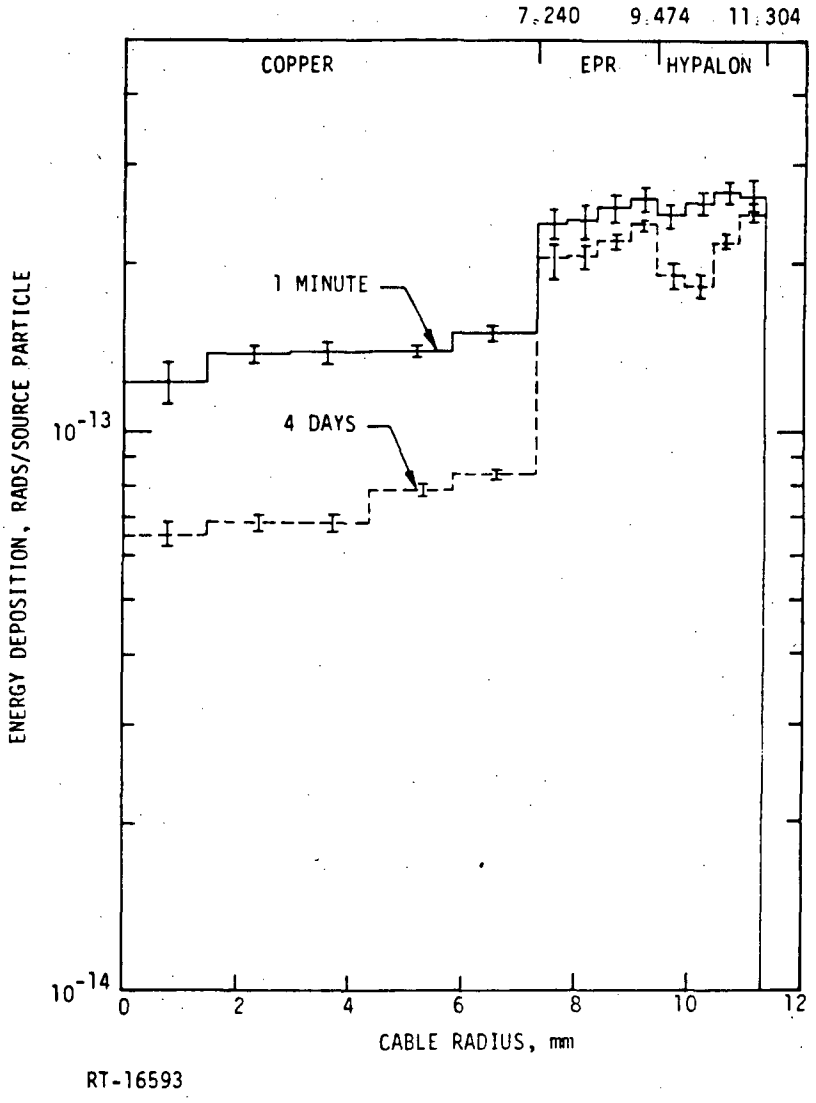

Figure 13. Depth-dose calculations for plate-out gamma-ray sources on cable (Source 2)

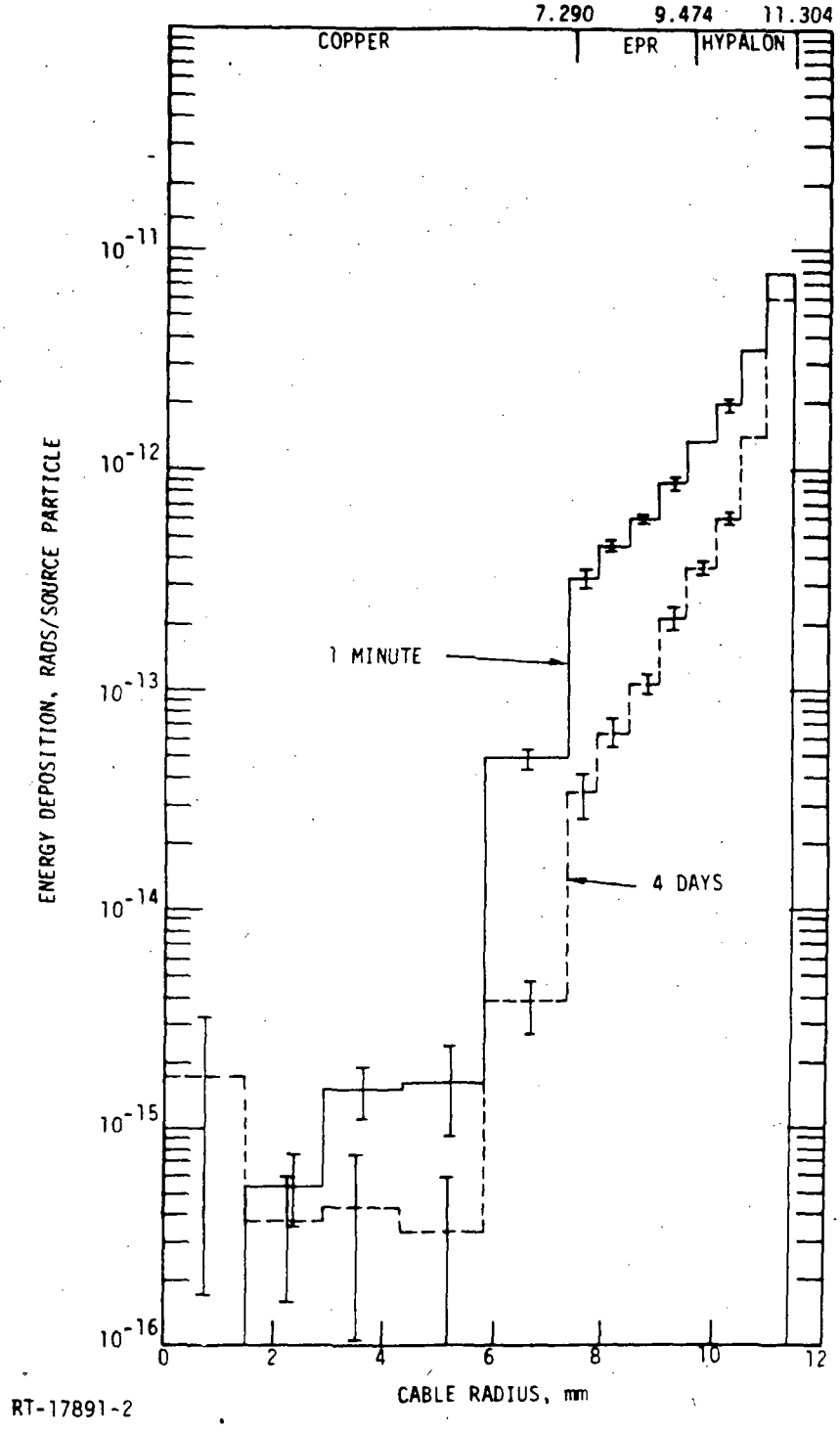

Figure 14. Depth-dose calculations for plate-out beta sources on cable (Source 1)

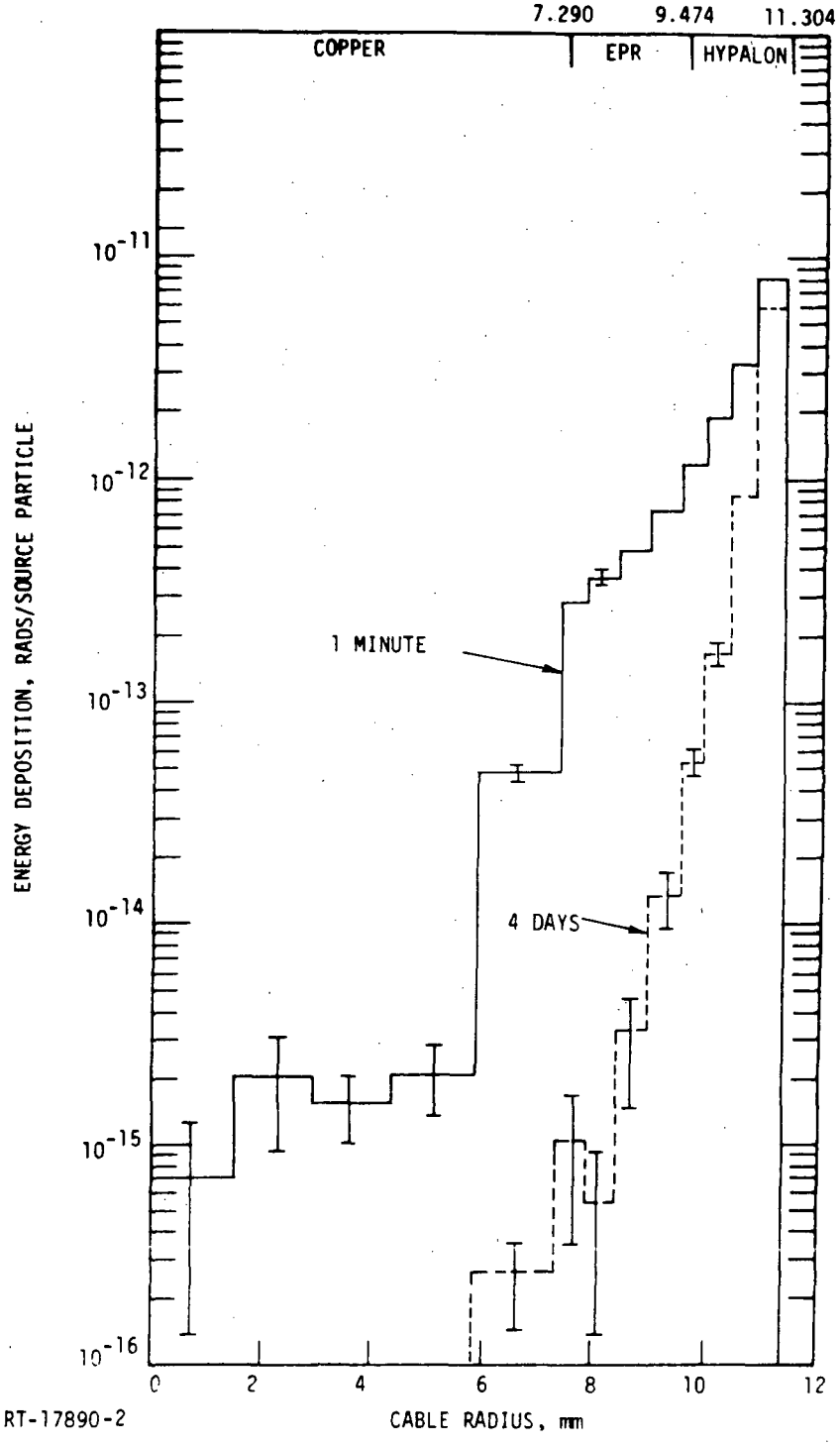

Figure 15. Depth-dose calculations for plate-out beta sources on cable (Source 2)

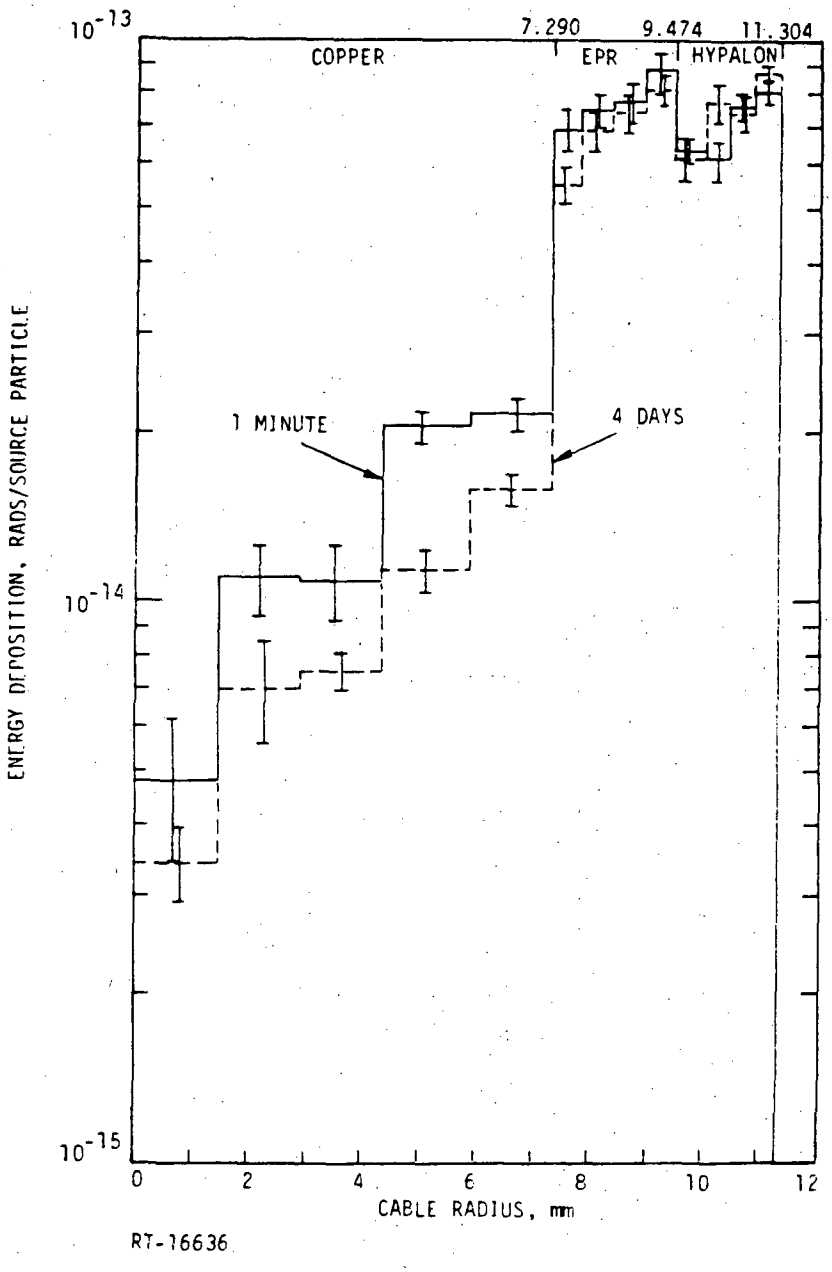

Figure 16. Depth-dose calculations for waterborne gamma-ray sources (Source 1)

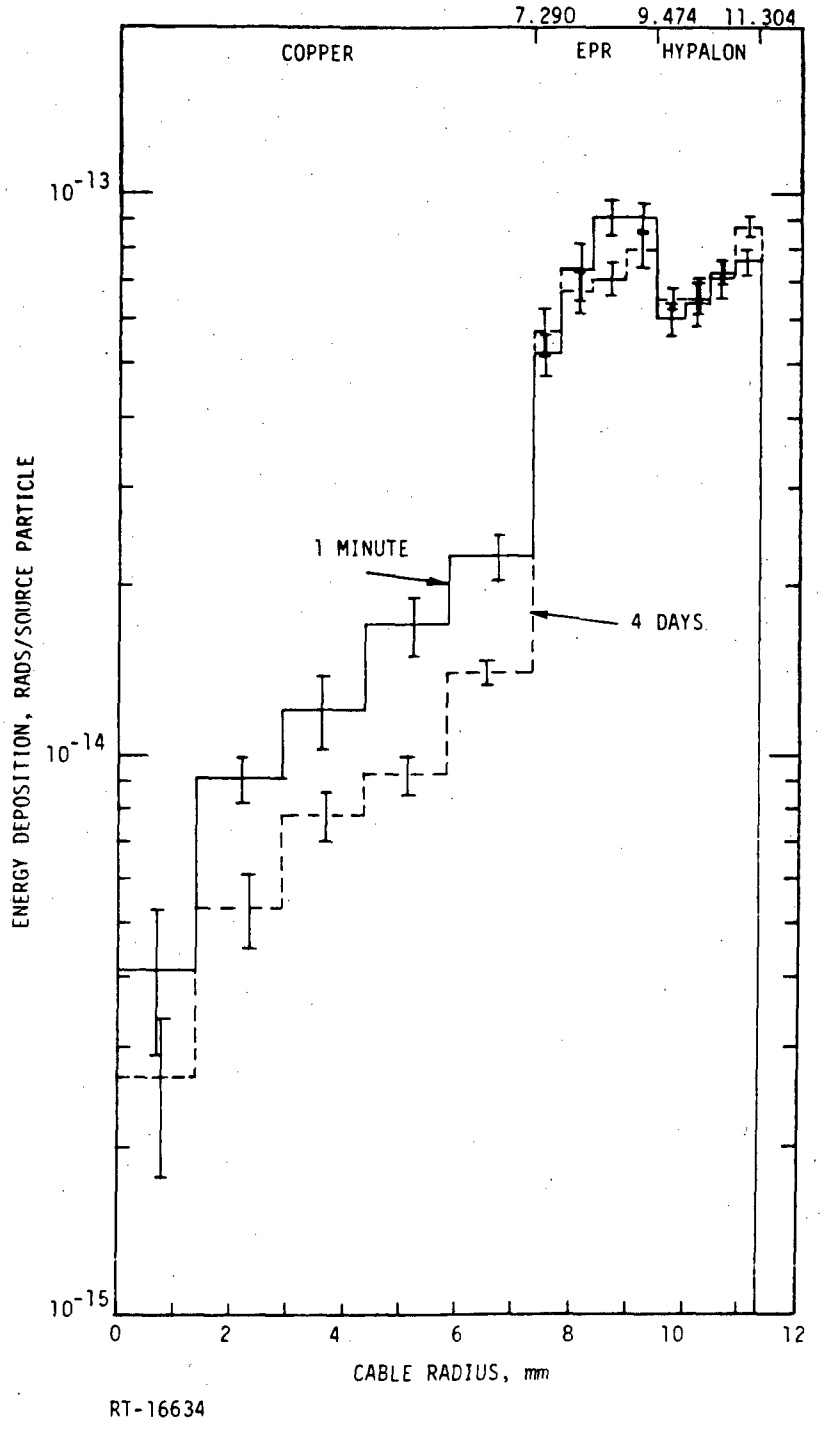

Figure 17. Depth-dose calculations for waterborne gamma-ray sources (Source 2)

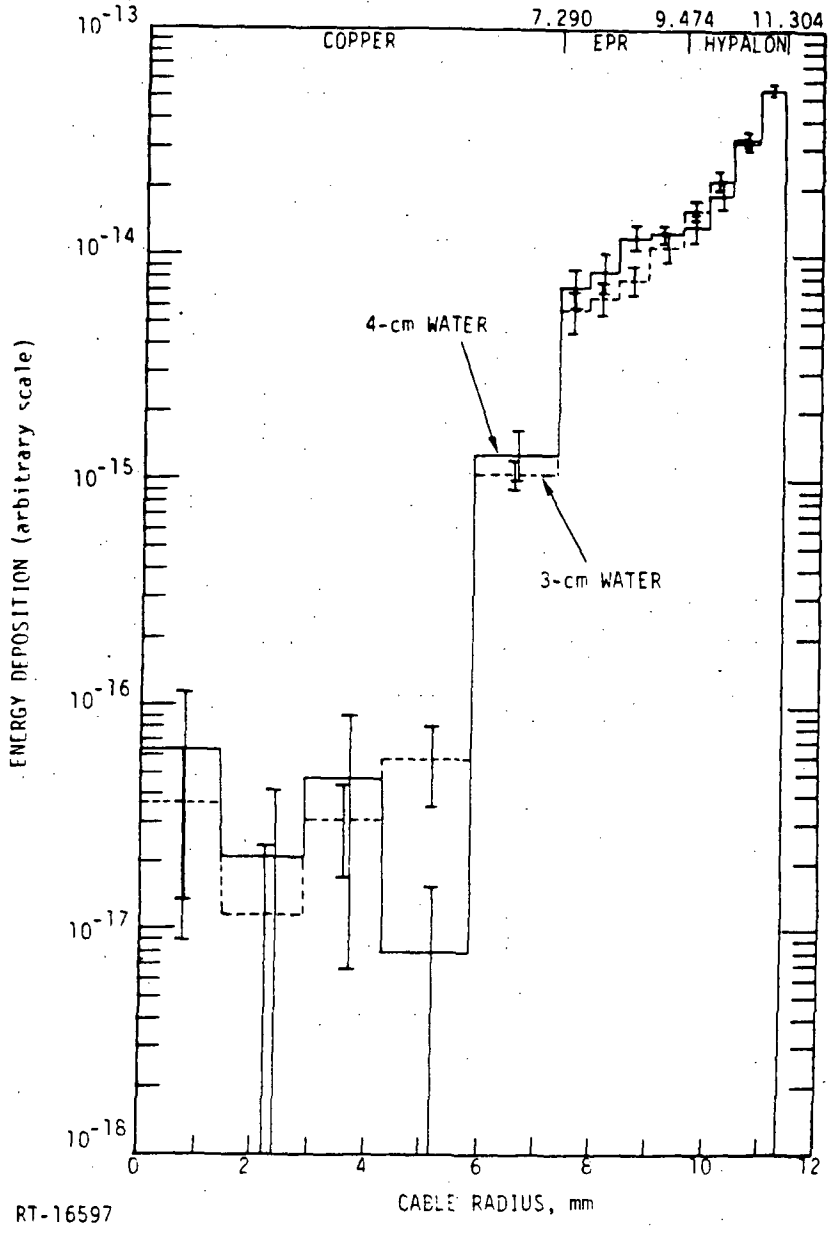

Figure 18. Comparison of two thicknesses of water layer on depth-dose results for waterborne beta spectrum at 1 minute (Source 1)

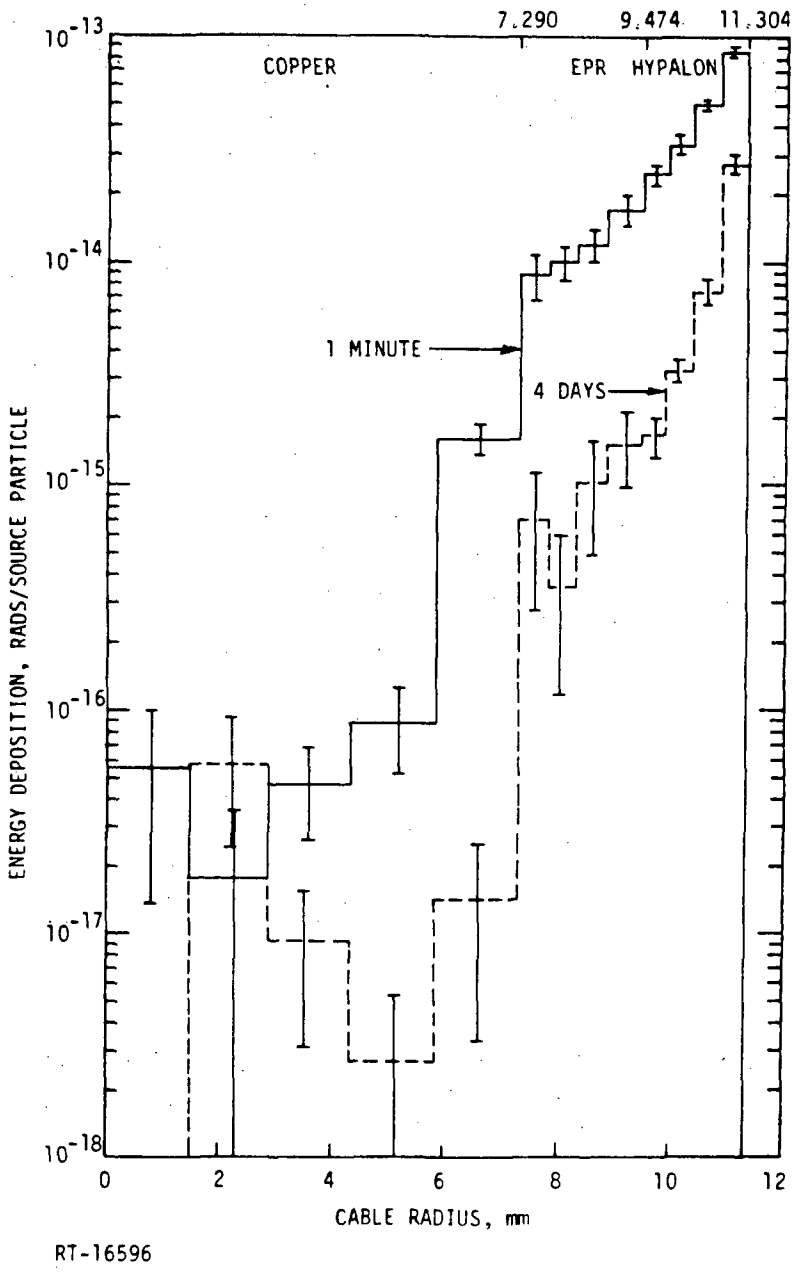

Figure 19. Depth-dose calculations for waterborne beta sources (Source 1)

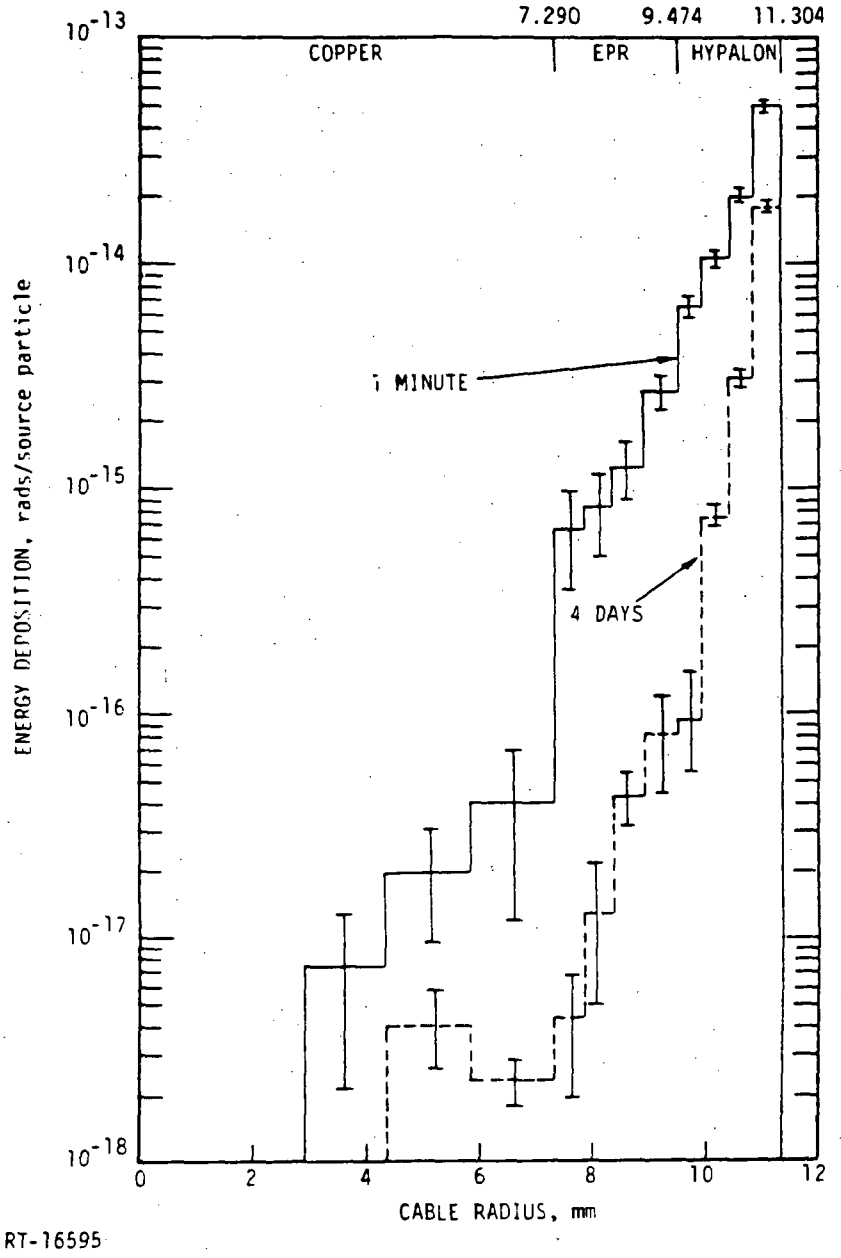

Figure 20. Depth-dose calculations for waterborne beta sources (Source 2)

shown in Figures 8 and 9 display little difference in the jacket and insulator for 1 minute and 4 days cooling in spite of the fact that the spectra are quite different. There is a large difference, however, in the energy deposited in the conductor between these two cases.

The results for the airborne beta sources, shown in Figures 10 and 11, are dramatically different for the two cooling times. The very soft betas at 4 days do not penetrate the insulator, depositing most of their dose in the surface layer of Hypalon.

For the case of the plate-out sources, the sources were assumed to be deposited on the surface of the cable. The results are shown in Figures 12 and 13 for the two gamma ray sources, and in Figures 14 and 15 for the beta sources. Again we find a dramatically different shape for the depth-dose profile for gamma rays and beta particles. The betas lose most of their energy in the first few layers of the jacket, whereas the gamma rays produce fairly uniform dose in both the jacket and insulator.

The results for waterborne gamma ray sources are shown in Figures 16 and 17. The observed profile is similar to the airborne and plate-out cases.

For beta particle sources distributed in water the range is relatively small which means that straightforward Monte Carlo calculations are feasible. Using the range of a 6 MeV beta particle as a limiting dimension, the thickness of the water layer surrounding the cable was taken to be 3 cm. This is a very conservative overestimate since there are very few betas at 6 MeV or higher in the source spectra. For the worst case - that is, the case where the spectra have the most high energy beta particles (Source 1 at 1 minute) - nearly 99 percent of the beta energy is lost in the water. As a further test, the thickness of the water layer was increased to 4 cm to determine if the depth-dose profile was affected. The results, shown in Figure 18, indicate that the thicker water layer has a negligible effect on the depth-dose profile within the statistical accuracy (1σ) of the calculations. Because the results were computed per source particle born in the water, the histograms shown in Figure 18 have been normalized at the outer zone of Hypalon.

Figures 19 and 20 show the depth-dose profiles in the cable from beta sources distributed in a 3 cm thick layer of water surrounding the cable.

4.3 CHARGE DEPOSITION RESULTS

A radiation damage mechanism that in certain cases could limit operation is charge buildup. Radiation induced nonuniform charge distributions in a dielectric could build to levels sufficient to cause breakdown of the dielectric. Although we have not made a detailed analysis of mechanisms for radiation damage in a reactor power cable, we attempted to investigate charge deposition in the model cable along with energy deposition. In fact, the SANDYL code automatically tallies net charge in each zone where energy is deposited. Net charge deposition for this purpose is defined as a number of electrons entering a zone in excess of those leaving a zone. Thus, a positive value for the net number of electrons deposited produces a net negative charge in that region. Conversely, a negative value of electrons deposited results in a positive charge.

The code does not provide information on the standard deviation of the charge deposition, but from repetitive runs it appears that the uncertainties are much greater than the uncertainties associated with the energy deposition.

The choices of zone sizes and number of histories run were optimized entirely on the basis of the energy deposition calculations. It is possible that different (thinner) regions and longer running times would be useful for studying the behavior of charge deposition in the cable.

The results of the calculations are summarized in Table 4. Net charge deposition in each layer is shown for ^{60}Co and for each of the sources investigated in this work. Charge deposition is to be interpreted as the instantaneous charge deposited for the various identified fission product sources. No mechanisms for leakage or other forms of dispersal of the charges have been included. The gamma-ray sources (including ^{60}Co) consistently produce a positive charge on the outer layer of the jacket (Hypalon), but on the interior of the cable no regular pattern is apparent. The beta sources, onthe other hand, produce much larger negative charge on the outermost region of the cable which falls off with decreasing radius. A much more regular behavior is observed. For the case of the cable surrounded by water, the charge buildup is about two orders of magnitude smaller. Of course, in a combined beta-gamma radiation field, there will be some compensation of the opposite signed charge depositions.

Interpretation of these results and their importance insofar as failure of the cable is concerned must await on analysis of the mechanisms of damage in the cable. We present the results of our charge deposition calculations without further analysis.

TABLE 4. CHARGE DEPOSITION IN THE CABLE

Net Electrons Deposited per 10^3 Source Gamma Rays Incident on a 10^3 cm Length of Cable

Material	Zone Outer Radius (mm)	^{60}Co	Airborne				Plate-Out				Waterborne			
			Source 1		Source 2		Source 1		Source 2		Source 1		Source 2	
			1 min	4 days	1 min	4 days	1 min	4 days	1 min	4 days	1 min	4 days	1 min	4 days
Hypalon	11.304	-5.10	-1.05	-0.30	-1.70	-0.45	-9.15	-8.15	-8.15	-5.00	-0.95	-0.85	-1.60	-0.75
"	10.847	-2.35	-0.25	0.10	-0.80	0.15	-0.55	0.25	-1.95	-0.80	-0.40	-0.15	0.35	0.05
"	10.390	0.45	-0.20	-0.05	0.20	-0.05	1.25	0.50	0.15	-0.35	0.60	0.20	-0.15	0.15
"	9.932	0.70	-0.60	0.30	0.35	0.15	0.25	0.80	-0.90	1.55	-0.30	0.10	0.15	-0.20
EPR	9.474	0.10	-0.25	-0.05	-0.10	0.15	-0.65	-1.20	0.75	-1.25	-0.10	0.10	0.25	0.35
"	8.928	-0.35	0.05	-0.25	0.15	-0.15	-1.05	0.75	-0.35	0.90	0.50	-0.10	-0.05	-0.25
"	8.382	-0.30	0.10	0.25	-0.15	-0.20	-1.05	0.25	0.05	-0.70	-0.20	0.05	-0.25	-0.10
"	7.836	0	0.30	-0.10	-0.40	0	0.95	-0.60	0.35	-0.35	-0.25	-0.25	-0.20	0.10
Copper	7.290	-0.60	0.10	0.10	0.25	0.20	0.20	0	-0.25	0.45	-0.15	-0.15	0.25	0.05
"	5.832	-0.25	-0.15	-0.10	-0.10	-0.20	0.55	0.60	0.60	0.30	0.35	0.10	0.10	0.05
"	4.374	1.50	-0.05	0.05	-0.05	0.05	-0.30	-0.30	0.10	-0.10	-0.25	-0.05	0	-0.05
"	2.916	-0.30	0.10	-0.05	0.20	-0.05	0	0.15	-0.40	0	0.05	0.05	0.05	0
"	1.458	-0.15	0.05	0	-0.05	0.05	0	-0.05	0.25	0	-0.05	0	0	0

Net Electrons Deposited per 10^3 Source Betas Incident on a 10^3 cm Length of Cable

Hypalon	11.304	-5.10	60.90	175.80	75.60	169.80	350.20	363.20	357.30	535.80	2.94	2.01	2.76	8.09
"	10.847	-2.35	29.00	10.70	29.30	11.90	114.50	116.70	119.60	65.50	1.34	0.40	0.88	1.08
"	10.390	0.45	22.60	0.60	22.70	2.00	60.50	61.33	56.50	11.50	0.84	0.15	0.40	0.27
"	9.932	0.70	17.30	0	17.10	0.20	34.90	39.00	34.00	3.40	0.46	0.05	0.24	0.02
EPR	9.474	0.10	14.20	0	14.90	0.10	19.80	17.33	17.90	0.60	0.33	0.06	0.11	0.01
"	8.928	-0.35	12.30	0	9.80	0	9.70	12.00	9.30	0.20	0.19	-0.01	0.03	0.01
"	8.382	-0.30	9.10	0	7.20	0	7.10	4.33	7.70	-0.10	0.11	0.02	0.03	0
"	7.836	0	8.20	0	5.20	0	4.80	3.33	3.20	0.10	0.13	0.02	0.02	0
Copper	7.290	-0.60	26.40	0	16.10	0	9.10	10.33	8.20	0	0.26	0	0.01	0
"	5.832	-0.25	0.50	0	0	0	0.10	0	0.10	0	0	0	0	0
"	4.374	1.50	0	0	0	0	0.10	0	0	0	0	0	0	0
"	2.916	-0.30	0	0	0	0	-0.10	0	0	0	0	0	0	0
"	1.458	-0.15	0	0	0	0	0	0	0	0	0	0	0	0

5. SIMULATOR SOURCES

There are several types of radiation sources either presently being used or proposed for use as simulators of the LOCA radiation sources for the purpose of qualification. These include ^{60}Co, ^{137}Cs, bremsstrahlung spectra, electrons from a linear accelerator and spent fuel elements. By far the most common testing source used today is ^{60}Co. It is inexpensive, readily available and requires relatively little labor. In this section we examine the energy deposition resulting from two of these sources using the same model for the cable that was used previously. The source configuration was selected as typical of the high power sources used in industry. Comparison of various simulator source results with the LOCA results will provide a basis for determining the suitability (and perhaps ranking) of the simulators for testing.

5.1 ^{60}Co SOURCE

The geometry adopted for the ^{60}Co source configuration is shown in Figure 21. The source was assumed to be bienergetic (1.173 and 1.332 MeV) on the surface of a cylinder of radius 12 in (30.48 cm), coaxial with the cable. Air at standard temperature and pressure (STP) with a density of 0.001293 g/cm^3 filled the space between source and cable.

Typically a test chamber is used to contain the test piece and its environment. The effect of a 1/4-inch (0.64 cm) steel test chamber with an inside radius of 10 inches (25.4 cm), also coaxial with the cable, was examined. Figure 22 shows the spectrum of photons at the cable surface after penetrating or backscattering from the steel. There is some degradation of the ^{60}Co photons, but nearly 82 percent are still in the broadened photopeak. The remaining photons are approximately uniformly distributed over the low energy portion of the spectrum. The average photon energy penetrating the test chamber is 1.156 MeV compared to 1.253 MeV without the chamber.

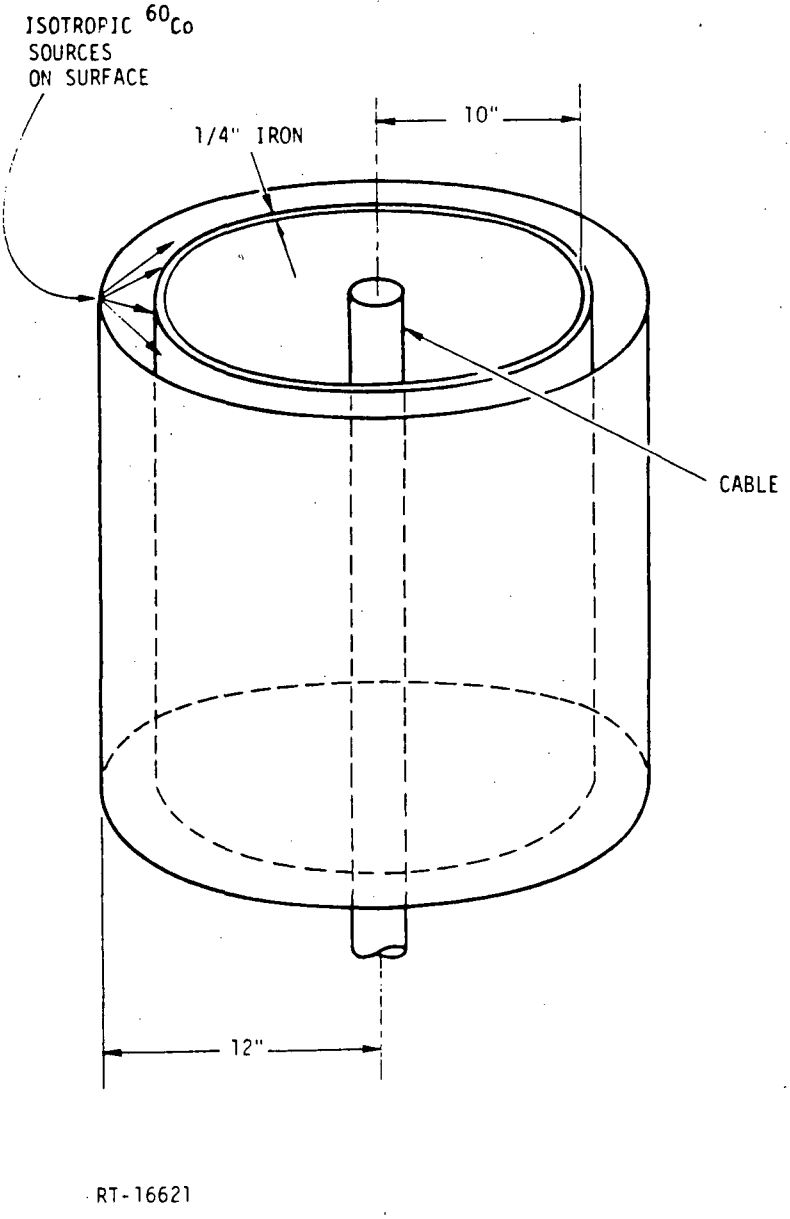

Figure 21. ^{60}Co source irradiation configuration

5.2 ^{137}Cs SOURCE

Another long-lived isotopic source suggested for use in qualification testing is ^{137}Cs. This isotope produces monoenergetic gamma rays of 0.662 MeV. For this study the same model was used for the source as was used for ^{60}Co. However, no steel test chamber was included, and no other processes were considered which degraded the source gamma rays before they impinged on the cable.

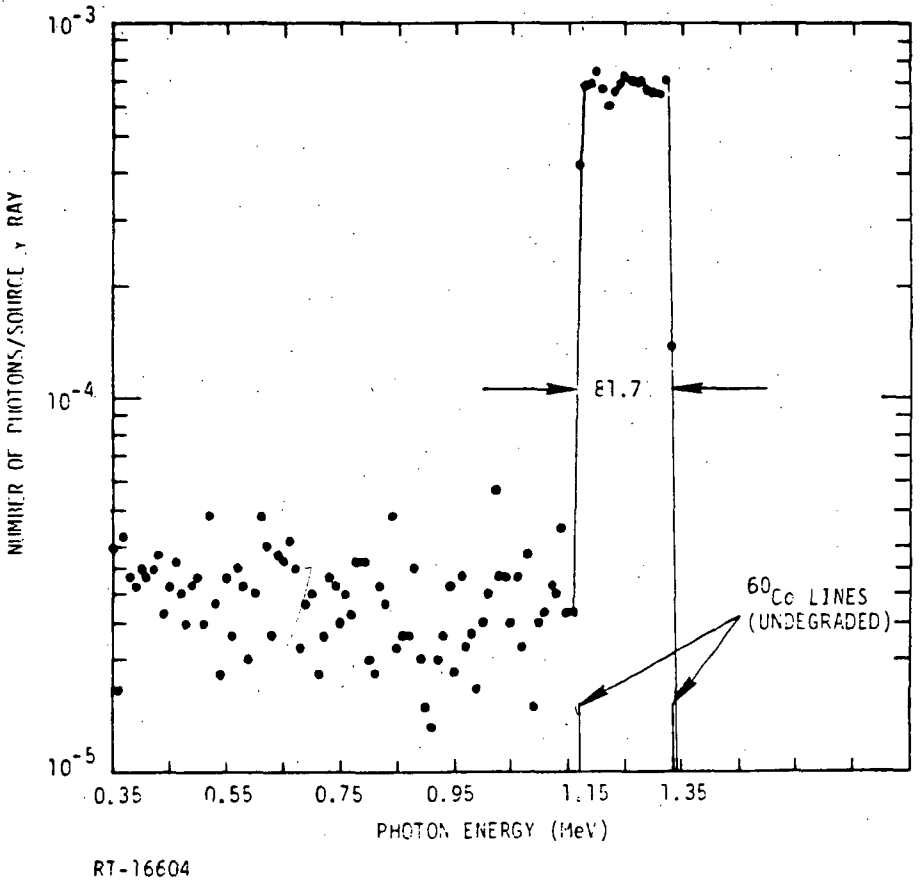

Figure 22. Degraded ^{60}Co energy spectrum at the cable surface with ⅛" iron liner.

5.3 DEPTH-DOSE RESULTS

Insofar as energy deposition in the model cable is concerned, the degradation of the ^{60}Co spectrum by the test chamber walls is negligible as may be seen from the depth-dose calculations in Figure 23. Calculations with and without the chamber are within the statistical uncertainties. The error bars represent one standard deviation (see subsection 3.4). Additional degradation of the source spectrum resulting from the source itself was not considered here. This may be important depending on the design of the source and the irradiation geometry (Ref 13).

The depth-dose results for ^{137}Cs are given in Figure 24. The softer gamma rays produce only a slightly different profile in the cable than ^{60}Co. The principal difference is in the dose in the conductor; the profile in the insulator and jacket are virtually identical for the two isotopes.

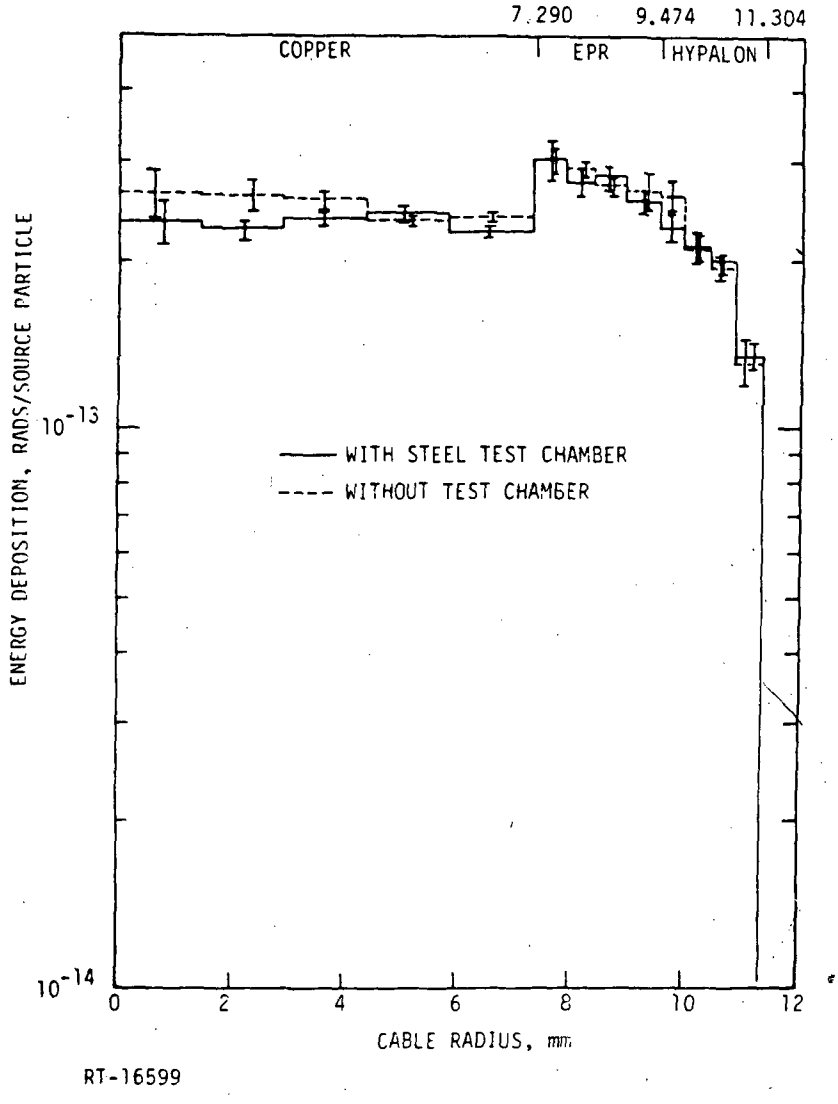

Figure 23. Depth-dose in cable due to ^{60}Co gamma rays with and without iron liner (test chamber)

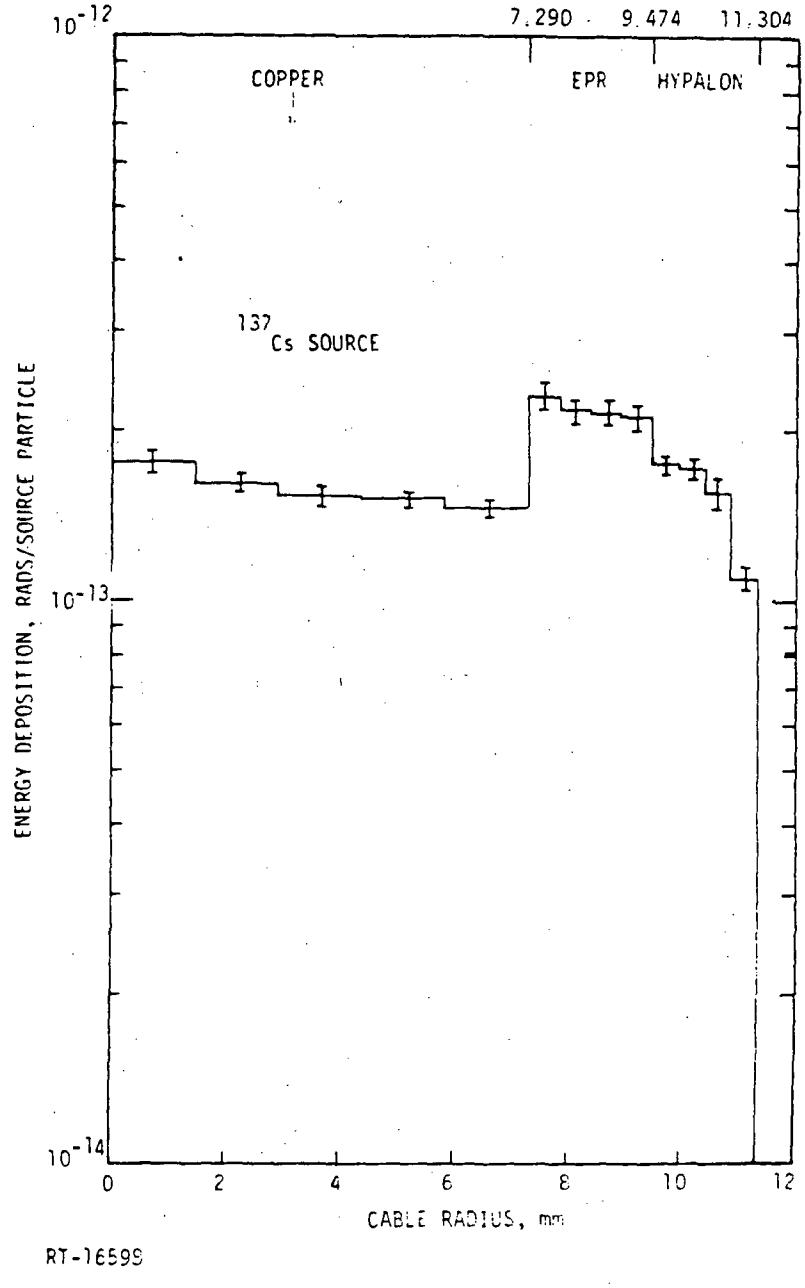

Figure 24. Depth-dose in cable for ^{137}Cs gamma rays

(This page intentionally left blank)

6. COMPARISONS OF RESULTS, DISCUSSION AND CONCLUSIONS

6.1 LOCA VERSUS SIMULATOR RESULTS

Depth-dose profiles for each of the sources studied are compared with the ^{60}Co results in Figures 25 through 36. Since there is so little difference between ^{60}Co and ^{137}Cs, we include the ^{137}Cs results in only a few cases. Since only the shapes of the depth-dose profiles are of consequence here, the simulator results were normalized to the LOCA calculations to give the same average dose in the outer layer of the jacket. Although this is an arbitrary choice, other normalizations would produce no different conclusions; for example, renormalizing the ^{60}Co result to give roughly equal dose in the EPR for the airborne gamma rays from Source 1 would result in seriously underestimating the dose in the jacket.

As is very clear from the comparisons shown, the ^{60}Co and ^{137}Cs sources do not produce depth-dose profiles in the cable that resemble the LOCA sources for any of the cases examined. If equivalence of these profiles is to be used as the only basis for judging simulator adequacy, then we must conclude that these isotopic sources are inadequate. It is also clear that the most serious discrepancy is with the beta sources, as expected. The penetrability and energy loss characteristics of beta particles are very different from gamma rays, and thus it is not surprising that monoenergetic gamma sources provide a poor simulation of the response to betas.

6.2 DISCUSSION AND CONCLUSIONS

6.2.1 Model Sensitivity

The importance or sensitivity that the model and assumptions have on the results and on the uncertainities associated with the results are not always transparent. One way that insight might be gained regarding model effects is to vary parameters of the model and repeat the calculations. Although resources did not permit extensive studies of model parameters such as cable diameter, insulator thickness, or material compositions, a few such calculations were made. In particular, a calculation with slightly

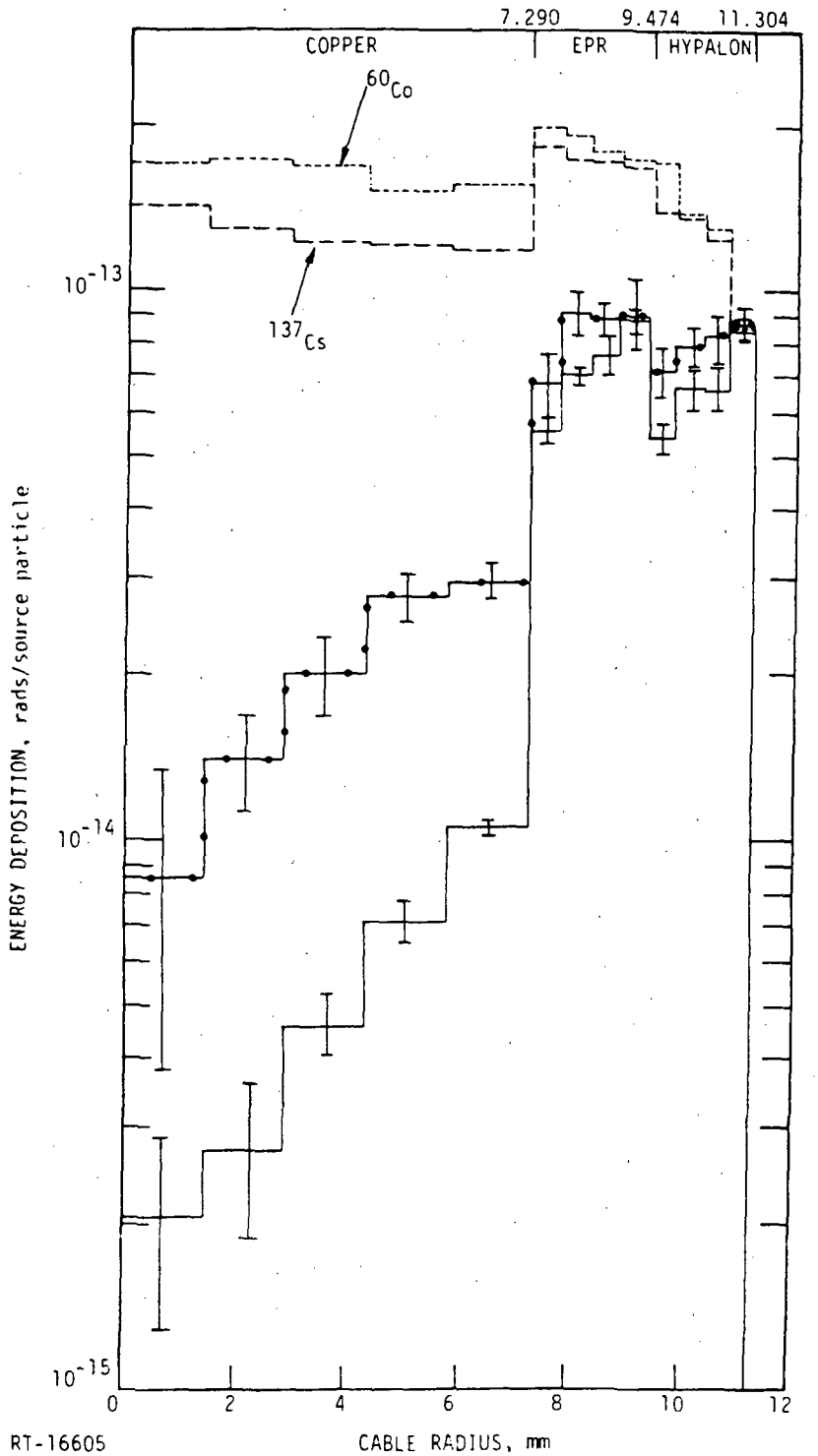

Figure 25. Comparison of depth-dose for ^{60}Co and ^{137}Cs with airborne gamma rays (Source 1). The isotopic source results have been normalized at the outer zone (surface) of hypalon.

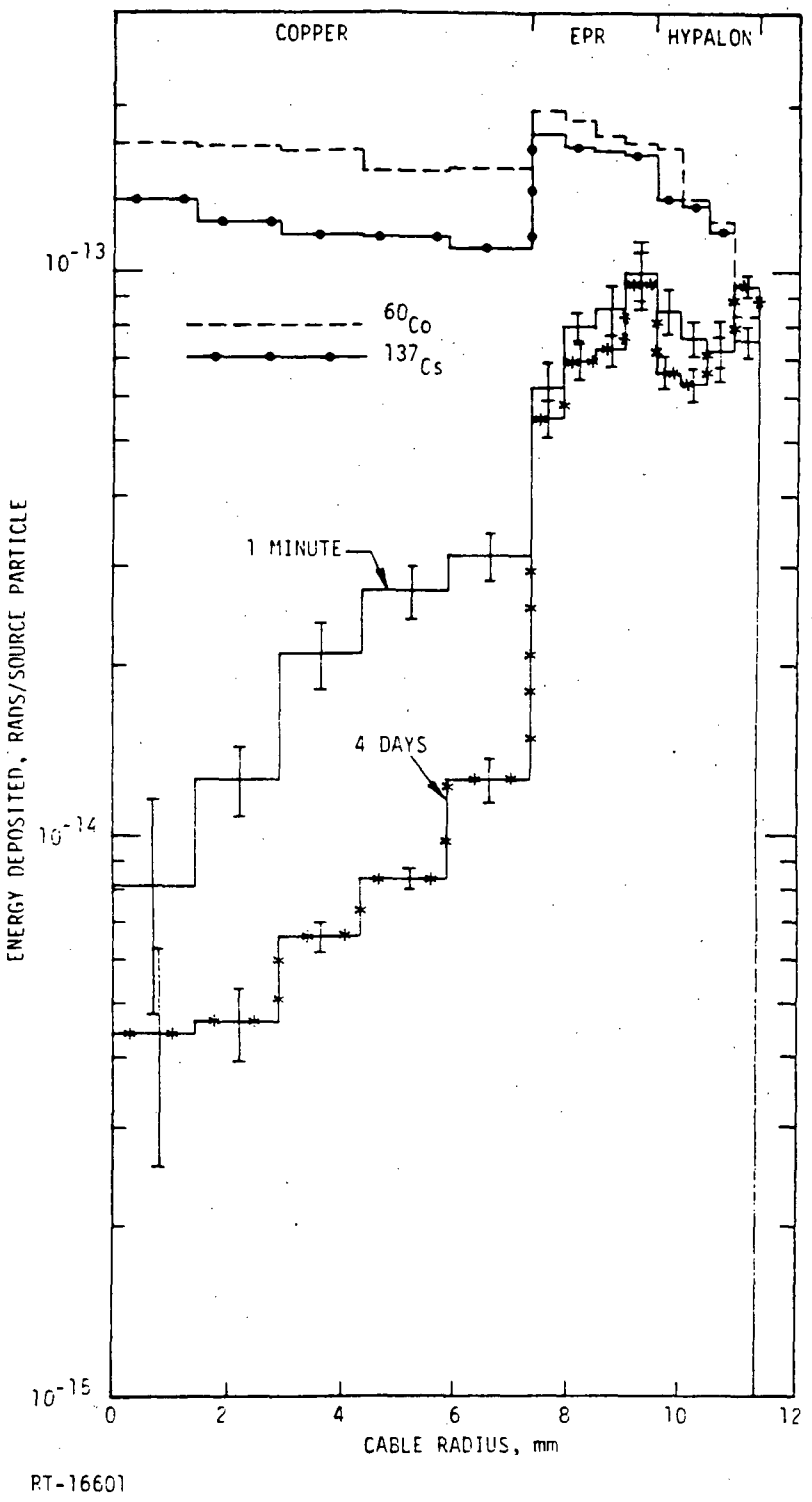

Figure 26. Comparison of depth-dose for ^{60}Co and ^{137}Cs with airborne gamma rays (Source 2). The ^{60}Co and ^{137}Cs results have been normalized to the average dose at the surface.

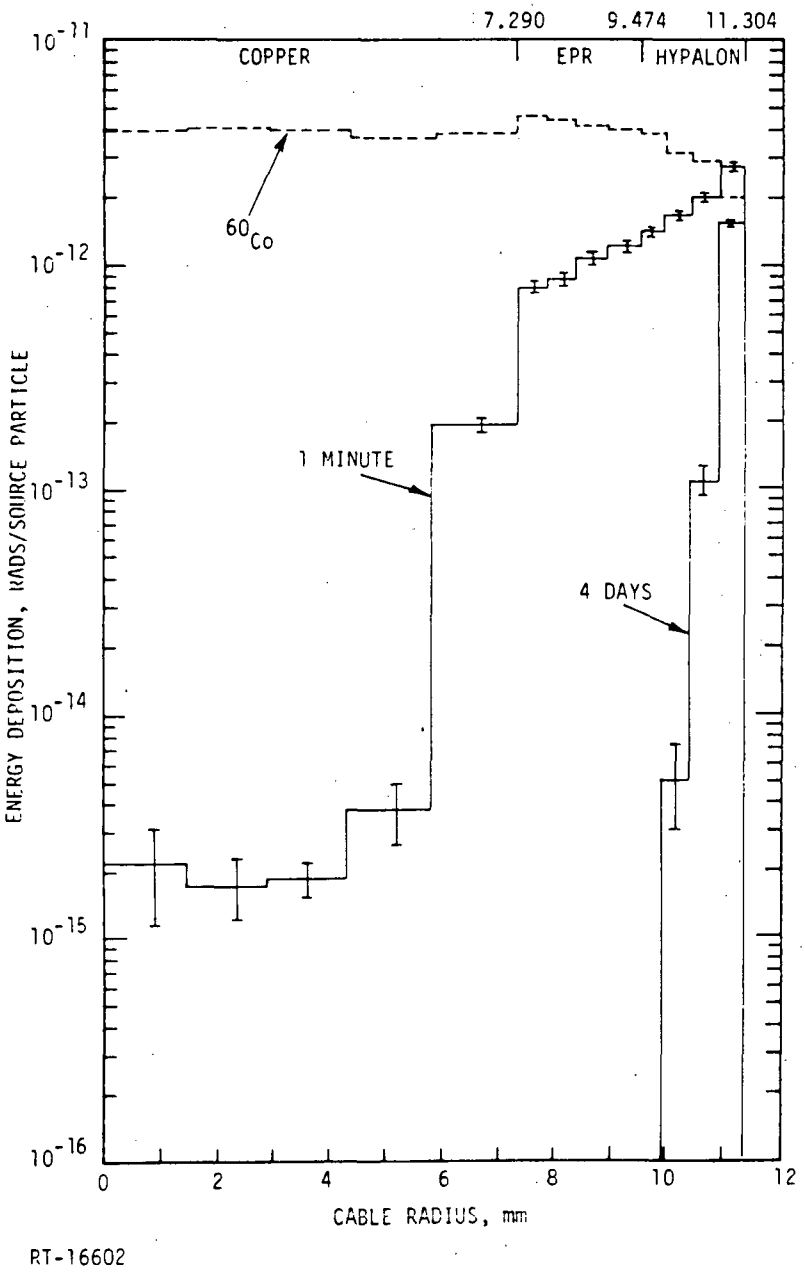

Figure 27. Comparison of depth-dose for ^{60}Co with airborne betas (Source 1). ^{60}Co result normalized to the average dose at the surface.

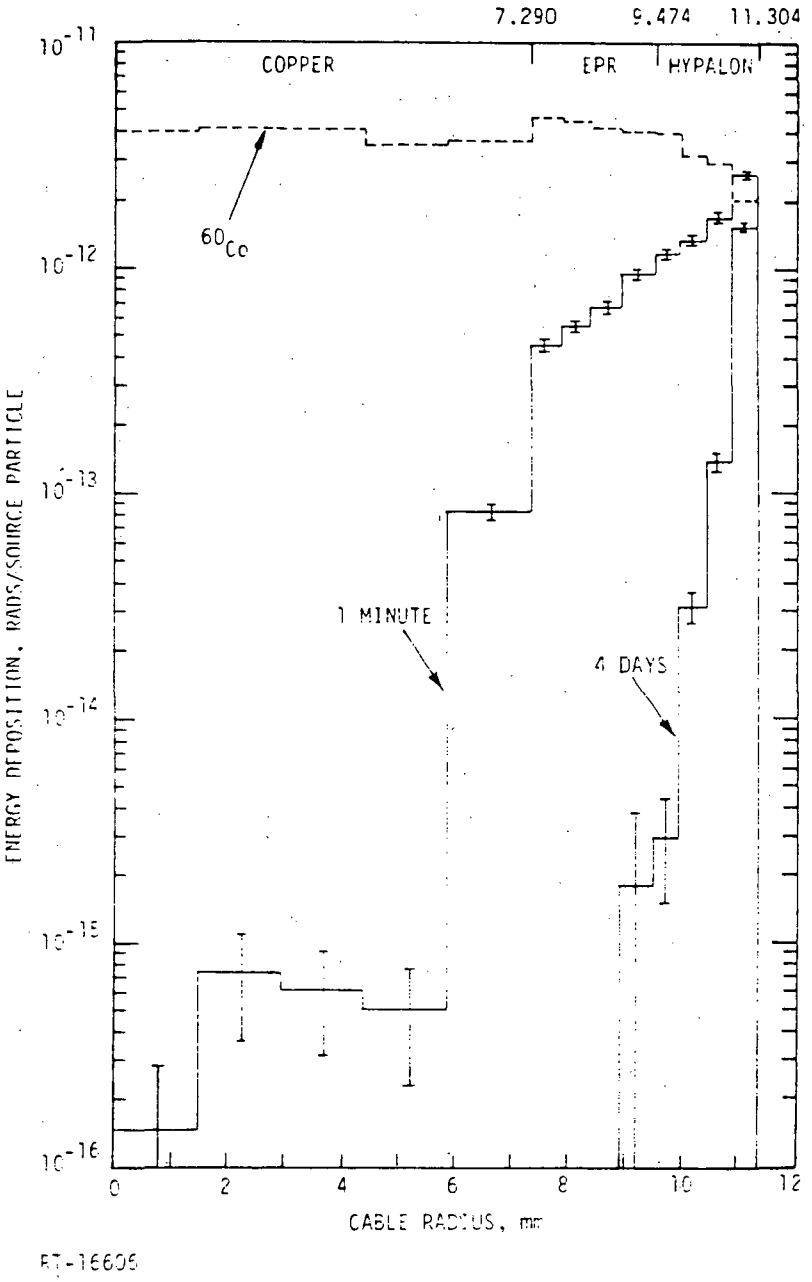

Figure 28. Comparison of depth-dose of ^{60}Co with airborne betas (Source 2); ^{60}Co result normalized at the average surface dose.

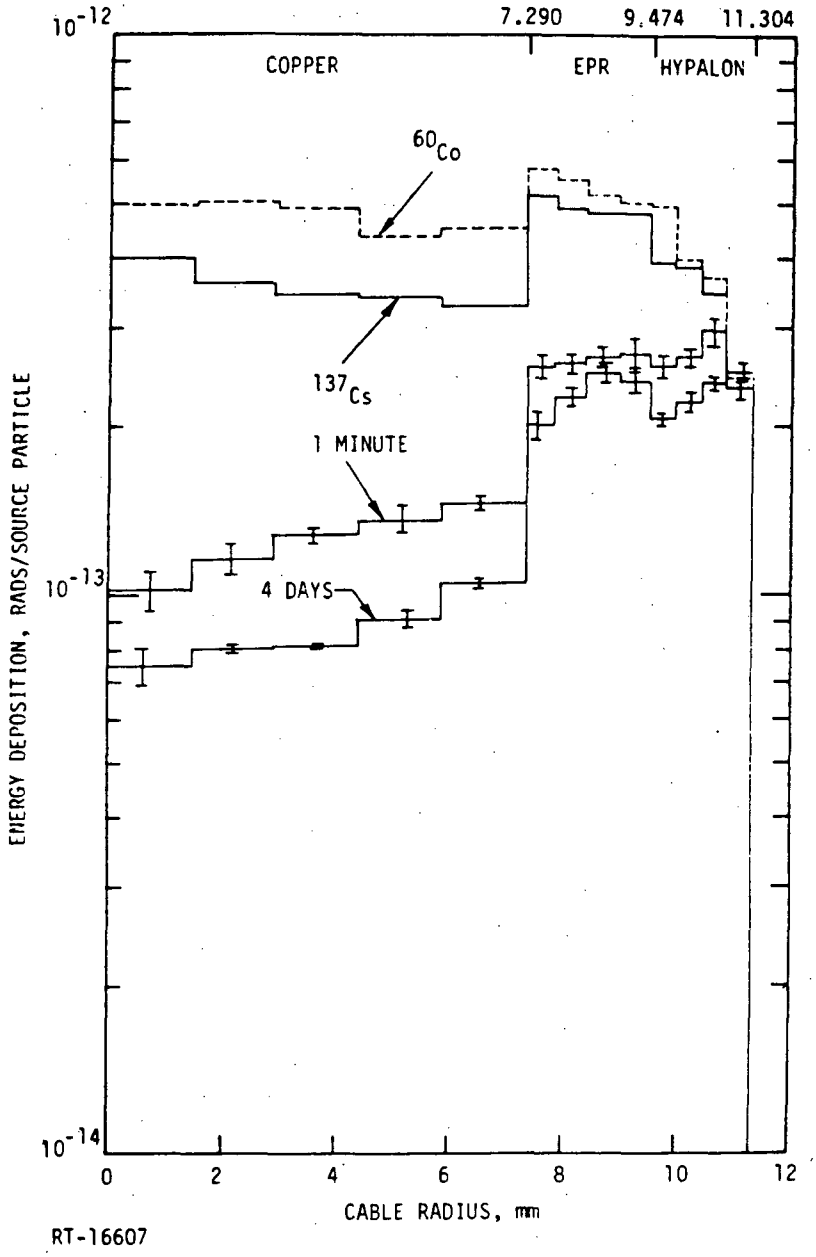

Figure 29. Comparison of depth-dose for ^{60}Co and ^{137}Cs with plate-out gamma rays (Source 1). Both the ^{60}Co and ^{137}Cs results have been normalized to the average surface dose.

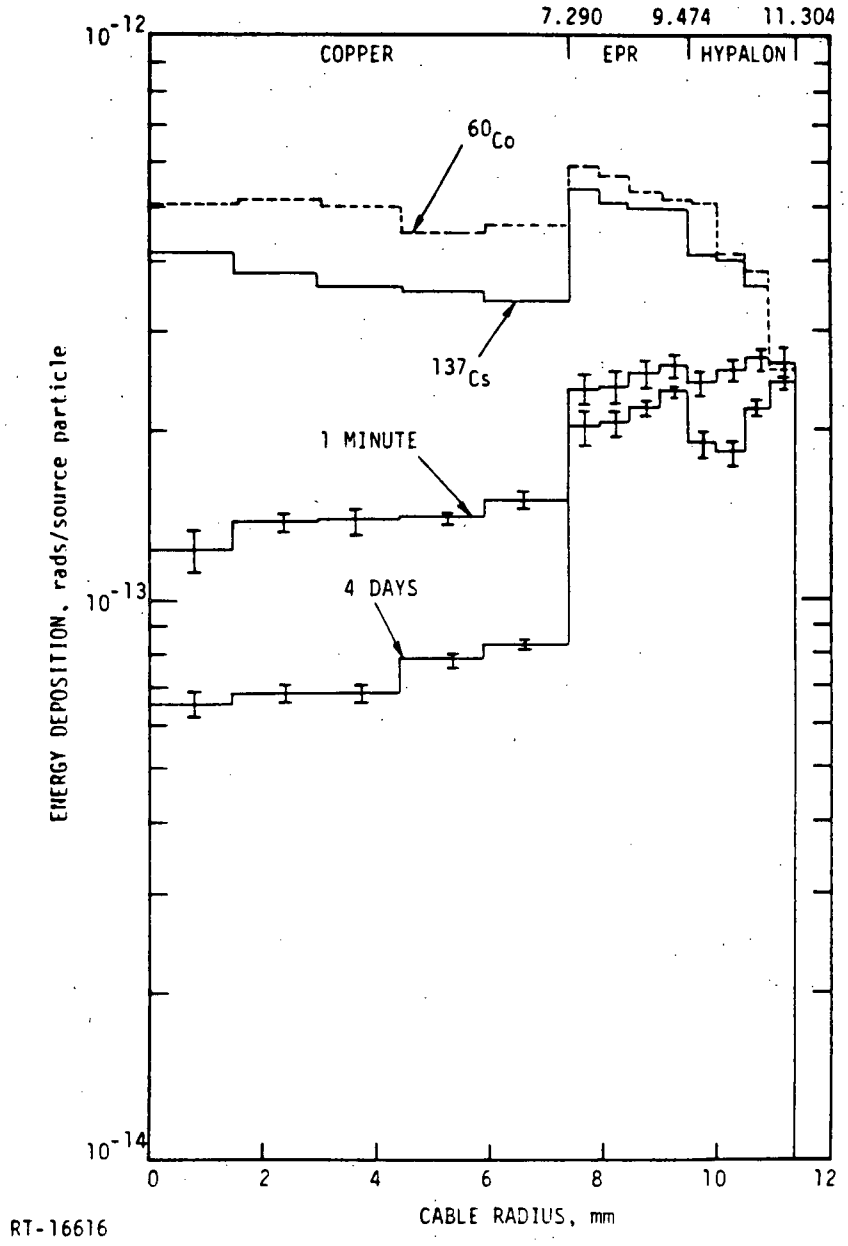

Figure 30. Comparison of depth-dose for ^{60}Co and ^{137}Cs with plate-out gamma rays (Source 2). Both ^{60}Co and ^{137}Cs have been normalized at the average surface dose.

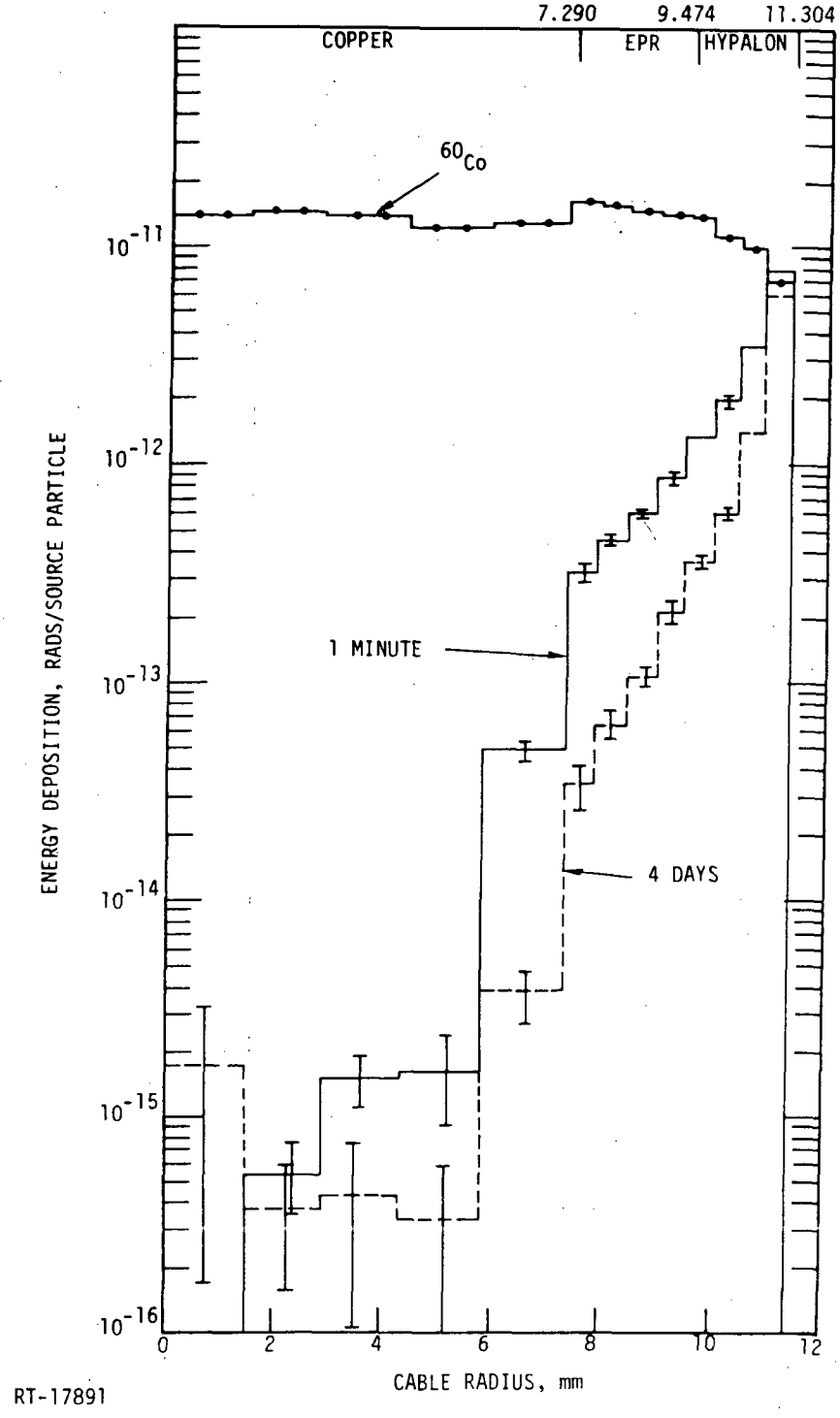

Figure 31. Comparison of depth-dose for ^{60}Co (normalized at average dose in surface zone) with plate-out betas (Source 1)

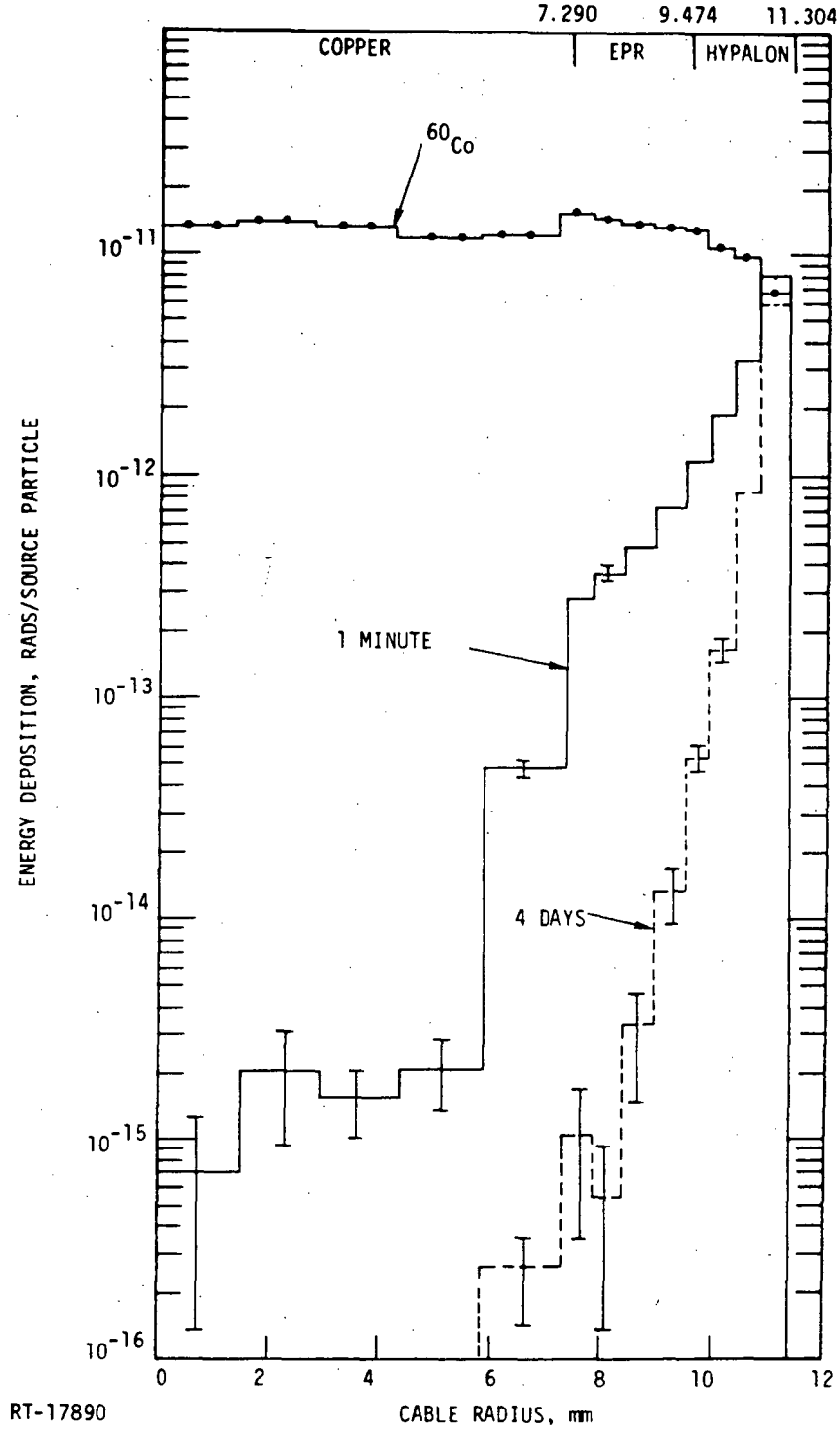

Figure 32. Comparison of depth-dose for ^{60}Co (normalized at average dose in surface zone) with plate-out betas (Source 2)

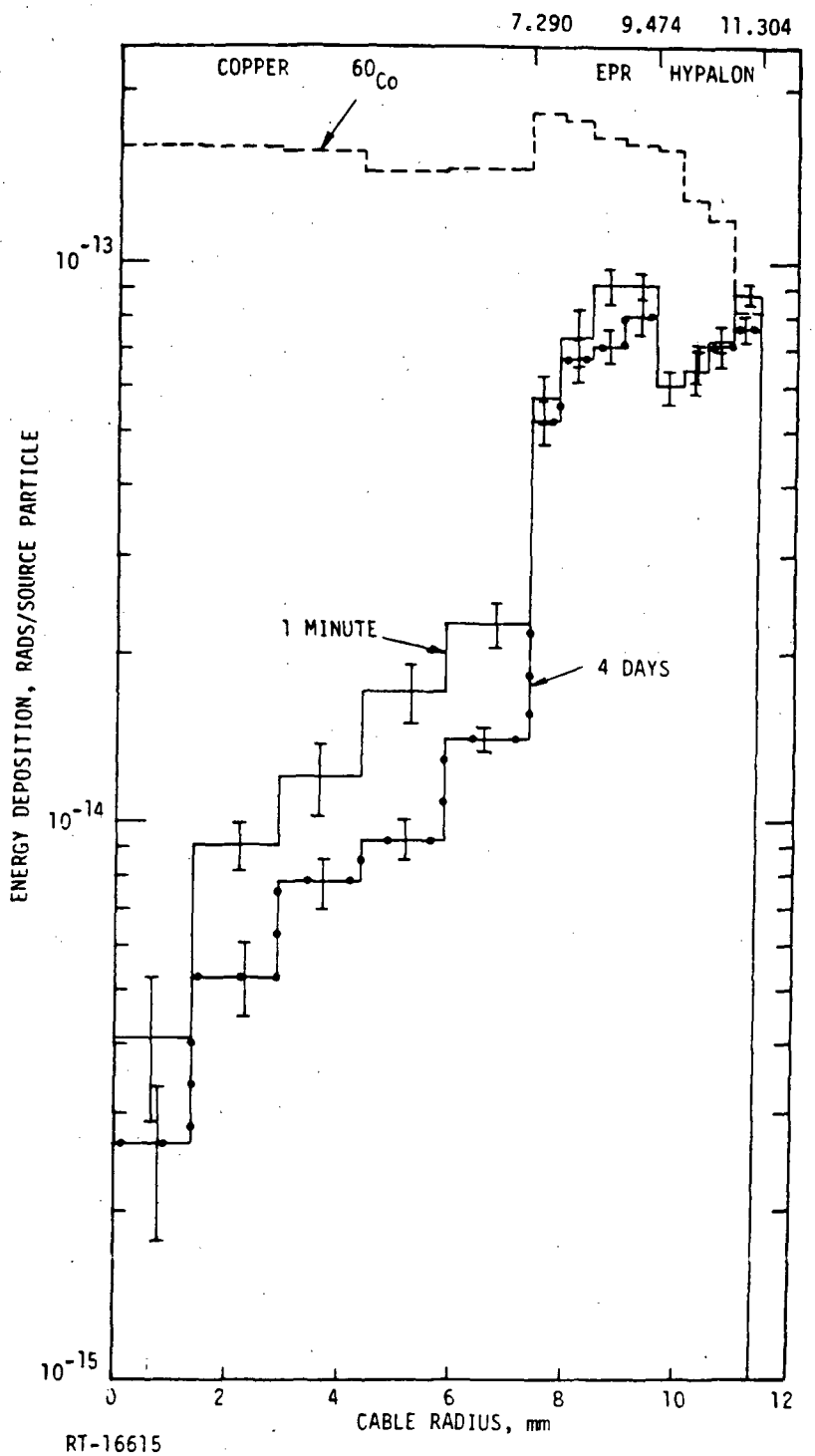

Figure 33. Comparison of depth-dose for ^{60}Co (normalized to average dose in surface zone) with waterborne gamma rays (Source 1)

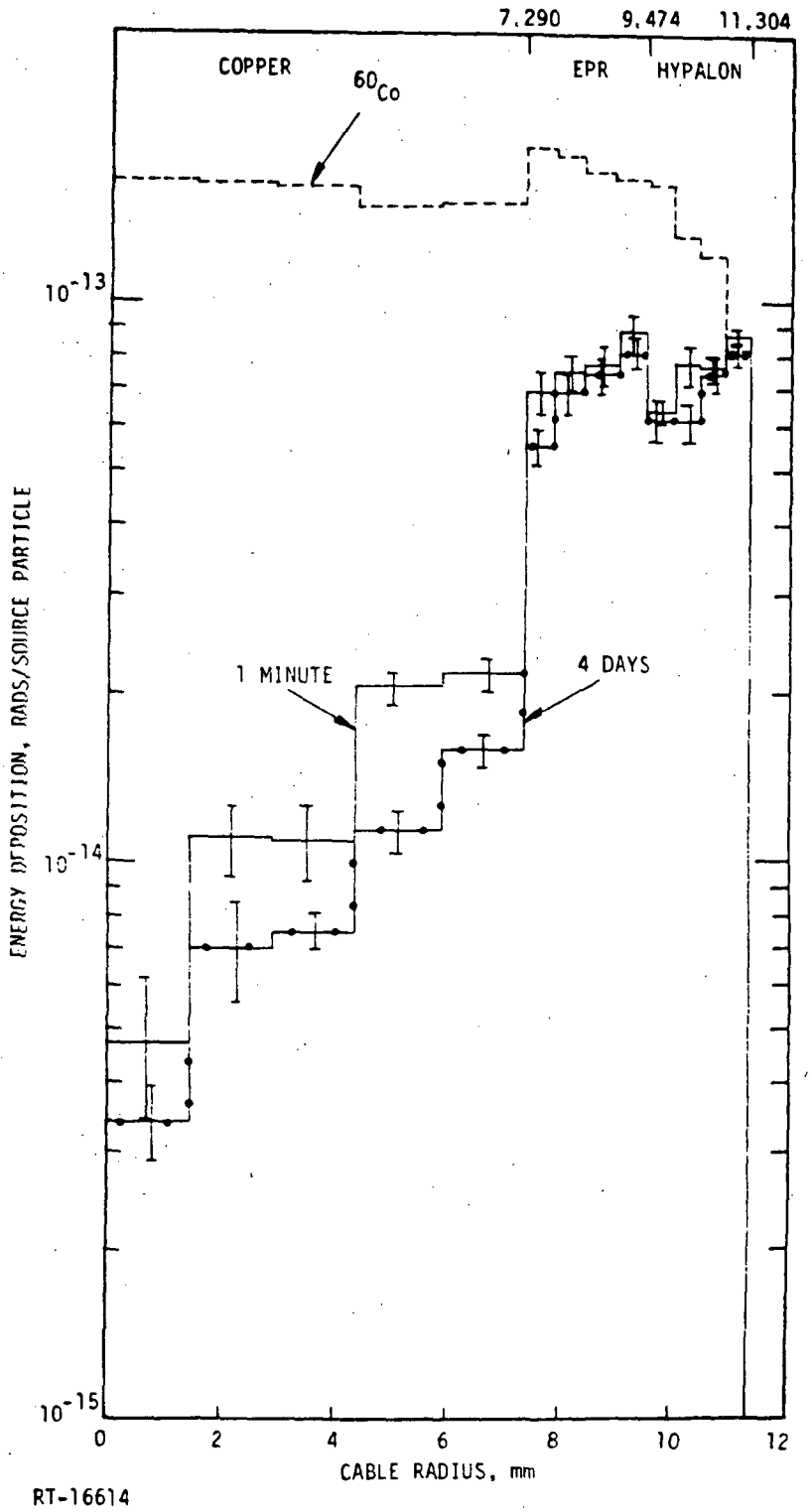

Figure 34. Comparison of depth-dose for ^{60}Co (normalized to average dose in surface zone) with waterborne gamma-rays (Source 2)

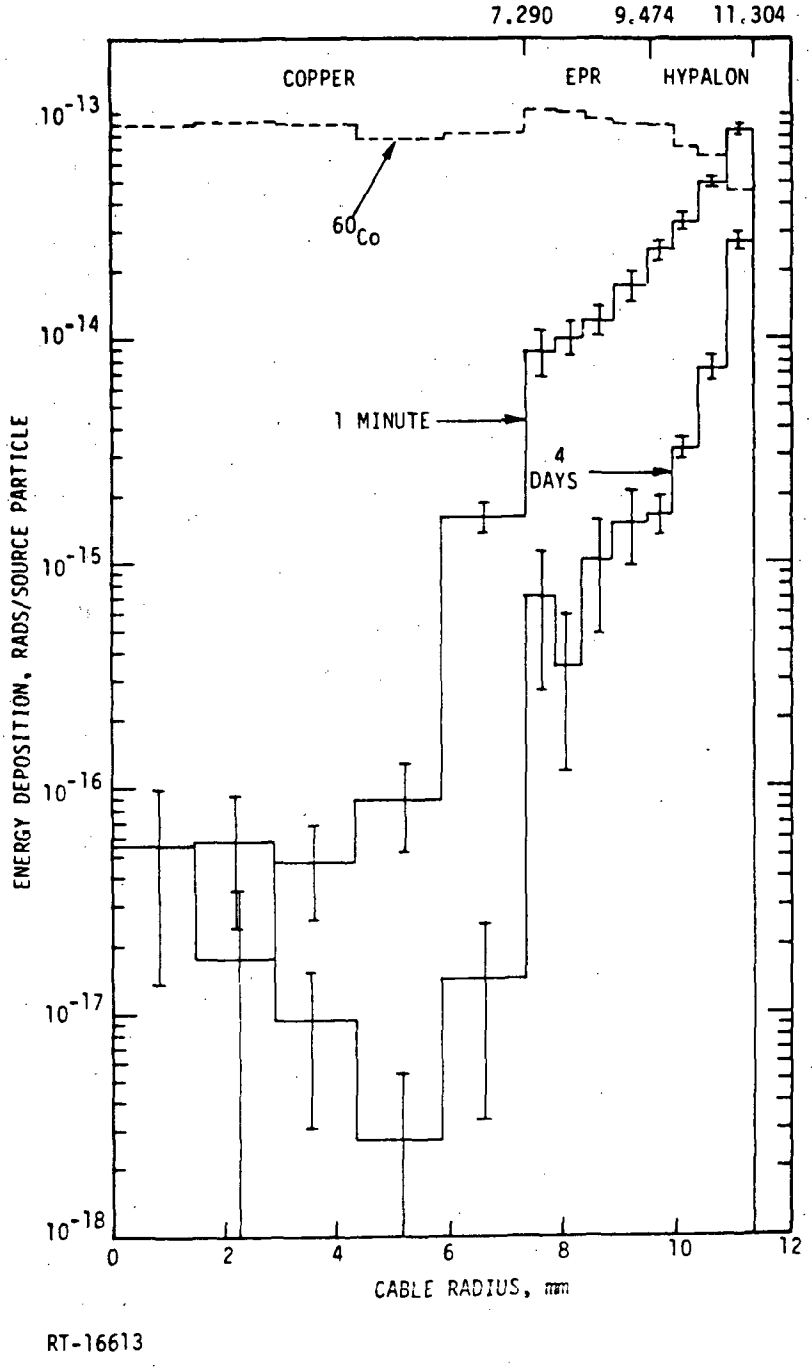

Figure 35. Comparison of depth-dose for ^{60}Co (normalized to average dose in surface zone) with waterborne betas (Source 1)

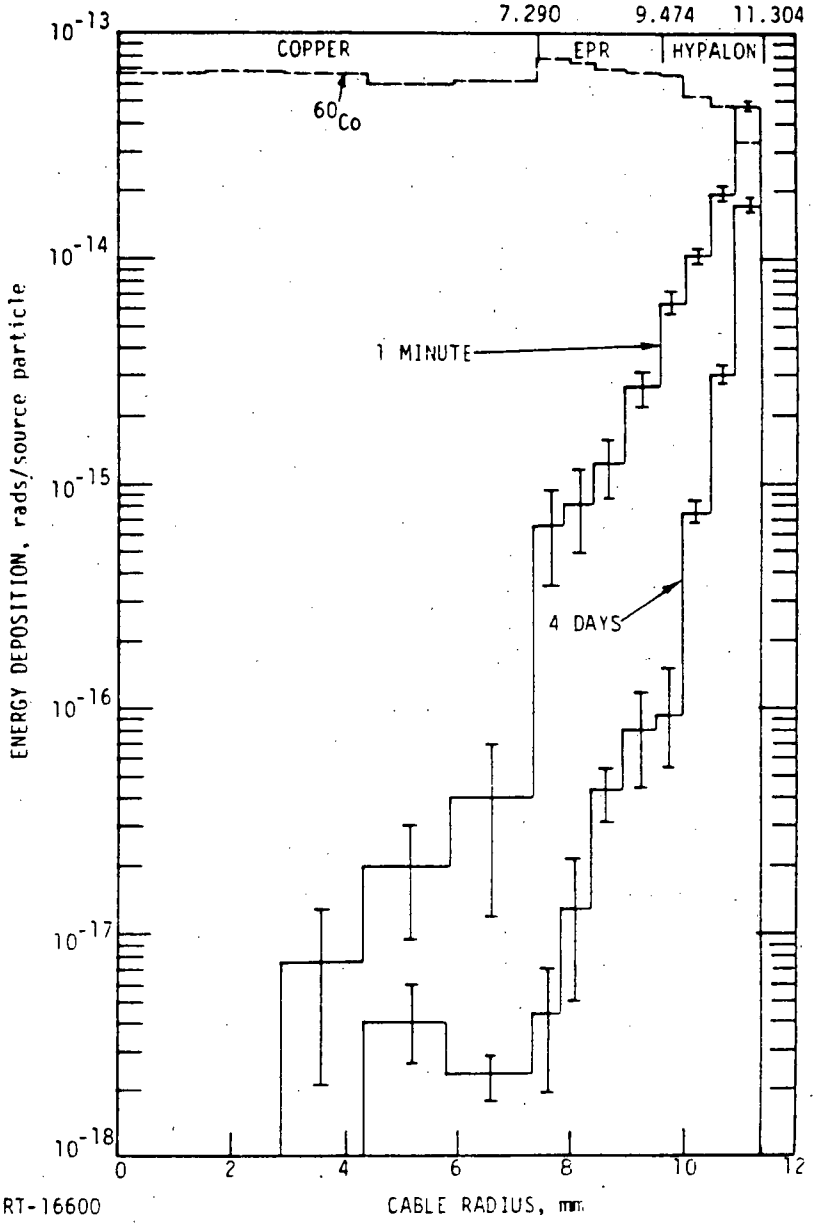

Figure 36. Comparison of depth-dose for ^{60}Co (normalized at surface) with waterborne betas (Source 2)

different compositon of elastomeric materials typical of the types used in power cables showed that slight changes in elemental composition of the jacket and insulator have no effect on the depth-dose results.

Another type of sensitivity calculation that was made has to do with the importance of steam in the containment atmosphere. For the airborne sources it was assumed that air plus 70 psig saturated steam filled the containment. The effects of

the steam were examined by repeating the calculations with only dry air as the medium surrounding the cable. The result of the fission product gamma ray source perturbation is illustrated in Figure 37. The absence of steam results in less perturbation of the source spectrum shape. The case shown in the figure is Source 1 at one hour.

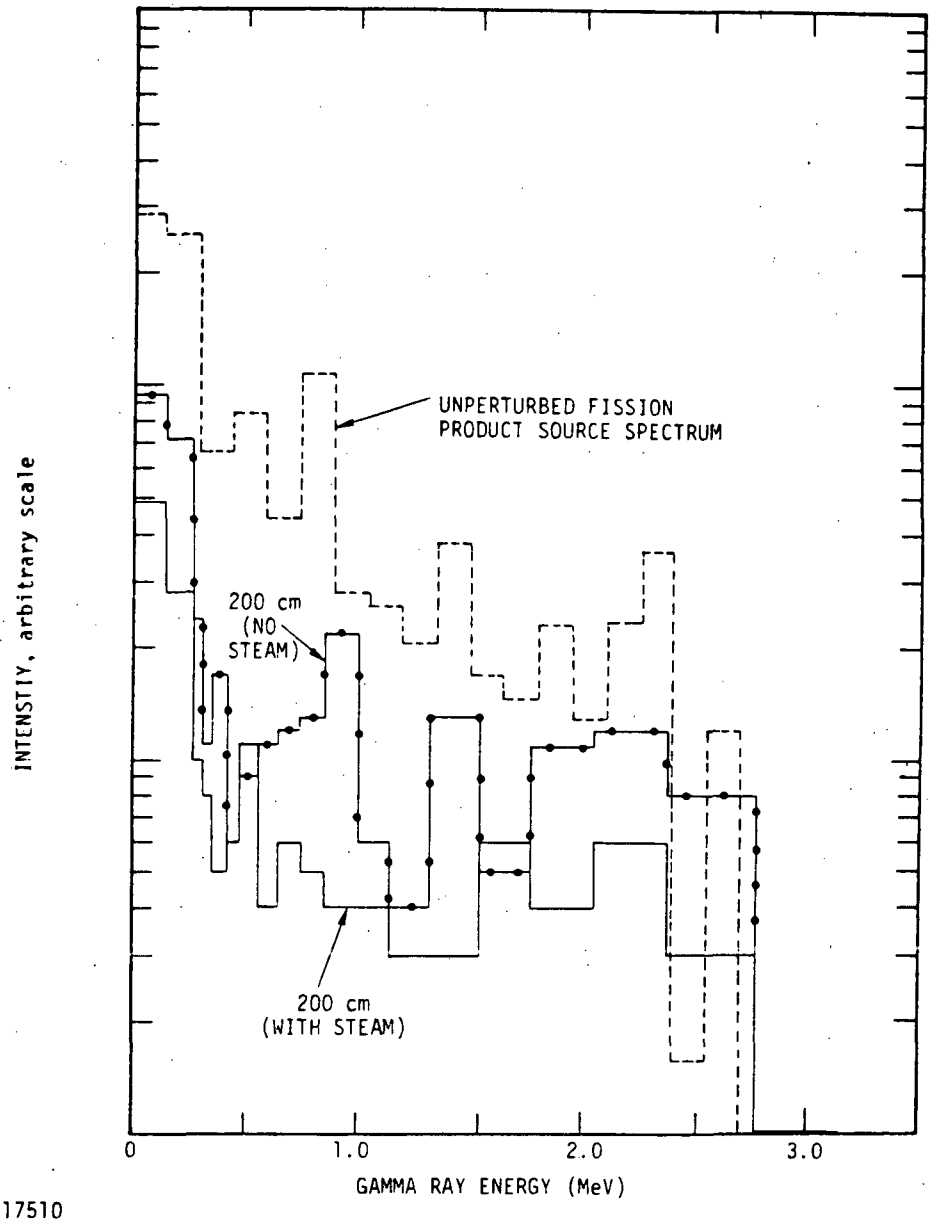

Figure 37. Influence of steam on the gamma ray source spectra (Source 1 at 1 hour)

The depth-dose profiles in the cable resulting from the two perturbed spectra given in Figure 37 are displayed in Figure 38. Within the statistical precision of the calculations there is no significant difference between the two cases. In other words, for this source the presence of steam in the medium surrounding the cable is of no consequence insofar as energy deposition in the cable is concerned.

An attempt was made to validate the approximate procedures used to treat the spatially extended sources. As discussed earlier, a "brute-force" calculation was made, but with a smaller region of air-steam surrounding the cable. The relative energy deposition results for the airborne gamma-ray source at one-minute are shown in Figure 39 (normalized at the outer zone of the jacket). The fact that two different size source regions were used complicates the interpretation of these results. In addition, the statistical uncertainties on the "brute-force" results are very large. One observes that the dose profiles in the jacket and insulator have approximately the same shape, whereas the dose in the conductor is about twice as large for the "brute-force" case. It is difficult to say if the latter difference is a result of the perturbation technique or the limited source thickness used for the exact calculation. However, since the cable performance is thought to be limited by the energy deposited in the dielectric, the difference in the deposition in the conductor is probably not significant.

6.2.2 Comparison Criteria

In this work the depth-dose profile in the cable has been used as a basis for comparing the various LOCA gamma-ray and beta sources with ^{60}Co and ^{137}Cs. Although depth-dose is probably the most sensitive test, and a sufficient condition to ensure adequacy of the simulation, it may not be a necessary condition. A proper basis for comparison depends on the radiation damage mechanism important for the particular piece of equipment of interest. If an evaluation of the damage mechanisms indicates that the depth-dose profile is the proper basis for evaluation, then other simulator sources should be considered. It is possible that the spectrally distributed sources will do a better job of simulating the LOCA dose profile.

In analyzing the results of the depth-dose comparisons it is tempting to argue that the ^{60}Co or ^{137}Cs sources produce a more conseravative situation since, if they are normalized at the surface, they always produce more dose in the inner regions of the cable than do the LOCA sources. Thus, according to this argument, if the cable survives the ^{60}Co irradiation test it will survive the LOCA radiation environment since the latter will deposit a smaller dose in the interior. In order for this argument to be

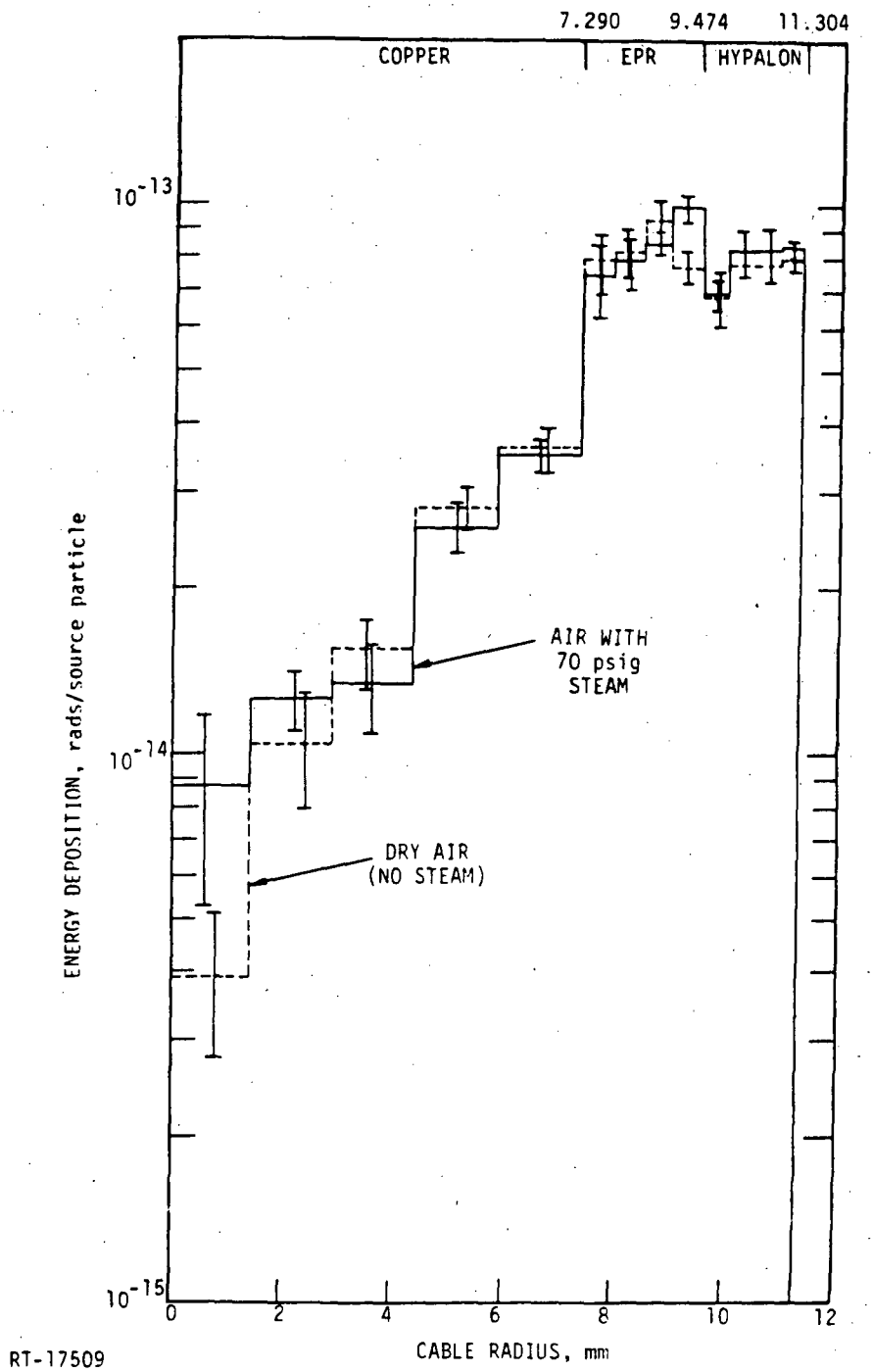

Figure 38. Depth-dose profile for Source 1 gamma rays at 1 hour with and without steam in the surrounding medium

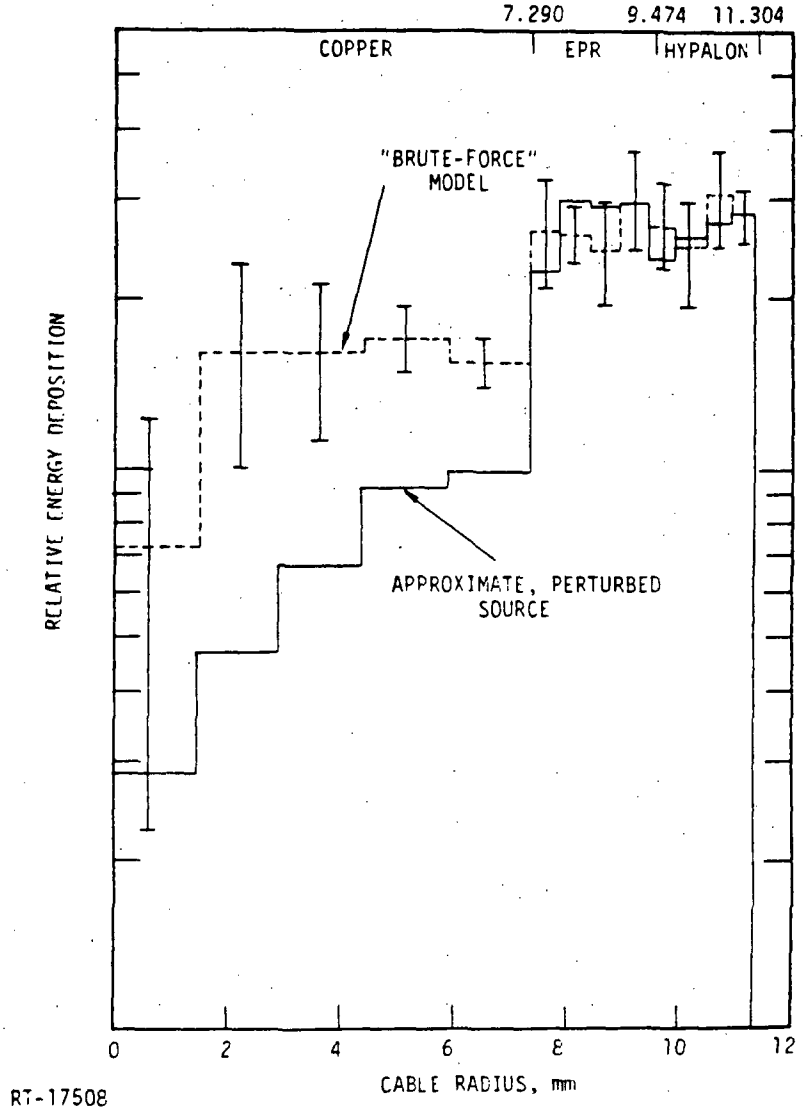

Figure 39. Comparison of airborne gamma ray energy deposition (Source 1 at 1 minute) for approximate, perturbed source and for "brute-force" model

valid it is necessary that the degradation of the cable be directly related to total dose. It is not clear that the problem is as simple as that. For example, charge buildup and dielectric breakdown are dependent upon the dose gradient in the cable. Other failures such as heating and gas evolution from the breakdown of polymeric materials and its subsequent migration and buildup could also depend upon the dose gradient.

Another argument against the "conservative" approach is that it could result in over-testing; that is, it could mean that the testing procedures are unnecessarily or overly conservative, which results in an unnecessarily high cost of testing or producing radiation hard cables. It is possible that laboratory testing and/or analysis of the details of damage in cables could answer this question.

The results for the charge deposition in the cable provide data for further analysis. It is clear that the ^{60}Co source does not reproduce the charge distribution produced by a beta spectrum. Further interpretation of these results are left for future consideration as the simulator adequacy evaluation evolves.

7. RECOMMENDATIONS FOR FURTHER WORK

During the course of this study a number of fertile areas of investigation were identified that were beyond the scope of this program, but nonetheless should be considered as possible areas for future study. We briefly describe each of the subject areas and suggest directions those topics might take.

7.1 CONSIDERATION OF DAMAGE MECHANISMS

The goals of the present work have been to provide comparative depth-dose calculations for simulator sources and for the calculated LOCA sources. Interpreation and evaluation of these comparisons remain to be done as part of the overall program effort to judge the adequacy of the test sources. Consideration of the mechanisms for failure should be a part of the interpretation of these results.

As discussed in subsection 2.2, the ultimate concern of the qualification program is to assure the operation of certain equipment in the reactor during both routine and accident conditions. For some such equipment or components it can be argued that the degradation is related to the total dose or dose profile. For other equipment dose may not be the controlling variable. Thus, the measure of adequacy of a testing program that simulates the expected radiation fields must be based upon the controlling damage mechanism.

Obviously, the evaluation of failure mechanisms for reactor equipment is complex and highly specific. That is, each piece of equipment must be examined with a knowledge of the details of its construction and operation. An example of the complexity of the analysis is given in Reference 5 for a cable.

One possible approach is for the major generic types of Class 1E electrical equipment subject to radiation qualification to be anlayzed for their radiation vulnerability. For each piece of equipment the controlling damage mechanisms might be identified so that a meaningful evaluation of qualification testing procedures can proceed. In the event that the dominant damage is not proportional to dose in the component, suitable analysis procedures will need to be developed.

7.2 OTHER SOURCE CALCULATIONS

The expense and time required to carry out depth-dose calculations necessarily limited the investigations to a few selected sources. The rationale for the choices was discussed in subsection 4.1; generally, bounding conditions were selected in order to see the extent of the variation that resulted in the depth-dose calculations. All the sources were derived from the low power, equilibrium operation results. It may be useful in the future to examine some of the more realistic cases, in other words, the higher power, shorter operation cases which include the effects of capture and depletion. Such spectra are available in Reference 2.

7.3 MODEL SENSITIVITY

The sensitivity of the cable model to the depth-dose calculations was only briefly studied. Sensitivity studies simply demonstrate how sensitive a result is to the assumptions used in the model. Parameters such as cable size, materials, inclusion of an electrical shield and others can be varied to determine their effect on the results. Calculations can also be extended to other types of cable used in nuclear power plants.

It may also be interesting to compare the LOCA and simulator results in very small regions around material interfaces where dose enhancement phenomena are important. The choices of zone thicknesses in the present work tended to average out dose enhancement. Previous experience has shown that one might expect very high local doses in regions near the conductor-insulator interface. Charge buildup at the interface could also be significant. The extent to which simulators reproduce interface effects should be investigated.

7.4 OTHER COMPONENTS AND SIMULATORS

The present study was restricted to cables. It may be useful to apply these methods to other Class 1E electrical equipment which must be qualified for use in nuclear power plants. Prior to doing the type of calculation reported here, it would be helpful to first assess the mechanisms for failure due to radiation in each component or piece of equipment. It would also be imformative to extend the calculations to other simulators such as bremsstrahllung sources, electron machines, and spent fuel assemblies which are spectrally distributed and can be tailored somewhat to produce variable spectra.

REFERENCES

1. "Qualification of Safety-Related Electric Equipment for Nuclear Power Plants," U.S. Nuclear Regulatory Commission Regulatory Guide 1.89, Revision 1 (Draft, November 1976).

2. N. A. Lurie, D. H. Houston and J. A. Naber, "Definition of Loss-of-Coolant Accident Radiation Source," IRT 8167-002/SAND 78-0090, IRT Corporation, prepared for Sandia Laboratories (February 1978).

3. L. L. Bonzon, "Radiation Signature Following the Hypothesized LOCA," SAND76-0740 (NUREG 76-6521), Sandia Laboratories (Sept. 1977, Rev. Oct. 1977).

4. J. A. Naber and N. A. Lurie, Nucl. Technology 36, 40-47 (1977).

5. R. E. Leadon, "Radiation Damage Mechanisms in Reactor Components," IRT Corporation (1977), unpublished.

6. H. M. Colbert, "SANDYL: A Computer Program for Calculating Combined Photon-Electron Transport in Complex Systems," SLL-74-0012, Sandia Laboratories (1974).

7. N. Vagelatos, N. A. Lurie, and J. P. Wondra, Proc. ERDA Symp. X-Ray and Gamma-Ray Sources and Detectors, Ann Arbor, MI, 1976 (CONF 760539) p. 51.

8. J. Kimlinger, E. F. Plechaty, and J. R. Terrall, "SORS Monte Carlo Photon Transport Code," UCRL-50358, Lawrence Livermore Laboratories.

9. M. J. Berger and S. M. Seltzer, "Electron and Photon Transport Programs," (I) NBS Report 9836, (II) NBS Report 9837.

10. M. J. Berger, in Methods in Computational Physics, (Academic Press, New York, 1963), Vol. I, p. 135.

11. J. A. Wall and E. A. Burke, IEEE Trans. Nucl. Sci. NS-17, (No. 6) 305 (1970).

12. E. A. Burke and J. C. Garth, "An Algorithm for Energy Deposition at Interfaces," IEEE Trans. Nucl. Sci. NS-23 (No. 6) 1938 (1976).

13. J. H. Aitken and W. H. Henry, Int. J. Appl. Radiation and Isotopes 15, 713-724 (1964).

(This page intentionally left blank)

APPENDIX

TABULATED DEPTH VERSUS DOSE IN CABLE

Table A-1. Calculated Depth-Dose in Model Cable Airborne Sources

	Radius (mm)	Gamma-Ray Dose (rads/source particle)[a]			
		Source 1 at 1 m	Source 1 at 4 d	Source 2 at 1 m	Source 2 at 4 d
COPPER	0				
	1.458	8.629-15	2.064-15	8.194-15	4.403-15
	2.916	1.407-14	2.724-15	1.262-14	4.662-15
	4.374	1.999-14	4.562-15	2.114-14	6.603-15
	5.832	2.789-14	7.194-15	2.722-14	8.344-15
	7.290	2.981-14	1.125-14	3.133-14	1.256-14
EPR	7.836	6.763-14	5.514-14	6.234-14	5.480-14
	8.382	9.019-14	6.952-14	7.972-14	6.961-14
	8.928	8.832-14	7.558-14	8.574-14	7.278-14
	9.474	8.927-14	8.708-14	9.911-14	9.556-14
HYPALON	9.932	7.044-14	5.365-14	8.539-14	6.637-14
	10.390	7.707-14	6.660-14	7.637-14	6.288-14
	10.847	8.247-14	6.591-14	7.628-14	7.215-14
	11.304	8.585-14	8.586-14	7.543-14	9.470-14

	Radius (mm)	Beta Dose (rads/source particle)[a]			
		Source 1 at 1 m	Source 1 at 4 d	Source 2 at 1 m	Source 2 at 4 d
COPPER	0				
	1.458	2.127-15		1.417-16	
	2.916	1.735-15		7.351-16	
	4.374	1.867-15		6.185-16	
	5.832	3.786-15		5.039-16	
	7.290	1.930-13		8.221-14	
EPR	7.836	7.799-13		4.534-13	
	8.382	8.589-13		5.573-13	
	8.928	1.067-12		6.764-13	
	9.474	1.209-12		9.388-13	1.743-15
HYPALON	9.932	1.399-12		1.170-12	2.954-15
	10.390	1.683-12	5.145-15	1.350-12	3.085-14
	10.847	2.011-12	1.054-13	1.678-12	1.380-13
	11.304	2.759-12	1.542-12	2.634-12	1.553-12

[a] Properly expressed as rads per single source particle on a ten-meter segment of cable, or rads/1.408×10^{-3} particles/cm^2

Table A-2. Calculated Depth-Dose in Model Cable Plate-Out Sources

	Radius (mm)	Gamma-Ray Dose (rads/source particle)[a]			
		Source 1 at 1 m	Source 1 at 4 d	Source 2 at 1 m	Source 2 at 4 d
	0				
COPPER	1.458	1.020-13	7.545-14	1.226-13	6.547-14
COPPER	2.916	1.166-13	8.033-14	1.373-13	6.841-14
COPPER	4.374	1.270-13	8.096-14	1.380-13	6.838-14
COPPER	5.832	1.367-13	9.059-14	1.397-13	7.866-14
COPPER	7.290	1.467-13	1.037-13	1.514-14	8.342-14
EPR	7.836	2.535-13	1.992-13	2.347-13	2.035-13
EPR	8.382	2.578-13	2.245-13	2.371-13	2.060-13
EPR	8.928	2.653-13	2.480-13	2.515-13	2.189-13
EPR	9.474	2.688-13	2.397-13	2.601-13	2.344-13
HYPALON	9.932	2.543-13	2.054-13	2.423-13	1.909-13
HYPALON	10.390	2.672-13	2.213-13	2.544-13	1.824-13
HYPALON	10.847	2.978-13	2.374-13	2.693-13	2.191-13
HYPALON	11.304	2.357-13	2.504-13	2.662-13	2.466-13

	Radius (mm)	Beta Dose (rads/source particle)[a]			
		Source 1 at 1 m	Source 1 at 4 d	Source 2 at 1 m	Source 2 at 4 d
	0				
COPPER	1.458			7.268-16	
COPPER	2.916	5.375-16	3.828-16	2.024-15	2.086-16
COPPER	4.374	1.530-15	4.472-16	1.598-15	7.216-17
COPPER	5.832	1.626-15	3.418-16	2.123-15	4.456-17
COPPER	7.290	4.851-14	3.844-15	4.757-14	2.584-16
EPR	7.836	3.200-13	3.429-14	2.820-13	1.057-15
EPR	8.382	4.451-13	6.672-14	3.632-13	5.406-16
EPR	8.928	5.877-13	1.066-13	4.707-13	3.041-15
EPR	9.474	8.900-13	2.102-13	7.157-13	1.305-14
HYPALON	9.932	1.322-12	3.600-13	1.185-12	5.210-14
HYPALON	10.390	1.985-12	6.066-13	1.876-12	1.647-13
HYPALON	10.847	3.491-12	1.441-12	3.339-12	8.695-13
HYPALON	11.304	7.865-12	6.117-12	7.819-12	5.766-12

[a] Properly expressed as rads per single source particle on a ten-meter segment of cable, or rads/1.408 x 10^{-3} particles/cm^2

Table A-3. Calculated Depth-Dose in Model Cable Waterborne Sources

	Radius (mm)	Gamma-Ray Dose (rads/source particle)[a] Source 1 at 1 m	Source 1 at 4 d	Source 2 at 1 m	Source 2 at 4 d
	0				
COPPER	1.458	4.788-15	3.432-15	4.115-15	2.562-15
COPPER	2.916	1.103-14	7.030-15	9.129-15	5.229-15
COPPER	4.374	1.092-14	7.527-15	1.207-14	7.778-15
COPPER	5.832	2.051-14	1.138-14	1.720-14	9.229-15
COPPER	7.290	2.166-14	1.578-14	2.247-14	1.397-14
EPR	7.836	6.900-14	5.524-14	5.213-14	5.709-14
EPR	8.382	7.483-14	6.889-14	7.342-14	6.698-14
EPR	8.928	7.771-14	7.410-14	9.130-14	7.070-14
EPR	9.474	8.796-14	8.129-14	9.092-14	7.985-14
HYPALON	9.932	6.322-14	6.137-14	5.988-14	6.489-14
HYPALON	10.390	6.140-14	7.768-14	6.405-14	6.497-14
HYPALON	10.847	7.581-14	7.381-14	7.164-14	7.242-14
HYPALON	11.304	8.092-14	8.703-14	7.641-14	8.761-14

	Radius (mm)	Beta Dose (rads/source particle)[a] Source 1 at 1 m	Source 1 at 4 d	Source 2 at 1 m	Source 2 at 4 d
	0				
COPPER	1.458	5.650-17			
COPPER	2.916	1.783-17	5.799-17		
COPPER	4.374	4.735-17	9.340-17	7.541-18	
COPPER	5.832	8.785-187	2.684-18	2.005-17	4.081-18
COPPER	7.290	1.575-15	1.421-17	4.084-17	2.289-18
EPR	7.836	8.751-15	6.890-16	6.618-16	4.342-18
EPR	8.382	9.840-15	3.492-16	8.267-16	1.256-17
EPR	8.928	1.175-14	1.031-15	1.251-15	4.307-17
EPR	9.474	1.696-14	1.506-15	2.704-15	7.988-17
HYPALON	9.932	2.446-14	1.668-15	6.582-15	9.297-17
HYPALON	10.390	3.293-14	3.256-15	1.041-14	7.466-15
HYPALON	10.847	4.937-14	7.401-15	1.990-14	3.070-15
HYPALON	11.304	8.537-14	2.749-14	4.987-14	1.807-14

[a] Properly expressed as rads per single source particle on a ten-meter segment of cable, or rads/1.408×10^{-3} particles/cm^2

Table A-4. Calculated Depth-Dose in Model Cable Simulator Sources

	Radius (mm)	Dose (rads/source particle)[a] ^{60}Co	^{60}Co (no test chamber)	^{137}Cs
	0			
COPPER	1.458	2.365-13	2.632-13	1.762-13
COPPER	2.916	2.278-13	2.660-13	1.619-13
COPPER	4.374	2.381-13	2.581-13	1.522-13
COPPER	5.832	2.413-13	2.331-13	1.512-13
COPPER	7.290	2.251-13	2.374-13	1.458-13
EPR	7.836	3.025-13	3.006-13	2.299-13
EPR	8.382	2.751-13	2.914-13	2.170-13
EPR	8.925	2.820-13	2.725-13	2.163-13
EPR	9.474	2.538-13	2.660-13	2.125-13
HYPALON	9.932	2.270-13	2.603-13	1.746-13
HYPALON	10.390	2.123-13	2.102-13	1.720-13
HYPALON	10.847	1.977-13	1.934-13	1.555-13
HYPALON	11.304	1.339-13	1.305-13	1.090-13

[a] Properly expressed as rads per single source particle on a ten-meter segment of cable, or rads/1.408×10^{-3} particles/cm^2

APPENDIX B

Evaluation of Radiation Damage Mechanisms in a Reactor Power Cable in a Loss-of-Coolant Accident

IRT 0056-002A

August, 1978

IRT 0056-002A

EVALUATION OF RADIATION DAMAGE MECHANISMS IN A REACTOR POWER CABLE IN A LOSS-OF-COOLANT ACCIDENT

Prepared by

J. F. Colwell, B. C. Passenheim, and N. A. Lurie

This report documents part of the Qualification Testing Evaluation (QTE) Program (A 1051-8) being conducted by Sandia Laboratories for the United States Nuclear Regulatory Commission under DOE Contract AT(29-1)-789.

Prepared for

SANDIA LABORATORIES
Albuquerque, New Mexico

Under

Contract 07-8944

August 1978

IRT Corporation

Instrumentation Research Technology

7650 Convoy Court • P.O. Box 80817
San Diego, California 92138

714 / 565-7171
Telex: 69-5412

ABSTRACT AND CONCLUSIONS

This analysis of the response of a reactor power cable to a loss-of-coolant accident (LOCA) discusses several different possible failure mechanisms.

In the first few fractions of a minute the electrical leakage currents flow and trapped electrons may discharge, inducing noise pulses into the cable. Quantitative analysis shows these effects are not serious for a power cable.

If the cable has poor heat contact with the external environment, within a few minutes radiation energy (dose) will raise the temperature from an already elevated temperature to approach the maximum service temperature for the insulators.

After a few days the accumulated dose is enough to deteriorate the cable insulation. This chemical and mechanical deterioration thus represents the ultimate failure mode of the cable.

It is noted that gamma ray simulators may understress the electrical effects and overstress the temperature effects. It is also noted that several parameters used in this study were extrapolated from the values for roughly similar materials in roughly similar environments. A final, definitive study might have to include a program to measure these parameters in the materials of interest.

TABLE OF CONTENTS

1. INTRODUCTION

The present work explores the expected failure modes of a power cable subjected to a loss-of-coolant accident (LOCA) environment in a nuclear power plant. The work is a more detailed numerical analysis of many of the effects outlined by Leadon in his preliminary analysis of the problem (Ref 1). An important source of input data for our present work is the energy deposition study carried out by Lurie, et al. (Refs 2,3).

The model for the cable which we use is identical to the one for which Lurie did the irradiation calculation. It is a copper conductor with an ethylene-propylene rubber (EPR) insulator covered by a chloro-sulfonated polyethylene (trade-name Hypalon) jacket. It is shown in Figure 1. The material properties for the various regions of the cable are listed in Table 1.

Table 1. Material Properties of the Cable

	Region Within the Cable		
Parameter, Symbol, Units	Copper	EPR	Hypalon
Outer Radius, r, cm	0.729	0.947	1.1304
Electrical Cond., σ, $(\text{ohm-cm})^{-1}$	5.7×10^{5}	6.4×10^{-10}	1.1×10^{-8}
Dielectric Strength, volt/cm	N/A	1.8×10^{-7}	1.0×10^{-5}
Dielectric Const., k, pure number	N/A	2.3	6.0
Dielectric Relaxation Time, sec	1.6×10^{-19}	2.2×10^{-4}	4.8×10^{-5}
Density, ρ, gm/cm^3	8.94	0.92	1.25
Thermal Cond., κ, $\text{watt/cm}^{\circ}\text{C}$	4.19	3.47×10^{-3}	1.9×10^{-3}
Tensile Strength, 1000 psi		<1	4.0
Service Temperature, max. $^{\circ}$C for continued use		177	163

In this task it is first necessary to define the environment to which the cable is expected to be subjected and then to calculate how this environment will influence the

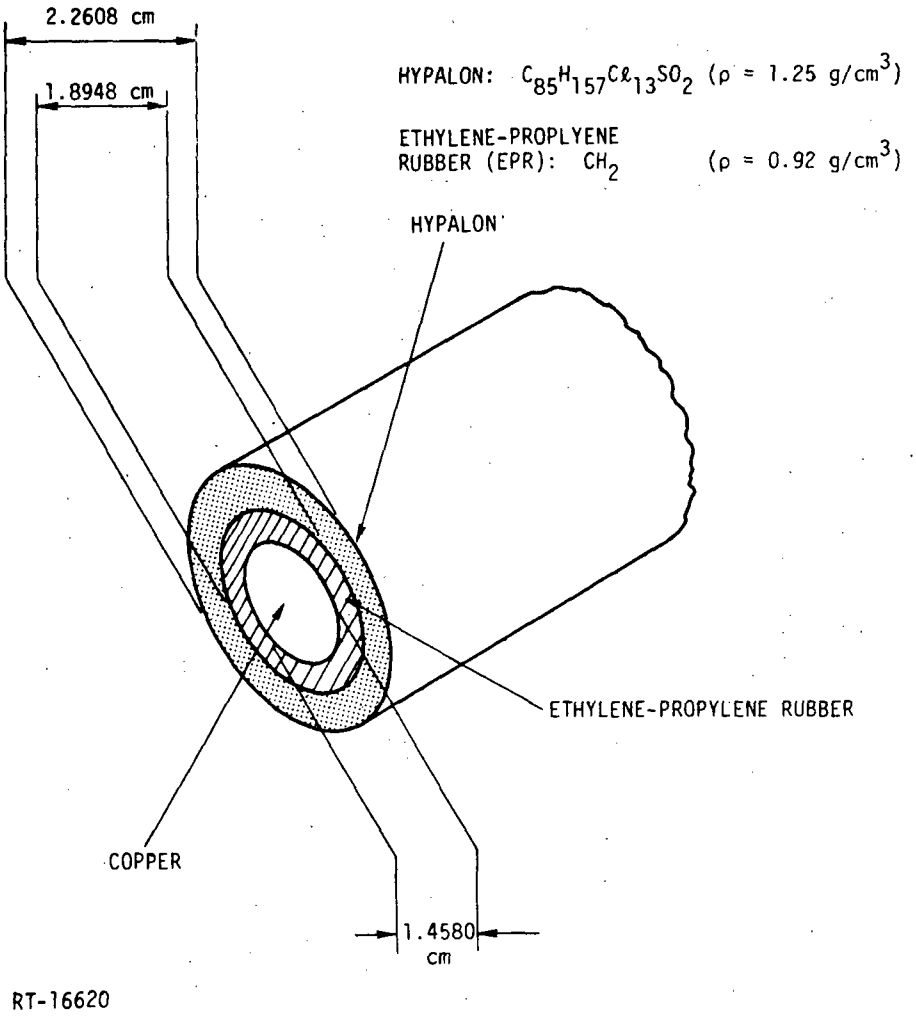

Figure 1. Model of the reactor power cable

operation of the cable. The definition of the assumed LOCA environment will be found in Section 2 of this report. The bulk of Section 2 is devoted to adapting the dose calculations of References 2 and 3 to the specified usage needed here. Section 3 is devoted to a calculation of the changes in electrical conditions. These changes include leakage current through the insulation because of its radiation and temperature enhanced conductivity, induced voltages from trapped charge, and the possibility of breakdown due to fields generated by this charge.

Section 4 briefly discusses temperature conditions. It should be remarked that both the electrical and temperature conditions depend on whether or not the cable is in

good enough contact with some external sink to exchange charge and thermal energy respectively. There will undoubtedly be some regions in poor contact with any ground plane where the fields and temperature can rise because there is no electrical or heat current flowing through the jacket. Sections 3 and 4 consider cases of both good and poor ground contact.

The mechanical and chemical deterioration which will occur are treated in Section 5. It turns out that disintegration or temperature and radiation enhanced deformation are the most likely failure modes of the cable.

This report follows the temporal development of effects in the cable after the LOCA environment is established. First the high dose rate will change the electrical conditions in seconds to fractions of a minute. The cable survives this challenge. Within a few minutes the radiation heat input will raise the insulator temperature near or above its normal service limit. The radiation and mechanical deteriorations induced by the radiation become serious only after many hours to a few days when the total accumulated dose has had a chance to build up to high levels.

2. CABLE ENVIRONMENT

For simplicity in discussing the attenuation of energy deposition from the cable edge into the cable interior, we have specialized our analysis to a single case: the airborne source case shown in Figures 8 and 10 of Reference 3. All sources discussed in Reference 3 attenuate in roughly the same manner as the airborne sources. An average over all sources will give substantially the same relative results as found for this one case. We also limit our analysis to a reactor power of 4,000 megawatts. All doses and dose rates are proportional to the reactor power so the final results presented here can be scaled up or down to fit a different particular case.

It is convenient to normalize the depth-dose profile to unity at the cable surface. The normalized doses per source particle are shown in Figure 2 for gamma radiation, and in Figure 3 for beta radiation. To get absolute dose deposition profiles, these energy loss curves must be multiplied by the total number of source particles at the cable surface.

Of course, not all of the fission product radiation impinges on the cable, so that an estimate of the local dose rate is also necessary. This has already been carried out by Bonzon (Ref 4); his results are shown in Figures 4 and 5. Note that these doses are due to combined environments from airborne, plate-out and waterborne sources. Values read from Figures 4 and 5 and converted to rads(Hypalon) are given in Table 2. These surface dose rates are then multiplied by the normalized dose-depth profiles shown in Figures 2 and 3 to obtain the total dose rates within the cable. The results of this procedure is exhibited in Figure 6. The leveling off a the EPR-Hypalon boundary is caused by backscatter into the Hypalon. The very rapid attenuation into the copper is caused by the rapid attenuation of betas, leaving only gammas which penetrate this far. The total gamma deposition is down from the total beta deposition by a factor of ten, so that the removal of betas drops the dose rate by a large factor.

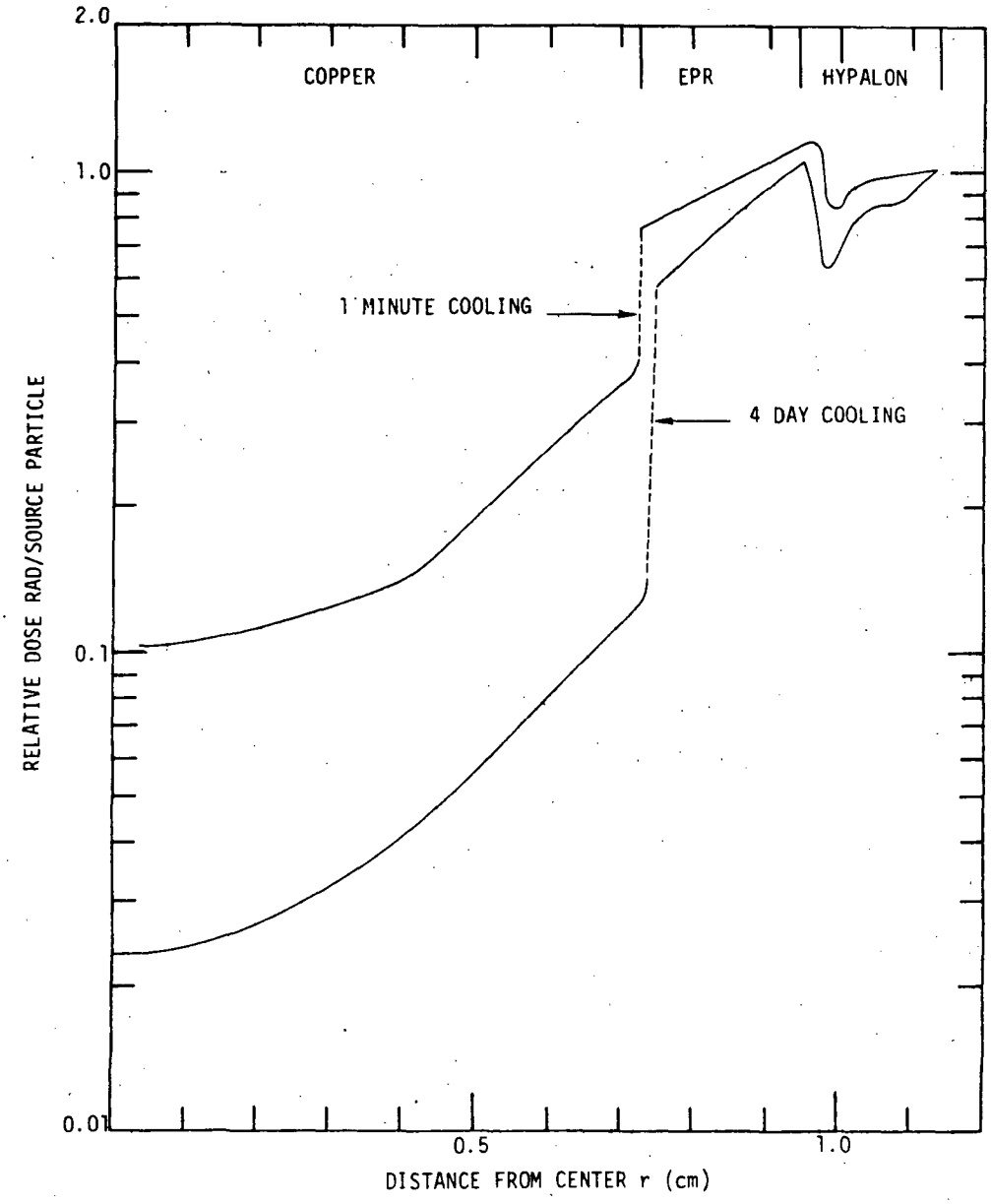

Figure 2. Normalized dose deposition profiles in a cable by gamma radiation in the LOCA radiation environment

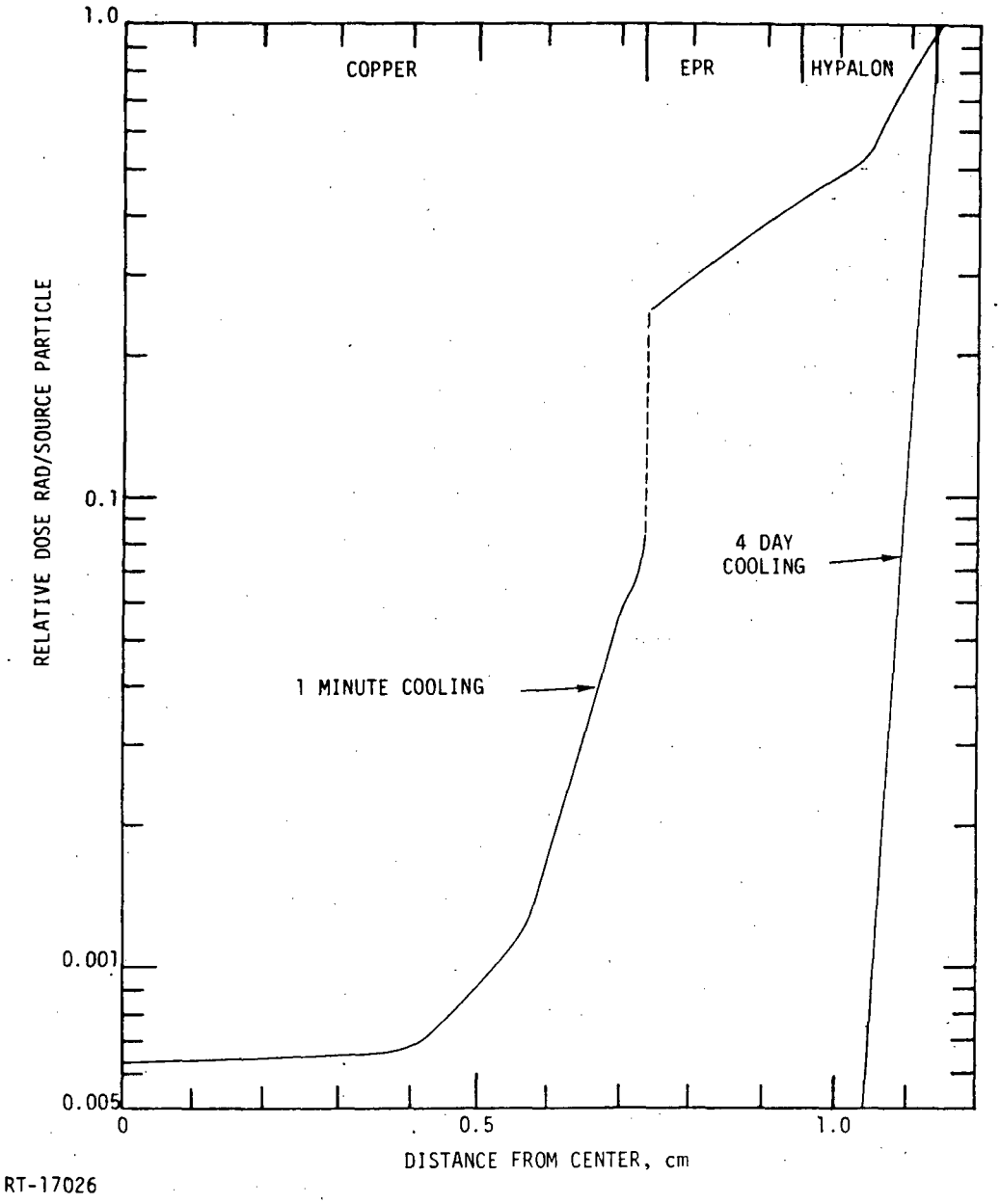

Figure 3. Normalized dose deposition profiles in a cable by beta radiation in a LOCA radiation environment

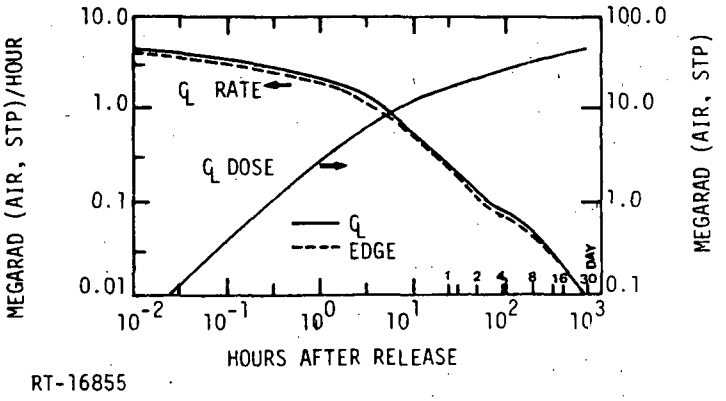

Figure 4. Typical dose rate and dose to air from the combined gamma sources; airborne source uniformly distributed in the containment volume, plate-out source uniformly distributed on the containment sidewall surface, 1/10 of the waterborne source assumed to be uniformly distributed in the containment volume.

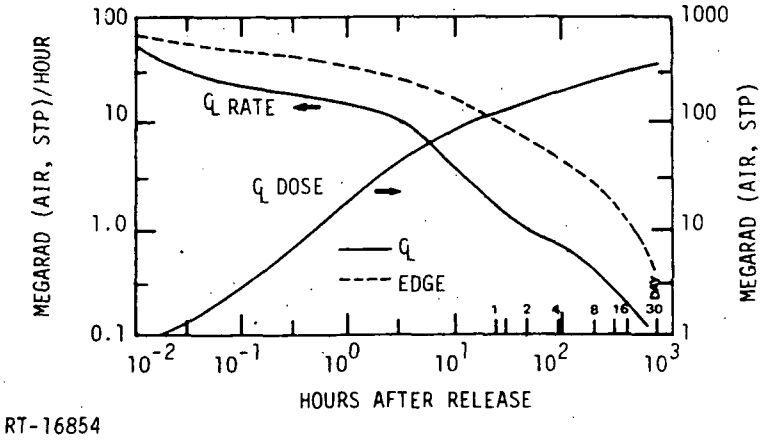

Figure 5. Typical dose rate and dose to air from the combined beta sources; airborne source uniformly distributed in the containment volume, plate-out source uniformly distributed on the containment sidewall surface, 1/10 of the waterborne source assumed to be uniformly distributed in the containment volume.

Table 2. Radiation Dose Rate in Rad (Hypalon)/Sec at Surface of Cables

	Radiation Source		
Time After Accident	Gamma	Beta	Total
1 minute	1.9×10^2	1.4×10^4	1.5×10^4
4 days	33	310	343

Other important environments include the external temperature which is taken to be steam at 60 psig. This results in a temperature of 143°C, which is rather high but still below the maximum service temperature shown in Table 1. The current expected is about 20 amps and the voltage is presumed to be a nominal 220V rms (i.e., 310V peak). The above data are summarized in Table 3. As a convenience in later discussions, the average dose rate in the different materials, as taken from Figure 6, is appended to Table 3.

Table 3. Worst Case Environment of the Cable

Reactor Power	4,000 Mwatt
External Temperature	140°C Peak
Potential of Inner Conductor	310 Volts Peak
Current Carried by Conductor	20 amps

Average Radiation Dose Rate Within the Given Region in Rad(Material)/Sec

Time After Accident	Copper	EPR	Hypalon
1 minute	585.0	6.4×10^3	1.1×10^4
4 days	1.9	26.0	100.0

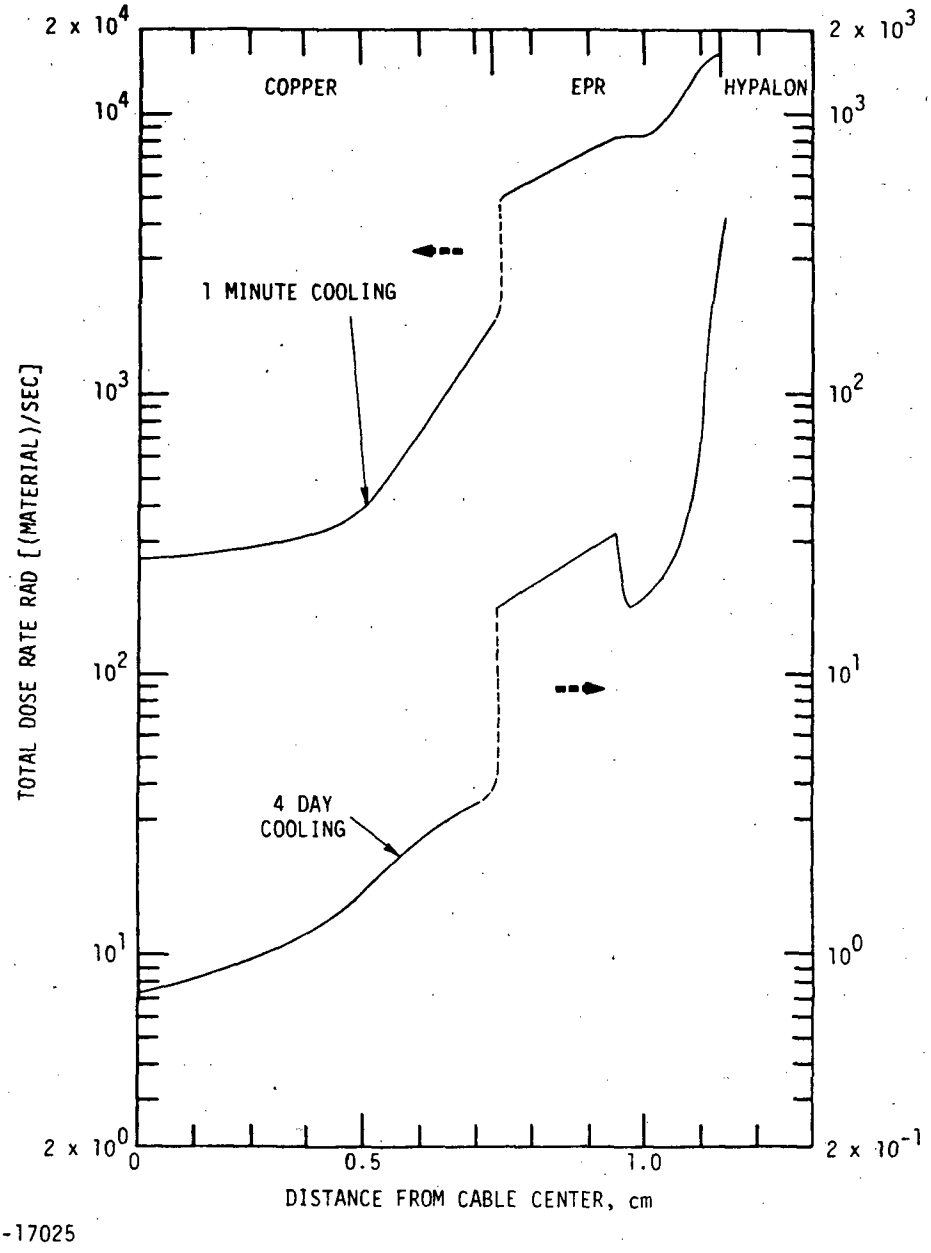

Figure 6. Total dose rate deposition profile in a cable due to the combined LOCA radiation environment.

3. ELECTRICAL CHANGES IN THE CABLE

3.1 SUMMARY OF THE ELECTRICAL PROBLEM

The dose rate, which is established soon after the accident will have several electrical consequences. The radiation induced conductivity, σ, will turn the pure insulator into a shunt resistor (albeit, still a very large one). This effect must be calculated from the value of conductivity of EPR at the radiation level and at the temperature listed in Table 3. Such data for EPR could not be found, but had to be estimated by comparison with data at the correct temperature for similar materials and for data at lower temperature for the same material. This procedure is acceptable since the electrical deviations remain small, although measurements on the material of interest in the environment of interest would be more satisfying. This work is described in subsection 3.2. The leakage current is the product of σ times the electric field, E. The field is derived in subsection 3.3, and σ and E are combined into an effective lumped shunt resistor in subsection 3.4. Noise pulses caused by release of trapped charge are discussed in subsection 3.5. Subsection 3.6 mentions differences between the LOCA radiation and gamma simulators.

3.2 DERIVATION OF THE CONDUCTIVITY

Several workers (Refs 5,7) have determined the electrical conductivity of a plastic insulator in a radiation environment. They all agree that the radiation induces a conductivity of the form

$$\sigma = A\dot{\gamma}^{\delta} \quad , \tag{1}$$

where $\dot{\gamma}$ is the dose rate, A is of order 10^{-15} to 10^{-20} (ohm-cm rad/sec)$^{-1}$ and δ is approximately 1.0. Assuming that δ equals 1 is accurate enough for our purpose.

The conductivity at an elevated temperature must also be found. Theoretically, the conductivity should be the product of the charge per carrier, e, the mobility, μ, and the numbers of carriers,n.

$$\sigma = n\, e\, \mu \quad . \tag{2}$$

The carriers are generated thermally as well as by the radiation

$$\sigma = n\, e\, \mu (n_{th} + n\dot{\gamma}) \quad , \tag{3}$$

where $n_{th} \approx n_o \exp(-E/kT)$.

The data of Harrison and Proulx (Ref 6) are plotted in Figure 7 as a function of inverse temperature (1000/T). This plot indicates that A has a temperature independent background plus an exponential variation. This is what would be expected from Equation 3 if μ is not a strong function of temperature. However, an analysis by Adamee and Calderwood (Ref 8) indicates that μ itself is an exponential function of T. Thus, it is safest to assume that the temperature dependence of A is parallel to the temperature dependence of σ. As an aid to this end, data from an NBS Monograph (Ref 9) are also plotted in Figure 5. It appears that at 143°C (1000/T = 2.40), A will be of the order of 10^{-13} for EPR. Hypalon is a better conductor than EPR so that, under the same temperature conditions the parameter for Hypalon (A) will be larger. We take A to be 10^{-12} for Hypalon. The values of σ quoted in Table 1 are found using the above values of A along with the 1 minute values of $\dot{\gamma}$ in the appropriate regions presented in Table 3. In Section 4 of this report, it is concluded that the temperature of the EPR may rise by as much as 15°C which could increase σ by a factor of 4. Nevertheless, as we are about to show, the conductivity does not appear to be large enough to cause any problem.

3.3 DERIVATION OF THE ELECTRIC FIELD

The electric field is the superposition of the field set up by any potential applied to the conductor and a field set up by charges trapped in the insulator. We will show that the field generated by trapped charge is insignificant compared to the normally applied voltage.

The trapped charge is the charge deposited per unit time, as calculated in Ref 3, times the charging time. The charging time is taken to be the dielectric relaxation

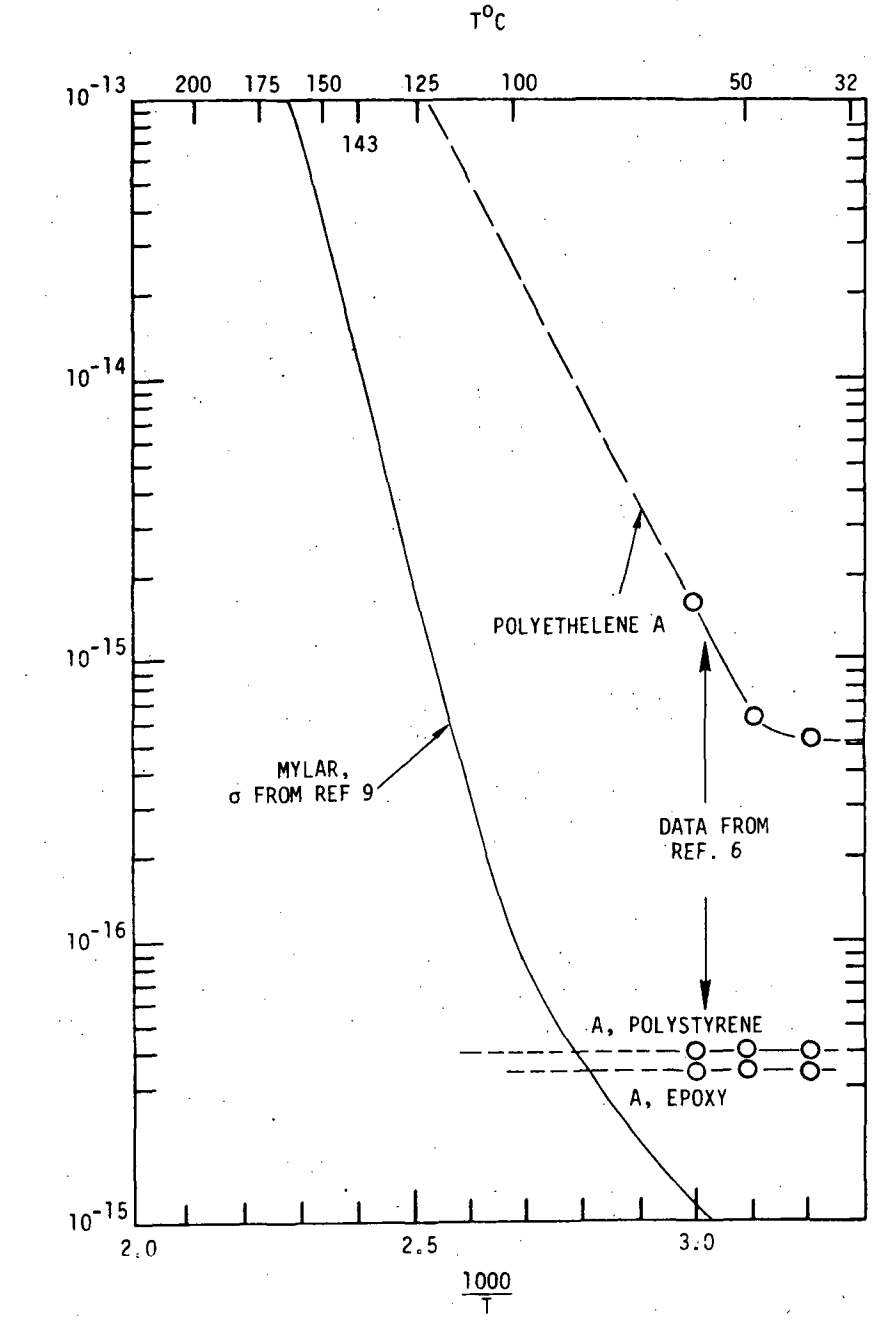

Figure 7. Electrical conductivity σ, and A as a function of temperature, T.

time presented in Table 1. Rather than treat each region separately, an average of 10^{-4} sec is used. For longer times, the field will be large enough to sweep most of the charges out of the cable. The total charge deposited within the copper is assumed to leak off immediately. This current represents a possible noise signal which has not been analyzed here because this is a power cable rather than a signal cable. Figure 8 shows the total charge per unit length $Q_T(r)$, in the dielectric from the copper out to radius, r. The charge starts at zero at r = 0.729 and goes negative because it is the accumulated electronic charge. The displacement, D, is found from the total charge by Gauss' Law applied to a unit length of the cable

$$2\pi r D_r = Q_T + Q_C \quad , \tag{4}$$

where Q_C is added to include image charges on the copper. The electric field is

$$E_r = D_r/\epsilon\epsilon_o = (Q_T + Q_C)/2\pi r\epsilon\epsilon_o \tag{5}$$

where ϵ is the dielectric constant of the medium and $\epsilon_o = 8.84 \times 10^{-14}$ F/cm is the permittivity of free space. The dielectric relaxation time is calculated from $\epsilon\epsilon_o/\sigma$. The constant Q_C in Equation 4 must be found from the voltage, V, across the cable. It is not a simple problem to decide what this voltage should be. In some places the outer jacket will make good contact with ground and will be at zero potential. Most places, it will charge up to an unknown voltage and then sweep the charge out. We shall examine both cases.

The relation between E and V is

$$E_r = - dV/dr \quad . \tag{6}$$

The solution to Equation 6 is written in terms of integrals over Q_T. To simplify notation we use r with subscripts C, E, and H to signify the outer radius of the three regions. Also subscripts E and H are added to ϵ to signify dielectric constants in these two regions. The final result is

$$V = V_C - \frac{1}{2\pi\epsilon\epsilon_o} \left[\int_{r_C}^{r} Q_T \, dr/r + Q_C \ell n \, (r/r_C) \right] . \tag{7}$$

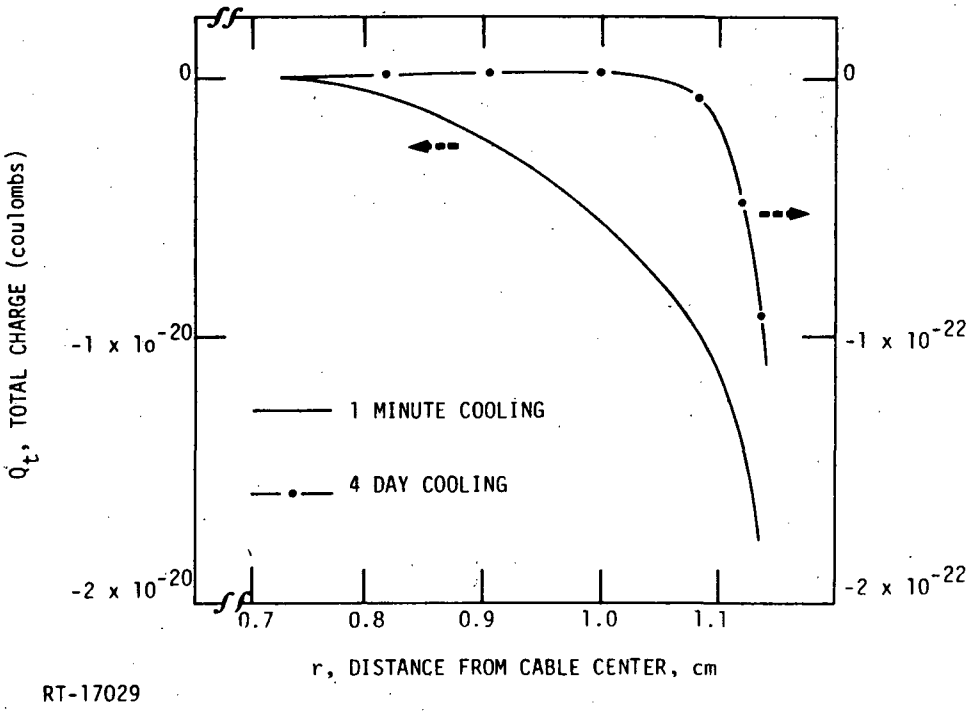

Figure 8. Total charge trapped in the cable insulation, Q_T, from the copper out to radius r.

The voltage at the Hypalon surface is

$$V_H = V_C - \left(\frac{1}{2\pi\epsilon\epsilon_0}\right)\left\{\frac{1}{\epsilon_E}\left[\int_{r_C}^{r_E} Q_T\, dr/r + Q_C \ell n\left(r_E/r_C\right)\right]\right.$$

$$\left. + \frac{1}{\epsilon_H}\left[\int_{r_E}^{r_H} Q_T\, dr/r + Q_C \ell n\left(r_H/r_E\right)\right]\right\} . \qquad (8)$$

The solution for Q_c is

$$Q_c = \left[(2\pi\epsilon_o \epsilon_E)\ (V_H - V_c) + \int_{r_c}^{r_E} Q_T\, dr/r \right.$$

$$\left. + 0.38 \int_{r_E}^{r_H} Q_T\, dr/r \right] / 1.1 \quad ,$$

where numerical values of the radii have been inserted into Equation 8.

This value of Q_c is inserted into Equation 5 to find the electric field,

$$E = \left(V_H = V_c + \frac{6.2 \times 10^{-21}}{\epsilon_E \epsilon_o} \right) / 1.1 = 266 + 2.6 \times 10^{-8} \text{ V/cm.}$$

The second term in E, caused by the trapped charge, is much less than the first term, caused by the applied voltage. The insulator is in no danger of breaking down if leakage current can drain off trapped charge as we assume here. The case where trapped charge builds up is discussed in subsection 3.5.

Also, this field will create a Joule heating of σE^2 which is about 5×10^{-5} watt/cm^3. This is much less than the power deposited by the radiation so there is no danger of "hot spots" driven by the positive feedback between increased σ with temperature and increased Joule heating with increased σ.

3.4 SHUNT RESISTANCE REPRESENTATION OF LEAKAGE CURRENT

The leakage current found above can be represented by a lumped shunt resistor, R_S, across the line:

$$R_S = \left(V_H - V_C \right) / \pi r L \sigma E = 1/\pi r L \sigma \approx 0.44/L\sigma \qquad (9)$$

where L is the length of the cable. The numerical value of R_s is about 70 MΩ if L is 10 cm, and it is 7 MΩ if L is 100 cm. If σ is increased because of increased insulator temperature then R_S will decrease by the same factor. All of these shunt resistances are high enough to be of no concern for the power cable considered here. It is possible, however, that they could represent an unacceptable loss in a high impedance measuring circuit.

3.5 THE NOISE PULSE GENERATED BY RELEASE OF TRAPPED CHARGE

We recognize that noise pulses from trapped charge discharges are probably not important to a power cable but would be for a signal cable. For completeness, we consider this topic. An estimate of this effect can be found by supposing that the field builds up to its breakdown limit, E_B, in some section of the cable which is not in good enough contact with a ground plane to allow ordinary leakage current to dispose of the trapped charge. The total charge built up per unit length, Q_B, under this circumstance can be found by inverting Equation 5 with $E_r = E_B \approx 10^6$ V/cm

$$Q_B = 2\pi r \epsilon \epsilon_o E_B \approx 1.3 \times 10^{-6} \text{ C/cm} \quad . \tag{10}$$

When the cable breaks down, the charge Q_B is transferred from the insulation to the copper where it neutralizes an equal image charge. In principle, the current flow during breakdown is perpendicular to the cable and it will not tend to induce an emf around the circuit to which the cable is connected. The exact magnitude of any induced emf depends on the geometry of the termination of the cable. If the charge transit time for the discharge is of order 10^{-6} sec, and the cable is a meter or more long, then it is unlikely that the induced emf would exceed a volt. The main noise will thus be a return current to establish a new image charge after the discharge. This current will flow over the period of about 10^{-6} sec so the 10^{-6} C/cm will be replaced by a current which is about one amp per cm of cable which failed. This current can be supplied from ground through the resistive load termination of the cable. If this load is very big then a large voltage has to be developed across the load. The charge can also be supplied from stray capacitance of the load termination. If this load capacitance is as big as the cable capacity of a few pf/cm, then it can supply the charge without changing its voltage by too much.

In summary, the amplitude of noise pulses built up by breakdown in the cable depends almost completely on the exact details of the cable termination. If the termination is either a small resistive load or a large capacitive load, then the noise spikes will not be large.

3.6 POSSIBLE ERRORS IN SIMULATION OF LOCA CABLE FAILURE

The trapped charge in the insulator is largely a consequence of the nonuiform dose deposited in the cable. The mechanism that applies here is that the secondary emission

leaving a volume element is not balanced by secondary emission from adjacent points because the adjacent points are not receiving the same primary radiation. The gamma source simulators do not show such a strong attenuation as does the true LOCA source so they will not properly simulate the trapped charge and any resultant noise spikes. However, because radiation induced leakage currents are judged to be inconsequential we suggest that the LOCA environment is adequately simulated by Co^{60}, as long as average doses are matched.

4. TEMPERATURE CHANGES IN THE CABLE

The total energy deposited inside any region of the cable is found by taking the dose rate within the region from Table 3 and converting the rad/sec to erg/gm-sec. This is then multiplied by density and converted to watts. The net result for copper is about 0.052 watt/cm^3. There is also a Joule heat generation from ½ I^2R losses in the copper. This is only about 10^{-3} watt/cm^3 when I is the nominal maximum of 20 amps; it is safely ignored compared with the radiation energy.

Two regions of the cable should be considered. The region considered first is in the middle where heat flow is radially through the insulator. The region near the ends is considered in the next paragraph.

Select a section of cable L cm long so the total power deposited into the cable is ($\pi r^2 L$) 0.052 watt. At equilibrium there will be a temperature gradient, ΔT, across the EPR which is big enough to conduct this heat to the external environment. In other words ΔT must satisfy

$$\frac{\Delta T}{\Delta r} (2\pi r L) \kappa_E = 0.052\, \pi r^2 L \quad . \tag{12}$$

The radius r is 0.729 cm and the thickness, Δr, is 0.18 cm which yields a value of ΔT of

$$\Delta T = \frac{0.052 \times 0.729 \times 0.18}{2 \times 3.47 \times 10^{-3}} = 1.0^{\circ}C \quad . \tag{13}$$

The radiation energy deposited in the Hypalon is 0.14 watt/cm^3. If this much heat flows radially out through the Hypalon itself, then a temperature change of about 7°C must exist within the Hypalon region. Such a rise above an ambient of 143 degrees is still safely below the service temperature of both EPR and Hypalon.

If the cable is in poor thermal contact at its outer radius, then the heat must flow into the copper and the heating problem becomes more serious. The heat must then flow out lengthwise to the ends of the cable or to regions where radial flow is again

permitted. For the case of linear flow in the copper, Equation 12 is recast as

$$\frac{\Delta T}{\Delta L} \pi r^2 \kappa_c = 0.04 \pi r^2 L$$

$$\Delta T = 0.04(L \Delta L)/4.19 \quad . \tag{14}$$

As an illustration, take $L \simeq \Delta L = 10$ cm and ΔT is about a degree. If L were a meter and if this were the only heat current allowed, then T could rise by ten to one hundred degrees, which does approach the temperature limit of the insulators.

On the other hand, the temperature rise may not be quite as large as indicated above since the two transport mechanisms will operate in parallel and allow the temperature to reach some lower temperature than that calculated by either mechanism by itself. In any event, however, some sections of the cable may approach the maximum service temperature of the insulators.

The ^{60}Co and ^{137}Cs simulation radiation sources do not reproduce the true LOCA attenuation into the cable so that the temperature profiles established by these simulators will not accurately reproduce the true LOCA profiles. In particular, the simulation fields are not attenuated in the cable as the true LOCA spectrum. Thus, the simulator will deposit too much power in the copper and inner portions of the Hypalon compared with the power deposited into the outer surface. If the simulation is performed so that the total doses are equivalent, then the simulator will exaggerate the heating of the inner insulator region. This is the inverse of the case of electrical effects generated by trapped charges where the simulator understresses the effect.

5. CHEMICAL AND MECHANICAL CHANGES IN THE CABLE

Several different chemical changes occur in a polymer or an elastomer (cf. Refs 1, 10-12) upon exposure to radiation: evolution of gases, crosslinking, and scission of bonds (also called unsaturation). The magnitudes of the effects are usually given by a G factor which gives the number of such events produced by 100 eV of absorbed radiation. The number of events per rad can be found by multiplying G/eV by 6.24×10^{11} eV/erg if desired. The values of G that are used here are given in Table 4. Some analysis, as discussed next, was done to obtain these numbers.

Table 4. G, the Number of Chemical Changes per Absorbed 100 eV at 140°C

Process	Polyethylene	Polypropylene
Crosslinking	3.3	1.0
Hydrogen Evolved	6.0	1.0 to 2.0
Unsaturation	3.0	0.8 to 1.0

The values for G for crosslinking and hydrogen evolution in polyethylene are given by Bolt and Carroll (Ref 10) as a function of temperature. We have used these values in Table 4. Reference 9 also contains G unsaturation for polyethylene, G crosslinking, and G unsaturation for polypropylene at 20°C. The increase in G with temperature will be similar to polyethylene so we have scaled these values up similar to the increase of polyethylene. Kircher and Bowman (Ref 11) indicate that an unsaturated hydrocarbon (polypropylene) evolves hydrogen at one-half to one-sixth the rate of a saturated hydrocarbon (polyethylene). This allows filling in the final entry in Table 4.

Bolt and Carroll's data indicate that the largest increase in G is already achieved by 140°C; a further increase to 200°C raises G by only five percent. There will not be a large synergistic effect between radiation and temperature above the steam temperature.

This analysis requires the total dose rather than the dose rate used heretofore. There are two factors to consider in integrating the dose rate over time to obtain dose.

The first factor is that the dose rate is steadily decreasing with time. This has already been accounted for by Bonzon (Ref 4) who presents total dose at the cable surface as a function of time. This can be used directly for total dose in the Hypalon region. The second factor is the energy degradation of the LOCA spectrum so that there is greater attenuation into the cable with increasing time. This factor was accounted for in the EPR layer by simply interpolating the attenuation factor between the one-minute and four-day cases. For later times the original data from Reference 2 is used to extrapolate the attenuation factor. The total dose so determined is shown in Figure 9.

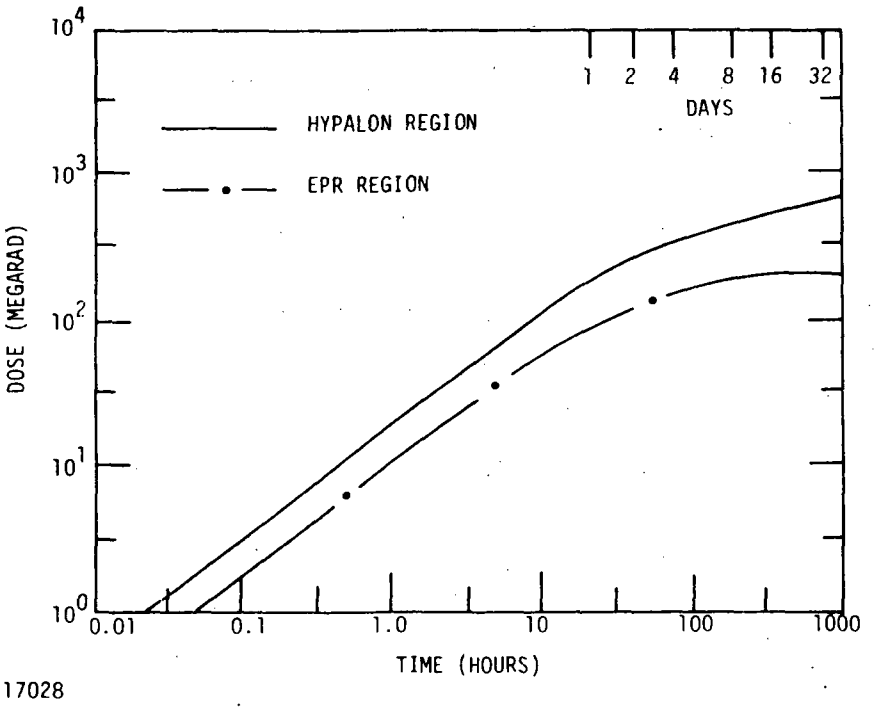

Figure 9. Total dose (material) deposited in the cable jacketing as a function of time for the LOCA radiation environment

To evaluate the effect of these doses, it is useful to consult Kircher and Bowman who derive the dose, γ (in rads), necessary to create one crosslink per mole in material with molecular weight, M:

$$\gamma = 4.8 \times 10^{11}/MG_{c\ell} \quad . \tag{15}$$

$G_{c\ell}$ will be between 1.0 and 3.3. For this example a G of 2.0 was selected. The value of γ to produce a crosslink per monomer (small molecule) with molecular weight M midway between polyethylene 14 and polypropylene 28, is about 10^4 Mrad. The unsaturation G is about the same as the crosslinking G, while the H_2 evolved is much larger. Thus by 10^4 Mrad (on the average), every monomer in the organic material has suffered a scission, or a crosslink. By the time this dose has accumulated, the polymer will be nearly disintegrated. It may be arbitrarily assumed that the material will retain some semblence of its structure if only one out of twenty monomers is decoupled or crosslinked. In this case, the acceptable dose is about 500 Mrad. This dose is reached in the Hypalon after approximately ten days in a LOCA environment, and may not be attained in the EPR region at all.

The mechanical evaluation in References 10 and 11 is also of interest in this regard. It essentially tells the same story as above. Hypalon starts to deteriorate at 90 Mrad (about ten hours) and loses stability seriously at 300 Mrad (eight days). The tensile strength of polyethylene and polypropalene will maintain up to 80 percent of their original value through 100 Mrad (one to two days) and will drop to 50 percent or less after 500 Mrad. The elongation and impact strength will deteriorate by 90 percent or more after 50 Mrad (which is accumulated after ten hours in a LOCA radiation environment). These later properties will determine the cable's resistance to vibration, which radiation environment should be specified in a LOCA.

We note that there is some uncertainty in the literature concerning the dose level at which Hypalon becomes seriously deteriorated. The values reported by Bolt and Carroll (Ref 10) are about a factor of 100 less than those given by Kircher and Bowman (Ref 11). The latter values are more consistent with failure levels in similar materials, and therefore they have been adopted here.

6. SUMMARY AND CONCLUSIONS

The most serious problems that will occur with the cable are chemical and mechanical deterioration which are expected to occur after a few hours to a day in LOCA environment. Impact strength and elongation changes by 50 percent within ten hours. In order to properly evaluate these effects the expected vibrational and bending stresses should be included in the specification of the LOCA environment.

The temperature rise in the insulation layers can approach the recommended service limit of Hypalon because of the energy deposited in the Hypalon and in the copper by the radiation field.

It is not expected that leakage resistance will be less than a megohm. Whether this impedance is a problem or not depends on what sort of circuits the cable connects. Voltage noise spikes will probably be of short duration. The amplitude of these spikes depends on the cable load impedance.

The gradient of dose rate into the cable, which is not simulated by standard gamma sources, has two consequences. The first is to allow the radiation to deposit charge into the insulator because the back and forward flow of secondary emission is not equal. The main role of this trapped charge is to create voltage noise spikes. These spikes may not be reproduced by a simulator. The second consequence of the $\dot{\gamma}$ gradient is that more energy is deposited in the interior by the nonattenuated simulator than is deposited by the LOCA radiation field. The simulator may exaggerate the interior temperature compared with the actual situation.

Several material parameters such as electrical conductivity and the radiation G values had to be interpolated from similar materials or from adjacent temperatures. If more accurate estimates than are presented here are ever needed, then a measurement program would be required.

REFERENCES

1. R. E. Leadon, "Radiation Damage Mechanisms in Reactor Components," IRT 4311-011, IRT Corporation (May 11, 1978).

2. N. A. Lurie, D. H. Houston, and J. A. Naber, "Definition of Loss-of-Coolant Accident Radiation Source," IRT 8167-004/SAND78-0091, IRT Corporation, prepared for Sandia Laboratories (May 1978).

3. N. A. Lurie, "Evaluation of Test Sources for Radiation Component Qualification," IRT 8167-010, Draft (March 1978).

4. L. L. Bonzon, "Radiation Signature Following the Hypothesized LOCA," SAND76-0740 (NUREG76-6521), Sandia Laboratories, Rev. October 1977.

5. C. Mallon and J. Wilkenfeld, "Measurement of Electrical Conductivity and Charge Storage of Insulating Materials," IRT 8172-002, IRT Corporation (March 1978).

6. S. E. Harrison and P. F. Proulx, "Measured Behavior of Gamma-Ray Photoconductivity in Organic Dielectrics," SCR-526 (June 1962).

7. T. J. Abrens and F. Wooten, "Electrical Conductivity Induced in Insulators by Pulsed Radiation," Trans. Nucl. Sci. NS-23, 1268 (June 1976).

8. V. Adamee and J. H. Calderwood, "Electrical Conductivity of Dielectrics at High Fields," J. Appl. Phys. 8, 551 (1975).

9. R. E. Schromm, A. F. Clark, and R. P. Reed, "A Compilation and Evaluation of Mechanical, Thermal, and Electrical Properties of Selected Polymers," NBS Monograph 132 (September 1973).

10. R. O. Bolt and J. G. Carroll (Eds.), Radiation Effects on Organic Materials, Academic Press (1963).

11. F. Kircher and E. Bowman (Eds.), Effects of Radiation on Materials and Components, Reinhold Publishing Company (1964).

12. A. Charlesby, Atomic Radiation and Polymers, Vol. I (Pergamon Press, 1960).

DISTRIBUTION:

U. S. Nuclear Regulatory Commission
(543 copies for RV)
Division of Document Control
Distribution Services Branch
7920 Norfolk Avenue
Bethesda, MD 20014

AMN Impianti Termici E. Nucleari
Via Pacinotti, 20
16151 Genova Sampierdarena,
Italy
Attn: G. Bottinelli

AMN spa
Via G. D'Annunzio 113
16121 Genova
Italy
Attn: P. Giordano

ASEA-ATOM (2)
Engineering
Box 53
S-721 04
Vasteras,
Sweden
Attn: G. Kvist
A. Kjellberg

ASEA KABEL AB
P. O. Box 42108
S-126 12
Stockholm,
Sweden
Attn: C. T. Jacobsen

Atomic Energy of Canada, Limited
Chalk River,
Ontario,
Canada
Attn: G. F. Lynch

Atomic Energy of Canada, Limited
Power Projects
Sheridan Park Research Community
Mississauga, Ontario L5K1B2
Canada
Attn: N. Cheesman

Battelle Institute V
Am Romerhof 35
D6000 Frankfurt/M
Federal Republic of Germany
Attn: B. Holzer

Belgonucleaire
rue de Champ-de-Mars, 25
B-1050 Brussels,
Belgium
Attn: J. P. van Dievoet

British Nuclear Fuels Ltd.
Springfield Works
Salwick, Preston
Lancs. England
Attn: W. G. Cunliffe, Bldg 396

Bundesanstalt fur Material Prufung
Unter den Eichen 87
1 Berlin 45
Germany
Attn: K. Wundrich

CERN
Laboraotorie 1
CH-1211 Geneva 23
Switzerland
Attn: H. Schonbacher

Centre d'Etudes Nucleaires de Saclay (3)
Boite Postale No. 21
91190 GIF-SUR-YVETTE
France 37.08
Attn: J. Laizier
E. Bouteiller
P. Tanguy

Conductores Monterrey, S.A.
APDO Postal 2039
Monterrey, N.L.
Mexico
Attn: Ing. Patricio G.
Murga G.

Electra de Viesgo, S.A.
Departmento Nuclear
Medio, 12 - SANTANDER
Spain
Attn: J. L. del Val

DISTRIBUTION: (cont)

Electricite de France (2)
Service Etudes et Projects
Thermigues et Nucleaires
Tour E.D.F.-G.D.F. Cedex No. 8
92080 PARIS LA DEFENSE
France
Attn: J. Roubault
M. Barbet

EURATOM
C.E.C. J.R.C.
Ispra (Varese)
Italy
Attn: G. Mancini

EURATOM
Joint Research Centre
Petten Establishment
European Communities
Petten
The Netherlands
Attn: M. Van de Voorde

Framatome (2)
77/81, Rue Du Mans
92403 Courbevoie
France
Attn: J. Meyer
G. Chauvin

Furukawa Electric Co., Ltd.
Hiratsuka Wire Works
1-9 Higashi Yawata 5 Chome
Hiratsuka, Kanagawa Pref.
Japan 254
Attn: E. Oda

Hitachi Cable Ltd. (2)
777 Third Avenue
New York, NY 10017
Attn: H. J. Amino
M. Sasson

Institute of Radiation Protection
Department of Reactor Safety
P. O. Box 268
00101 Helsinki 10
Finland
Attn: M. Heikkila

ITT Cannon Electric Canada
Four Cannon Court
Whitley, Ontario, LIN 5V8
Canada
Attn: B. Marshall

Japan Atomic Energy Research Inst. (2)
Takasaki Radiation Chemistry
Research Establishment
Watanuki-Machi
Takasaki, Gunma-Ken
Japan
Attn: Y. Nakase
S. Machi

Japan Atomic Energy Research Institute
Tokai-Mura
Naka-Gun
Ibaraki-Ken
Japan
Attn: A. Kohsaka

Kansai Electric Power Co., Inc.
1725 K. St. N.W.
Suite 810
Washington, DC 20006
Attn: J. Yamaguchi

Meideusha Electric Mfg. Co. Ltd.
1-17, 2-Chome Osaki
Shinagawa-Ku
Tokyo
Japan
Attn: M. Kanazashi

Universidade Federal do Rio de Janeiro
Av. N.S. Copacabana 661/1201
22050 Rio de Janeiro -RJ
Brazil
Attn: Paulo Fernando Melo

Oy Stromberg Ab,
Helsinki Works
Box 118
SF-00101
Helsinki 10
Finland
Attn: P. Paloniemi

DISTRIBUTION: (cont)

Rhein-Westf TUV
Steuben Str 53
D-43 Essen
Federal Republic of Germany
Attn: R. Sarturi

Studsvik Energiteknik AB
S-61182
Nykoping
Sweden
Attn: E. Hellstrand

Tokyo Electric Power Co., Inc.
No. 1-3 1-Chome Uchisaiwai-Cho
Chiyoda-Ku, Tokyo
Japan
Zip Code 100
Attn: H. Hamada

Traction & Electricite
Rue de la Science 31
1040 Brussels
Belgium
Attn: P. A. Dozinel

Waseda University
Dept. of Electrical Engineering
170-4, Shinjuku, Tokyo
Japan
Attn: K. Yahagi

Westinghouse Nuclear Europe (3)
Rue de Stalle 73
1180 Brussels
Belgium
Attn: R. Minguet
R. Doesema
J. Cremader

4000 A. Narath
4200 G. Yonas
4300 R. L. Peurifoy, Jr.
4400 A. W. Snyder
4410 D. J. McCloskey
4420 J. V. Walker
4440 G. R. Otey
4441 M. Berman
4442 W. A. von Riesemann
4443 D. A. Dahlgren
4444 S. L. Thompson
4445 L. O. Cropp
4445 L. L. Bonzon (15)
4445 W. H. Buckalew
4445 J. A. Lewin
4445 F. V. Thome
4450 J. A. Reuscher
4500 E. H. Beckner
4700 J. H. Scott
5000 J. K. Galt
5800 R. S. Claassen
5810 R. G. Kepler
5811 L. A. Harrah
5811 R. L. Clough
5813 J. G. Curro
5813 K. T. Gillen
5813 E. A. Salazar
5815 R. T. Johnson
8266 E. A. Aas
3141 T. L. Werner (5)
3151 W. L. Garner (3)
for DOE/TIC (Unlimited Release)
3154-3 R. P. Campbell (25)
for NRC distribution to NTIS